MITOCHONDRIAL PYRUVATE METABOLISM

INDUCES PSEUDOHYPOXIA

AND MITOPHAGY

by

Ashot Sargsyan

A dissertation submitted to the faculty of
The University of Utah
in partial fulfillment of the requirements for the degree of

Doctor of Philosophy

Department of Biochemistry

The University of Utah

May 2017

Copyright © Ashot Sargsyan 2017

All Rights Reserved

The University of Utah Graduate School

STATEMENT OF DISSERTATION APPROVAL

The dissertation of **Ashot Sargsyan**

has been approved by the following supervisory committee members:

Jared Rutter	, Chair	**12/13/2016** Date Approved
Adam Hughes	, Member	**11/28/2016** Date Approved
Elizabeth Leibold	, Member	**12/13/2016** Date Approved
Dennis Winge	, Member	**12/13/2016** Date Approved
Dana Carroll	, Member	**11/28/2016** Date Approved

and by **Christopher P. Hill and Wesley I. Sundquist** , Co-Chairs of

the Department of **Biochemisrty**

and by David B. Kieda, Dean of The Graduate School.

ABSTRACT

Mitochondria play a central role in cellular energy metabolism, and they supply most cellular adenosine triphosphate (ATP). During production of ATP, mitochondria also produce reactive oxygen species that could be damaging to mitochondria and to other cellular compartments. To limit and control the production of excessive reactive oxygen production, mitochondria have developed several quality control mechanisms that ensure mitochondrial integrity. Degradation of mitochondria through autophagy is the last step in mitochondrial quality control. Although mitochondrial dysfunctions are described in many human diseases including neurological diseases, diabetes, and cancer, there is little known about whether mitophagy plays any role in the etiology of these diseases. Partly this could be explained by the fact that for a long time mitophagy has been considered a nonselective process. Now several lines of evidence suggest that mitophagy is a steady state process, and in metabolically active tissues, the half-life of mitochondria is as low as two days. Possibly another reason for the slow progress in mitophagy research has been the lack of easily applicable and sensitive methods for mitophagy detection, and most mitophagic research has been done in settings of extreme mitochondrial stress. For example, carbonyl cyanide m-chlorophenyl hydrazone (CCCP), an uncoupling agent of the mitochondrial proton gradient, has been extensively used. Although CCCP and

other global mitochondrial stressors are excellent inducers of mitophagy, they affect the entire mitochondrial pool, and in most cases, do not recapitulate any given physiological or pathophysiological condition. Here we report a sensitive and highly quantifiable method for detection of mitophagy and autophagy in parallel that could be applied to physiological conditions of cells. This method relies on lysosomal delivery of mitochondrial targeted pH-sensitive Rosella biosensors and could reliably detect even very weak induction of mitophagy. Moreover, using this method we identified that pyruvate metabolism in mitochondria induces mitophagy. This mitophagy is mediated by pseudohypoxic induction of hypoxia inducible factor 1α. Interestingly, we discovered that even close to physiological levels of glucose can induce this pathway. Importantly, this process is completely blocked with pharmacological inhibitors of the mitochondrial pyruvate carrier. Thiazolidinediones, a class of insulin sensitizing medications, are known to inhibit the mitochondrial pyruvate carrier. Here, we show that thiazolidinediones are effective inhibitors of pyruvate induced pseudohypoxia. This observation is particularly interesting since thiazolidinediones are actively prescribed. Whether this phenomenon is clinically relevant remains to be studied.

TABLE OF CONTENTS

ABSTRACT iii

LIST OF FIGURES vii

ACKNOWLEDGMENTS viii

Chapters

1. INTRODUCTION 1

Overview of mitochondria 2
Mitochondria in energy production 3
Mitochondria as reactive oxygen species (ROS) source 4
Mitochondrial quality control 7
Discussion 16
References 18

2. RAPID PARALLEL MEASUREMENTS OF MACROAUTOPHAGY AND MITOPHAGY IN MAMMALIAN CELLS USING A SINGLE FLUORESCENT BIOSENSOR 28

Abstract 29
Introduction 29
Results 30
Discussion 36
Materials and methods 36
References 38

3. MITOCHONDRIAL PYRUVATE METABOLISM INDUCES PSEUDOHYPOXIA AND MITOPHAGY 40

Abstract 41
Introduction 42
Results 45
Conclusion 52
Discussion 53
Materials and methods 54

References.....59

4. CONCLUSIONS.....74

Mito-Rosella.....75
Mitochondrial pyruvate metabolism induces pseudohypoxia and mitophagy.....76
Future directions.....77
References.....79

APPENDIX: HEPATOCYTES ARE THE PRINCIPAL SOURCE OF CIRCULATING RBP4 IN MICE.....80

LIST OF FIGURES

Figures

2.1. Rosella pH-responsive fluorescent biosensors. 31

2.2. Single-cell measurements of autophagy and mitophagy based on biosensor responses to CCCP treatment. 32

2.3. Parallel quantification of autophagy and mitophagy under the same conditions by flow cytometry (FCM) measurement of biosensor responses. 34

2.4. Quantification of CCCP induced mitophagy in HEK-293 and HCT-116 cells and deferiprone (DFP)-induced mitophagy in HeLa cells. 35

3.1. Pyruvate stabilizes HIF-1α and induces expression of BNIP3 65

3.2. Expression of BNIP3 and mitophagy are mediated by HIF-1α 66

3.3. HIF-1α stabilization is dependent on mitochondrial pyruvate metabolism 67

3.4. Glucose and glycolysis product levels 68

3.5. Pyruvate metabolism inhibits OGDH in HepG2 cells 69

3.6. Dimethyl 2-ketoglutarate induces stabilization of HIF-1α and mitophagy 70

3.7. TZDs are effective inhibitors of pyruvate mediated pseudohypoxia 71

3.8. Pyruvate induces degradation of OGDH that is reversed by pioglitazone and NAC 72

3.9. Pyruvate metabolism increases ROS production 73

5.1. Generation of LRKO mice 84

5.2. LRKO mice lack circulating RBP4 85

ACKNOWLEDGMENTS

I would like to thank my mentor, Dr. Timothy Graham, for his patience and continuous support in my transition to an independent scientist. I am also extremely grateful to my thesis committee members, Drs. Dana Carroll, Elizabeth Leibold, Dennis Winge, Adam Hughes, Jared Rutter, and Donald McClain, who guided me through my studies. I am especially indebted to Dr. Rutter for allowing me to continue my studies in his laboratory, and Dr. Winge and Dr. Hughes for their encouragement and many stimulating conversations about science. I am also thankful to Dr. Elizabeth Leibold, Dr. Sihem Boudina, and Dr. Amnon Schlegel, as their office doors were always open for me. I would like to thank Dr. Dean Li and Dr. Simon Fisher for arranging financial support in my last year in the program. I am also thankful to my friends who made Salt Lake City, a home away from home, especially Laura, Tanya, Josh, Cole, Spencer, Dustin, Camille, Andres, Zaven, and Greg. I am also eternally grateful to my family, for their continuous support throughout the years, without having a clear picture of what I am trying to do. Lastly, I want to thank my girlfriend, Anna, for her unconditional support, understanding, and patience during my countless late night adventures in the lab.

CHAPTER 1

INTRODUCTION

Overview of mitochondria

Mitochondria are essential organelles that reside within the cytoplasm of every eukaryotic cell except for some specialized cells such as erythrocytes and lens cells[1, 2]. Mitochondria are segregated from the cytoplasm with double membranes: a porous mitochondrial outer membrane (MOM) and impermeable inner membrane (MIM). The space between those two membranes is called the intermembrane space (IMS), and the mitochondrial core is called the matrix. Mitochondria are functionally multifaceted and are pivotal in cellular metabolism. Unlike other organelles in eukaryotic cells, mitochondria possess circular deoxyribonucleic acid (DNA) and DNA replication machinery. Phylogenetic analysis of mitochondrial genes [3, 4] suggests that mitochondria evolved from alpha proteobacteria after engulfment by an eukaryotic ancestor. This engulfment eventually evolved into an endosymbiotic state, where most of the genes encoding mitochondrial proteins were transferred to the nucleus of the cell, and only 13 out of 1000+ proteins[5] are encoded in circular mitochondrial DNA (mtDNA). Mitochondria have structurally distinct ribosomes that translate mtDNA encoded genes. These 13 genes encode essential oxidative phosphorylation proteins. The rest of the mitochondrial proteome requires cytoplasmic translation and import of proteins. Importantly, there is a great degree of dynamic and rapid regulation of both mitochondrial and cytosolic translation of mitochondrial proteins[6]. For the import processes, most mitochondrial proteins in the cytoplasm are translated with a mitochondrial localization presequence, which directs them to mitochondria where the presequence is proteolytically cleaved upon import [7, 8]. Mitochondrial

outer membrane proteins lack this presequence and instead contain mitochondria targeting sequences within mature proteins. These targeting sequences are recognized by mitochondrial translocase of outer membrane (TOM)-associated receptors. After crossing the outer membrane, these newly imported proteins are directed to either Translocase of Inner Membrane 23 complex (TIM23) for import to the mitochondrial matrix, or to Translocase of Inner Membrane 22 complex (TIM22), that facilitates insertion of those proteins into the inner membrane. Importantly, the mitochondrial proton gradient is essential for both inner membrane translocase complexes[9]. Mitochondria also rely on other cellular compartments and organelles for their lipid needs. Although some of the mitochondrial lipids such as phosphatidylglycerol and cardiolipin are mitochondria specific and are synthesized in mitochondria[10, 11], other lipids are imported from the endoplasmic reticulum (ER).

Mitochondria in energy production

Historically, mitochondria have been looked at primarily as powerhouses of cells, although now their diverse functions are widely recognized. Mitochondria are involved in many aspects of cellular processes such as fatty acid and amino acid metabolism, iron[12] and calcium homeostases[13], induction of apoptosis[14], and autophagy[15]. Perhaps the most recognized function of mitochondria is the generation of ATP through a complex and highly regulated process of the tricarboxylic acid cycle (TCA) and oxidative phosphorylation. Through a series of reactions in the tricarboxylic acid cycle, acetyl-CoA, derived from different sources,

is oxidized to carbon dioxide and water. During these reactions, the TCA generates reduced nicotinamide adenine dinucleotide (NADH) and reduced flavin adenine dinucleotide ($FADH_2$), which transfer their electrons to the electron transfer chain (ETC) in the mitochondrial inner membrane. The ETC is comprised of four different protein complexes termed complex I through IV. Through redox reactions complex I accepts two electrons from NADH and simultaneously pumps protons into the mitochondrial intermembrane space. Electrons from $FADH_2$ are accepted by complex II, while complexes III and IV transfer additional protons to the intermembrane space. This proton gradient generated by the ETC across the mitochondrial inner membrane is released by complex V (ATP synthase) that uses this electrochemical gradient to phosphorylate adenosine diphosphate (ADP) to triphosphate (ATP), the main energy carrier molecule of eukaryotic cells. This electrochemical gradient is also used in generation of heat in brown and beige adipocytes, through the actions of Uncoupling Protein 1(UCP1).

Mitochondria as reactive oxygen species (ROS) source

The electron transport chain is also a significant source of reactive oxygen species production and it is estimated that up to 2% of oxygen consumed is converted to reactive oxygen species (ROS). ROS formation in mitochondria is a result of electron leak from the ETC and subsequent reduction of molecular oxygen. The ETC primarily generates superoxide ($O_2^{\cdot-}$) by reduction of oxygen at complexes I and III, where superoxide coming from complex I is released to the matrix, while complex III produced superoxide is found in both matrix and

intermembrane space. Historically, ROS were considered harmful, although now several lines of evidence suggest that ROS have important physiological roles and serve as signaling molecules[16]. For example, ROS production is required for proper function of some growth factors, and inhibition of ROS production blocks their downstream tyrosine kinase signaling[17, 18]. Mitochondrial ROS also regulate several physiological responses. Particularly, mitochondrial ROS is critical in the hypoxic response[19-21], induction of autophagy[22], inflammation response[23, 24] and vascular constriction[25]. Although well-regulated production of ROS is important in cellular signaling, several conditions could increase production of ROS and inflict significant oxidative damage both to mitochondria and to other cellular compartments. Increased levels of NADH in the matrix accompanied by decreased oxidative phosphorylation (OXPHOS) activity could result in excessive superoxide production. In addition, high membrane potential causes increased ROS production by reverse electron transport[26]. Importantly, reverse electron transport generated ROS recently have been implicated in reperfusion injury[27]. Mitochondria originated oxidative stress can be damaging to almost all biological macromolecules (DNA, proteins, and lipids), and mitochondrial ROS have been implicated in many disease states and aging. Oxidative damage to DNA is thought to be one of the mechanisms of mutagenesis and eventually carcinogenesis[28, 29], and many cancer types exhibit increased ROS production[30]. Moreover, ROS is also known to activate the MAPK/Erk1/2 pathway in some cancer types, which increases cell proliferation[31, 32]. Interestingly, different ROS are shown to have countering effects on cell proliferation: Low doses of hydrogen peroxide coupled

with superoxide are known to induce proliferation, while high levels of hydrogen peroxide promote senescence[33]. ROS is also implicated in type 2 diabetes and it is well established that hyperglycemia induces increased ROS production[34, 35]. Furthermore, β cell dysfunction during diabetes could be attributed to chronic hyperglycemic induction of ROS production[36]. ROS also can act in peripheral tissues by interfering with insulin receptor signaling [37] and by activating the JNK pathway that promotes peripheral insulin resistance. Consistent with this theory, it has been shown that antioxidant therapy could reverse the progression of type 2 diabetes[38, 39]. Another major area of ROS related pathologies are neurological diseases. For example, Alzheimer's disease (AD) is characterized by abnormal levels of oxidative damage[40, 41] and mitochondria associated mutations[42, 43]. Amyotrophic lateral sclerosis (ASL), another debilitating disease, is directly linked to mitochondria and ROS and 20% of familial cases of ALS are known to arise from mutations in the superoxide dismutase gene[44]. Furthermore, mitochondrial dysfunction and ROS are also involved in Parkinson's disease, another prevalent pathology. Growing evidence suggests that mutations in familial forms of Parkinson's disease are often accompanied by increased ROS production and decreased activity of complex I[45-47]. ROS are also thought to be central in aging theory[48-50] as they contribute to the decline of mitochondrial function over time.

Mitochondrial dysfunction not related to excessive ROS production is also implicated in human diseases. For example, dysregulation of TCA cycle enzymes can lead to selective accumulation of metabolites that are implicated in progression of various cancers, mainly by inhibition of enzymes responsible for degradation of

hypoxia inducible factor 1α (HIF-1α). For example, mutations in the succinate dehydrogenase complex and fumarate hydratase lead to pheochromocytomas and paragangliomas[51-54].

Mitochondrial quality control

Unlike any other organelle in eukaryotic cells, mitochondria have their own DNA that encodes 13 proteins for the ETC, 2 mitochondrial ribosomal RNAs, and 22 transfer RNAs. The proximity of ROS generation sites makes mitochondrial DNA susceptible to oxidative damage. It has been estimated that mutation rates in mtDNA are 10 to 15 times higher than in nuclear DNA[55, 56]. Over time this damage contributes to the decrease in mitochondrial function. Apart from mtDNA, mitochondrial proteins and lipids also sustain significant oxidative damage. In particular, the ETC is known to be a target of oxidative modifications[57] and there is an increase of oxidative damage to the ETC complexes with age[58]. In addition, proteins that are not associated with ETC are also known to undergo oxidative modifications. For example, mitochondrial aconitase is sensitive to oxidative stress[59], and upon being damaged could also contribute to ROS production[60]. Alpha ketoglutarate dehydrogenase is another target for ROS and subsequent impairment is implicated in Alzheimer's disease[61, 62]. Other significant targets for oxidative damage are mitochondrial lipids. Oxidative damage to lipids on mitochondrial membranes is shown to impair mitochondrial function[63, 64].

As a source and a target of ROS, mitochondria possess several quality control mechanisms that ensure the mitochondrial integrity and homeostasis.

Mitochondrial quality control mechanisms can be divided into four distinct parts: 1) Regulation and detoxification of reactive oxygen species by antioxidant defense mechanisms, 2) Identification and repair/degradation of misfolded or oxidized proteins by mitochondrial resident proteases, 3) Segregation of damaged or excessive proteins into distinct compartments and budding off of mitochondria, and 4) destruction of a whole mitochondria by means of autophagy.

Mitochondrial antioxidant defense

In physiological states, production of ROS by the ETC in mitochondria is highly regulated by several mechanisms. Mitochondrial Uncoupling Proteins 2 and 3 (UCP 2-3) are thought to limit excessive ROS production by decreasing the proton gradient formation[65]. Moreover, it has been shown that UCPs are activated by ROS, which serve as a negative feedback mechanism. Superoxide formed at the ETC is converted to hydrogen peroxide by mitochondrial resident protein superoxide dismutase (SOD2). Hydrogen peroxide, in turn, is converted to water and oxygen by the action of catalase enzyme, which is also present in mitochondria of some tissues[66]. Mitochondria also have other enzymes with antioxidant properties such as peroxiredoxins[67], which in combination with thioredoxin and thioredoxin reductase[68] catalyze conversion of hydrogen peroxide into water. It has been estimated that the superoxide dismutase and peroxiredoxin/thioredoxin/thioredoxin reductase system are the main mitochondrial antioxidant defense systems[69]. In addition to proteins that catalyze conversion of ROS to water and molecular oxygen, a major antioxidant defense

system is tripeptide glutathione[70] which is present in high concentrations in mitochondria as well as in cytosol and nuclei. Glutathione can directly scavenge ROS and act as a cofactor for some enzymes involved in antioxidant defense such as glutathione peroxidase.

Mitochondrial proteases

Mitochondria have three major classes of ATP-dependent proteases, Lon protease, Clp-like, and AAA-protease[71]. The last two are found in the matrix and on the inner mitochondrial membrane and facilitate degradation of misfolded and oxidized proteins[72, 73]. Hydrophobic surfaces are thought to serve as a recognition domain for both proteases. Lon protease plays a critical role in the degradation of oxidized aconitase[74] , Cytochrome C Oxidase Subunit 4 Isoform 1, Succinate Dehydrogenase Subunit 5, and other damaged proteins[75]. Furthermore, Lon deficient cells exhibit significant mitochondrial defects that lead to cell death[76]. Mitochondrial proteases have been shown to participate in numerous other aspects of mitochondrial integrity such as the mitochondrial unfolded protein response, mitochondrial morphology changes, mitophagy, and apoptosis[75].

Mitochondria-derived vesicles and compartments

In 2008, Neuspiel and colleagues identified a new class of vesicular transport from mitochondria and peroxisomes that is cargo selective[77]. Importantly, only a subset of mitochondria-derived vesicles (MDV) was targeted to peroxisomes. In 2012, the same group identified the second destination for MDV as the lysosome[78].

Interestingly, these vesicles form after oxidative stress induction and bud directly from respiring mitochondria that do not yet exhibit excessive ROS damage signs. It appears that actively respiring mitochondria without any additional oxidative stress can produce hundreds of MDVs, indicating a steady state process. Later, it was determined that MDVs are enriched for oxidized mitochondrial proteins[79]. Moreover, PINK1 and Parkin have been shown to play a direct role in MDV formation[80]. This finding is particularly interesting since it appears that these proteins are involved in multistage mitochondrial quality control and can mediate MDV formation as well as mitophagy. A similar pathway of vesicular transport from mitochondria to lysosomes, called mitochondria-derived compartments (MDC), has been recently identified in budding yeast[81]. Although similar in concept, these two pathways are distinct in their cargo selection. MDCs contain mainly mitochondrial outer, and a subset of inner membrane proteins belonging to the carrier family. Importantly, inhibition of the MDC pathway results in deterioration of mitochondrial membrane potential, suggesting that MDCs play a protective role and are part of mitochondrial quality control.

Degradation of mitochondria by autophagy

The above mentioned mitochondrial quality controls are nondestructive ways to maintain mitochondrial integrity. It is presumed that if these mechanisms fail to preserve mitochondrial homeostasis, parts of mitochondria are targeted for destruction by autophagy, a process of degradation in which cells catabolize some parts of the cytosol and the organelles through delivery to lysosomes. General

autophagic pathways are conserved through yeast to mammals and involve the ATG proteins. Currently, about 37 ATG proteins have been identified[82]. The most prevalent form of autophagy, termed macroautophagy, is a nonselective process that is triggered by starvation and provides cells with necessary nutrients. During general autophagy, the phagophore membrane, also called the isolation membrane, engulfs a portion of cytoplasm and segregates its contents. Eventually, the phagophore membrane closes to form double membrane vesicles known as autophagasomes. Autophagasomes then fuse either with other autophagasomes or lysosomes where their contents are degraded by lysosomal enzymes. The substrates later are released as free amino acids and other molecules. Mitophagy is a special form of autophagy, where mitochondria are selectively targeted for lysosomal degradation by the autophagic machinery. The primary role of mitophagy is to eliminate defective and old mitochondria. Mitophagy is also critical in erythrocyte development and destruction of paternal mitochondria during conception. In early research, lysosomal degradation of mitochondria was thought to be a “bystander” process, where induction of general autophagy affected some mitochondria. The first case of mitophagy was reported in 1962 by Ashford and Porter[83], where the authors described mitochondria in the lysosomes of hepatic tissues after glucagon treatment. Later, it was established that mitochondria could be targeted for degradation independently of other organelles such as peroxisomes. Notably, during starvation mammalian mitochondria are preferentially spared from autophagic destruction by elongation and formation of interconnected networks, thus escaping engulfment by the phagophore memb-

rane[84]. Significant progress in the identification of mediators of mitophagy has been accomplished in yeast systems, where genetic screens identified close to 40 proteins that are required for mitophagy, but not for general autophagy[85]. For example, ATG32 localizes to mitochondria and recruits the canonical autophagic machinery[86]. Another protein involved in mitophagy in yeast is ATG11, which functions as a cargo receptor between mitochondria and ATG8[87]. A mammalian homologue of ATG32 was recently discovered[88, 89], but a homologue of ATG11 has not yet been identified. In yeast, mitochondrial degradation is closely regulated by the carbon source[90], and mitophagy does not take place when a carbon source is non fermentable. In contrast, there is robust mitophagy with fermentable carbon sources, since oxidative phosphorylation is no longer critical for growth.

PINK1/PARKIN pathway. Perhaps the most well studied mammalian pathway of mitophagy is PTEN-Induced Putative Kinase 1(PINK1)/Parkin cytosolic E3 ubiquitin ligase-mediated degradation of mitochondria. These two genes are often mutated in autosomal recessive Parkinson's disease (PD). In patients with PD, there is an accumulation of dysfunctional mitochondria. In *Drosophila* models, deletion of PINK1 and Parkin proteins causes accumulation of dysfunctional mitochondria in neuronal and muscle tissues that results in neurodegeneration[91, 92]. Subsequent experiments demonstrated that Parkin and PINK1-dependent mitophagy can be induced by mitochondrial depolarization with carbonyl cyanide m-chlorophenyl hydrazone (CCCP)[93]. In normal ''nonstressed" conditions PINK1 is recruited to mitochondrial membranes by mitochondrial membrane potential and undergoes degradation facilitated by mitochondrial processing peptidase and

proteases[94]. In defective mitochondria, where membrane potential is decreased, PINK1 is stabilized on mitochondrial membranes and is no longer degraded. This, in turn, recruits Parkin, which is normally found in the cytoplasm, to mitochondria[95]. After recruitment to the mitochondrial membrane, Parkin ubiquitinates several mitochondrial proteins and initiates mitophagy. Among the ubiquitinated proteins are numerous outer membrane proteins, including Mitofusins 1 and 2, MIRO and DRP1. Although the exact roles of these ubiquitinated proteins and sites are not well understood, they trigger degradation of mitochondrial proteins and whole mitochondria by the ubiquitin proteasome system[96,97] and autophagic machinery. The latter is mediated by recruitment of mammalian homologue of ATG8 (LC3) to mitochondrial membranes. Recently, it has been reported that upon stabilization on the mitochondrial membranes, PINK1 is autophosphorylated at multiple sites that are critical for Parkin recruitment[98]. PINK1 also phosphorylates Parkin on Ser 65 and leads to activation of Parkin's E3 ligase activity[99]. Moreover, PINK1 can phosphorylate Ser65 on ubiquitin molecules which leads to activation of Parkin as well[100]. Ubiquitinated proteins cannot directly bind to the autophagic machinery, and therefore, there are a number of scaffolding proteins that bridge ubiquitinated proteins to LC3. To date, Optineurin, NDP52, and p62 have been reported to bridge mitochondria and LC3[101-103].

BNIP3 and BNIP3L mediated mitophagy. Another well recognized mitophagic pathway is mediated by BCL2 and Adenovirus E1B 19-kDa-interacting Protein 3 (BNIP3) and BNIP3-like (BNIP3L, also known as NIX) proteins[104]. Both are BH3-only mitochondrial single-pass outer membrane proteins that also contain an LIR

(LC3 interacting domain) that binds and facilitates the interaction between mitochondria and LC3[105, 106]. Studies in mice have shown that NIX is critical in mitochondrial clearance during erythrocyte development[107, 108]. In contrast, BNIP3 is involved in hypoxia and fasting induced mitophagy in the liver[109, 110], and BNIP3 KO mice develop increased mitochondrial mass and dysfunction accompanied by excessive accumulation of lipids in the liver[111]. In addition, phosphorylation of BNIP3 on Ser17 and Ser24 increases the affinity for the LC3 interacting domain, therefore augmenting mitophagy[112]. Apart from their mitophagic roles, both BNIP3 and NIX play important roles in induction of apoptosis.

FUNDC1 mediated mitophagy. Recently, FUN14 Domain-Containing Protein1 (FUNDC1) has been identified as a novel mitophagy receptor. In *in vitro* studies, FUNDC1 mediates hypoxia induced mitophagy, as FUNDC1 KD cells failed to induce mitophagy[113]. FUNDC1 is an outer mitochondrial membrane protein with three transmembrane domains that has its N-terminus exposed to the cytoplasm and C-terminus extended into the intermembrane space. Mechanistically, studies have shown that FUNCD1 has a LIR domain and can interact with LC3. Moreover, FUNDC1 is posttranslationally regulated by phosphorylation events. Under normoxic conditions, FUNDC1 is phosphorylated by SRC and CK2 at Tyr18 and Ser13, which impairs its interaction with LC3. Under hypoxic or uncoupling conditions, these phosphorylation events are reversed by the action of mitochondrial PGAM5 phosphatase[114], therefore enabling the interaction of LC3 with its binding domain on FUNDC1. In addition to these inhibitory phosphorylation events, there is an activation-inducing phosphorylation site, Ser13, that under

hypoxia is phosphorylated by ULK1[115]. In addition to posttranslational modification of FUNDC1, there is also transcriptional regulation mediated by miRNA 137. During hypoxia, there is a decrease in levels of miRNA 137 that leads to upregulation of FUNDC1[116].

Cardiolipin mediated mitophagy. Recently, cardiolipin has been shown to act as a mitochondrial degradation receptor in mammalian primary neurons and SH-SY5Y cells[117]. Cardiolipin is an inner mitochondrial membrane phospholipid that is essential in mitochondrial cristae formation and stabilizes proteins of the ETC. Upon treatment with CCCP or either rotenone, staurosporine or 6-hydroxydopamine, cardiolipin is translocated to the outer mitochondrial membrane with the help of the mitochondrial NDPK-D protein[118], where it is exposed to cytoplasm. This allows cardiolipin to interact with LC3 and recruit autophagic machinery to mitochondria.

Energetic balance and mitophagy. Mitochondria are pivotal in energy metabolism and perform a variety of metabolic functions. Perhaps the most important aspect of mitochondrial biology is the ability to produce ATP through the ETC that takes place on the inner mitochondrial membrane. The ETC is often leaky, and therefore produces reactive oxygen species by complexes I and III. A majority of the cell's need for ATP is met by mitochondrial oxidative phosphorylation, while the rest is supplied through glycolysis. In times of greater demand for ATP or when the carbohydrate source can only be metabolized in mitochondria, cells increase the mitochondrial load which in turn increases reactive oxygen species production. This could be potentially damaging to the cells and to

mitochondria as well. In 2013, Melser and colleagues showed that increased mitochondrial activity induces mitochondrial degradation mediated by NIX and the small GTPase RHEB independently of mTOR[119]. Importantly, these authors showed that RHEB and NIX mediated mitophagy are protective by increasing mitochondrial OXPHOS activity, while RHEB and NIX deficiency has deleterious effects on mitochondrial function mediated by ROS damage.

Discussion

Although mitochondrial degradation via lysosomes was first reported five decades ago, there has been little progress in elucidating the role of mitophagy and its regulatory networks in health and disease. The majority of mitophagic pathways described in this work have been discovered in the last decade. Except for a few proteins (PINK1/PARKIN and BNIP3/NIX), the exact mechanisms and physiological or pathological roles of mitophagy or its impairment are not well understood. Mitochondria are a source and a target of ROS damage, and undergo recycling, presumably to avoid excessive damage accumulation. In experimental murine and *in vitro* cell systems, the half-life of mitochondria is estimated to be from less than 2 to 10 days[120-122]. This fast recycling rate requires that efficient quality control mechanisms must be present in mitochondria, and that alterations in these processes could lead to accumulation of impaired mitochondria. Despite the significant rate of mitochondrial turnover, research on mitophagy has primarily been focused on mitochondrial toxin-induced mitophagy, and many known mediators of mitophagy have been discovered with stressors like CCCP, Antimycin

A, and rotenone, and so forth. While these inducers have been powerful tools and were instrumental in many discoveries, most cases do not have physiologically related conditions, at least when we consider the amplitude of the applied stress. For example, some studies have failed to detect Parkin recruitment and mitophagy in primary neurons with endogenous Parkin upon depolarization with CCCP[123,124]. Another important aspect of mitophagic research is that in most experimental conditions we use stressors that are uniformly applied to all mitochondria in the cell, while in physiological conditions mitochondria tend to segregate ‘’bad” parts and target them for degradation. This perhaps could be explained by the fact that mitophagy has been hard to detect when it is not massively induced. In recent years, there has been a surge of new methods to better quantify mitophagy, and it should become relatively easy to identify and quantify mitophagy in more physiological conditions, as well as pathologies directly connected to impairment of mitophagy. There are numerous disease states that often are accompanied with mitochondrial dysfunction. Whether mitophagy, an ultimate checkpoint in mitochondrial quality, is implicated in these disease states remains to be studied.

References

1. Bassnett, S. & Beebe, D. C. Coincident loss of mitochondria and nuclei during lens fiber cell differentiation. *Dev. Dyn.* **194**, 85-93 (1992).

2. Gronowicz, G. *et al.* Maturation of the reticulocyte *in vitro*. *J. Cell Sci.* **71**, 177-197 (1984).

3. Lang, B .F. *et al.* Mitochondrial genome evolution and the origin of eukaryotes. *Annu. Rev. Genet.* **33**, 351-397 (1999).

4. Gray, M. W. Mitochondrial evolution. *Cold Spring Harb. Perspect. Biol.* **4**, a011403 (2012).

5. Pagliarini, D. J. *et al.* A mitochondrial protein compendium elucidates complex I disease biology. *Cell* **134**, 112-123 (2008).

6. Couvillion, M. T. *et al.* Synchronized mitochondrial and cytosolic translation programs. *Nature* **533**, 499-503 (2016).

7. Horwich, A. L. *et al.* A leader peptide is sufficient to direct mitochondrial import of a chimeric protein. *EMBO J.* **4**, 1129-1135 (1985).

8. Hurt, E. C. *et al.* The cleavable prepiece of an imported mitochondrial protein is sufficient to direct cytosolic dihydrofolate reductase into the mitochondrial matrix. *FEBS Lett.* **178**, 306-310 (1984).

9. Pfanner, N. & Geissler, A. Versatility of the mitochondrial protein import machinery. *Nat. Rev. Mol. Cell Biol.* **2**, 339-349 (2001).

10. Zinser, E. *et al.* Phospholipid synthesis and lipid composition of subcellular membranes in the unicellular eukaryote Saccharomyces cerevisiae. *J. Bacteriol.* **173**, 2026-2034 (1991).

11. Davidson, J. B. & Stanacev, N. Z. Biosynthesis of cardiolipin in mitochondria isolated from guinea pig liver. *Biochem. Biophys. Res. Commun.* **42**, 1191-1199 (1971).

12. Lill, R. *et al.* The role of mitochondria in cellular iron–sulfur protein biogenesis and iron metabolism. *BBA-Mol. Cell Res.* **1823**, 1491-1508 (2012).

13. Rizzuto, R. *et al.* Mitochondria as sensors and regulators of calcium signalling. *Nat. Rev. Mol. Cell Biol.* **13**, 566-578 (2012).

14. Wang, C. & Youle, R .J. The role of mitochondria in apoptosis. *Annu. Rev. Genet.* **43**, 95-118 (2009).

15. Hailey, D. W. *et al.* Mitochondria supply membranes for autophagosome biogenesis during starvation. *Cell* **141**, 656-667 (2010).

16. Finkel, T. Signal transduction by reactive oxygen species. *J. Cell Biol.* **194**, 7-15 (2011).

17. Sundaresan, M. *et al.* Requirement for generation of H2O2 for platelet-derived growth factor signal transduction. *Science* **270**, 296-299 (1995).

18. Bae, Y. S. *et al.* Epidermal growth factor (EGF)-induced generation of hydrogen peroxide. Role in EGF receptor-mediated tyrosine phosphorylation. *J. Biol. Chem.* **272**, 217-221 (1997).

19. Brunelle, J. K. *et al.* Oxygen sensing requires mitochondrial ROS but not oxidative phosphorylation. *Cell Metab.* **1**, 409-414 (2005).

20. Guzy, R. D. *et al.* Mitochondrial complex III is required for hypoxia-induced ROS production and cellular oxygen sensing. *Cell Metab.* **1**, 401-408 (2005).

21. Mansfield, K. D. *et al.* Mitochondrial dysfunction resulting from loss of cytochrome c impairs cellular oxygen sensing and hypoxic HIF-alpha activation. *Cell Metab.***1**, 393-399 (2005).

22. Scherz-Shouval, R. *et al.* Reactive oxygen species are essential for autophagy and specifically regulate the activity of Atg4. *EMBO J.* **26**, 1749-1760 (2007).

23. Bulua, A. C. *et al.* Mitochondrial reactive oxygen species promote production of proinflammatory cytokines and are elevated in TNFR1-associated periodic syndrome (TRAPS). *J. Exp. Med.* **208**, 519-533 (2011).

24. Zhou, R. *et al*. A role for mitochondria in NLRP3 inflammasome activation. *Nature* **469**, 221-225 (2011).

25. Liu, Y. *et al.* Mitochondrial sources of H2O2 generation play a key role in flow-mediated dilation in human coronary resistance arteries. *Circ. Res.* **93**, 573-580 (2003).

26. Murphy, M. P. How mitochondria produce reactive oxygen species. *Biochem. J.* **417**, 1-13 (2009).

27. Chouchani, E. T. *et al.* Ischaemic accumulation of succinate controls reperfusion injury through mitochondrial ROS. *Nature* **515**, 431-435 (2014).

28. Marnett, L. J. Oxyradicals and DNA damage. *Carcinogenesis* **21**, 361-370 (2000).

29. Valko, M. *et al.* Role of oxygen radicals in DNA damage and cancer incidence. *Mol. Cell. Biochem.* **266**, 37-56 (2004).

30. Szatrowski, T. P. & Nathan, C. F. Production of large amounts of hydrogen peroxide by human tumor cells. *Cancer Res.* **51**, 794-798 (1991).

31. Irani, K. *et al.* Mitogenic signaling mediated by oxidants in Ras-transformed fibroblasts. *Science* **275**, 1649-1652 (1997).

32. Kumar, B. *et al.* Oxidative stress is inherent in prostate cancer cells and is required for aggressive phenotype. *Cancer Res.* **68**, 1777-1785 (2008).

33. Sarsour, E. H. *et al.* Manganese superoxide dismutase activity regulates transitions between quiescent and proliferative growth. *Aging Cell* **7**, 405-417 (2008).

34. Schulze, P. C. *et al.* Hyperglycemia promotes oxidative stress through inhibition of thioredoxin function by thioredoxin-interacting protein. *J. Biol. Chem.* **279**, 30369-30374 (2004).

35. Nishikawa, T. *et al.* Normalizing mitochondrial superoxide production blocks three pathways of hyperglycaemic damage. *Nature* **404**, 787-790 (2000).

36. Robertson, A. P. Chronic oxidative stress as a central mechanism for glucose toxicity in pancreatic islet beta cells in diabetes. *J. Biol. Chem.* **279**, 42351-42354 (2004).

37. Rudich, A. *et al.* Prolonged oxidative stress impairs insulin-induced GLUT4 translocation in 3T3-L1 adipocytes. *Diabetes* **47**, 1562-1569 (1998).

38. Haber, C. A. *et al.* N-acetylcysteine and taurine prevent hyperglycemia-induced insulin resistance *in vivo*: Possible role of oxidative stress. *Am. J. Physiol. Endocrinol. Metab.* **285**, E744-E753 (2003).

39. Jacob, S. *et al.* Oral administration of rac-α-lipoic acid modulates insulin sensitivity in patients with type-2 diabetes mellitus: A placebo-controlled pilot trial. *Free Radic. Biol. Med.* **27**, 309-314 (1999).

40. Giasson, B. I. *et al.* The relationship between oxidative/nitrative stress and pathological inclusions in Alzheimer's and Parkinson's diseases 1,2 1 2. *Free Radic. Biol. Med.* **32**, 1264-1275 (2002).

41. Ferreiro, E. *et al.* Mitochondrial- and endoplasmic reticulum-associated oxidative stress in alzheimer's disease: from pathogenesis to biomarkers. *Int. J. Cell Biol.* **2012**, 735206 (2012).

42. Dumont, M. *et al.* Mitochondrial dihydrolipoyl succinyltransferase deficiency accelerates amyloid pathology and memory deficit in a transgenic mouse

model of amyloid deposition. *Free Radic. Biol. Med.* **47**, 1019-1027 (2009).

43. Reddy, P. H. Mitochondrial oxidative damage in aging and Alzheimer's disease: implications for mitochondrially targeted antioxidant therapeutics. *J. Biomed. Biotechnol.* **2006**, 31372 (2006).

44. Ferri, A. *et al.* Familial ALS-superoxide dismutases associate with mitochondria and shift their redox potentials. *Proc. Natl. Acad. Sci. U. S. A.* **103**, 13860-13865 (2006).

45. Gandhi, S. *et al.* PINK1-associated Parkinson's disease ss caused by neuronal vulnerability to calcium-induced cell death. *Mol. Cell* **33**, 627-638 (2009).

46. Palacino, J. J. *et al.* Mitochondrial dysfunction and oxidative damage in parkin-deficient mice. *J. Biol. Chem.* **279**, 18614-18622 (2004).

47. Devi, L. *et al.* Mitochondrial import and accumulation of α-synuclein impair complex I in human dopaminergic neuronal cultures and parkinson disease brain. *J. Biol. Chem.* **283**, 9089-9100 (2008).

48. Shigenaga, M. K., Hagen, T. M. & Ames, B. N. Oxidative damage and mitochondrial decay in aging. *Proc. Natl. Acad. Sci. U.S.A.* **91**, 10771-10778 (1994).

49. Harman, D. Aging: a theory based on free radical and radiation chemistry. *J. Gerontol.* **11**, 298-300 (1956).

50. Harman, D. The biologic clock: the mitochondria? *J. Am. Geriatr. Soc.* **20**, 145-147 (1972).

51. Niemann, S. & Muller, U. Mutations in SDHC cause autosomal dominant paraganglioma, type 3. *Nat. Genet.* **26**, 268-270 (2000).

52. Pollard, P. J. *et al.* The TCA cycle and tumorigenesis: the examples of fumarate hydratase and succinate dehydrogenase. *Ann. Med.* **35**, 632-639 (2003).

53. Baysal, B. E. *et al.* Mutations in SDHD, a mitochondrial complex II gene, in hereditary paraganglioma. *Science* **287**, 848-851 (2000).

54. Hao, H. X. *et al.* SDH5, a gene required for flavination of succinate dehydrogenase, is mutated in paraganglioma. *Science* **325**, 1139-1142 (2009).

55. Mecocci, P. *et al.* Oxidative damage to mitochondrial DNA shows marked age-dependent increases in human brain. *Ann. Neurol.* **34**, 609-616 (1993).

56. Richter, C. *et al.* Normal oxidative damage to mitochondrial and nuclear DNA is extensive. *Proc. Natl. Acad. Sci. U. S. A.* **85**, 6465-6467 (1988).

57. Choksi, K. B. *et al*. Oxidatively damaged proteins of heart mitochondrial electron transport complexes. *Biochim. Biophys. Acta* **1688**, 95-101 (2004).

58. Choksi, K. B. *et al*. Age-related increases in oxidatively damaged proteins of mouse kidney mitochondrial electron transport chain complexes. *Free Radic. Biol. Med.* **43**, 1423-1438 (2007).

59. Yan, L. J. *et al.* Oxidative damage during aging targets mitochondrial aconitase. *Proc. Natl. Acad. Sci. U. S. A.* **94**, 11168-11172 (1997).

60. Cantu, D. *et al.* Oxidative inactivation of mitochondrial aconitase results in iron and H_2O_2-mediated neurotoxicity in rat primary mesencephalic cultures. *PLoS One* **4**, e7095 (2009).

61. Starkov, A. A. *et al.* Mitochondrial alpha-ketoglutarate dehydrogenase complex generates reactive oxygen species. *J. Neurosci.* **24**, 7779-7788 (2004).

62. Tretter, L. & Adam-Vizi, V. Alpha-ketoglutarate dehydrogenase: a target and generator of oxidative stress. *Philos. Trans. R. Soc. Lond., B, Biol. Sci.* **360**, 2335-2345 (2005).

63. Hermes-Lima, M. *et al.* Characteristics of Fe(II)ATP complex-induced damage to the rat liver mitochondrial membrane. *Mol. Cell. Biochem.* **145**, 53-60 (1995).

64. Castilho, R. F. *et al.* Oxidative damage of mitochondria induced by Fe(II)citrate is potentiated by Ca2+ and includes lipid peroxidation and alterations in membrane proteins. *Arch. Biochem. Biophys.* **308**, 158-163 (1994).

65. Echtay, K. S. *et al.* Superoxide activates mitochondrial uncoupling proteins. *Nature* **415**, 96-99 (2002).

66. Radi, R. *et al.* Detection of catalase in rat heart mitochondria. *J. Biol. Chem.* **266**, 22028-22034 (1991).

67. Chang, T. S. *et al.* Peroxiredoxin III, a mitochondrion-specific peroxidase, regulates apoptotic signaling by mitochondria. *J. Biol. Chem.* **279**, 41975-41984 (2004).

68. Arnér, E. S. J. & Holmgren, A. Physiological functions of thioredoxin and thioredoxin reductase. *Eur. J. Biochem.* **267**, 6102-6109 (2000).

69. Rabilloud, T. *et al.* The mitochondrial antioxidant defence system and its response to oxidative stress. *Proteomics* **1**, 1105-1110 (2001).

70. Masella, R. *et al.* Novel mechanisms of natural antioxidant compounds in biological systems: involvement of glutathione and glutathione-related enzymes. *J. Nutr. Biochem.* **16**, 577-586 (2005).

71. Bulteau, A. L. *et al.* Mitochondrial protein oxidation and degradation in response to oxidative stress and aging. *Exp. Gerontol.* **41**, 653-657 (2006).

72. Käser, M. & Langer, T. Protein degradation in mitochondria. *Semin. Cell Dev. Biol.* **11**, 181-190 (2000).

73. Van Dyck, L. & Langer, T. ATP-dependent proteases controlling mitochondrial function in the yeast Saccharomyces cerevisiae. *Cell. Mol. Life Sci.* **56**, 825-842 (1999).

74. Bota, D. A. & Davies, K .J. A. Lon protease preferentially degrades oxidized mitochondrial aconitase by an ATP-stimulated mechanism. *Nat. Cell Biol.* **4**, 674-680 (2002).

75. Quiros, P. M. *et al.* New roles for mitochondrial proteases in health, ageing and disease. *Nat. Rev. Mol. Cell Biol.* **16**, 345-359 (2015).

76. Bota, D. A. *et al.* Downregulation of the human Lon protease impairs mitochondrial structure and function and causes cell death. *Free Radic. Biol. Med.* **38**, 665-677 (2005).

77. Neuspiel, M. *et al.* Cargo-selected transport from the mitochondria to peroxisomes is mediated by vesicular carriers. *Curr. Biol.* **18**, 102-108 (2008).

78. Soubannier, V. *et al.* A vesicular transport pathway shuttles cargo from mitochondria to lysosomes. *Curr. Biol.* **22**, 135-141 (2012).

79. Soubannier, V. *et al.* Reconstitution of mitochondria derived vesicle formation demonstrates selective enrichment of oxidized cargo. *PLoS One* **7**, e52830 (2012).

80. McLelland, G. L. *et al.* Parkin and PINK1 function in a vesicular trafficking pathway regulating mitochondrial quality control. *EMBO J.* (2014).

81. Hughes, A. L. *et al.* Selective sorting and destruction of mitochondrial membrane proteins in aged yeast. *eLife* **5**, e13943 (2016).

82. Lamb, C. A. *et al.* The autophagosome: origins unknown, biogenesis complex. *Nat. Rev. Mol. Cell Biol.* **14**, 759-774 (2013).

83. Ashford, T. P. & Porter, K. R. Cytoplasmic components in hepatic cell lysosomes. *J. Cell Biol.* **12**, 198-202 (1962).

84. Gomes, L. C. *et al.* During autophagy mitochondria elongate, are spared from degradation and sustain cell viability. *Nat. Cell Biol.* **13**, 589-598 (2011).

85. Ashrafi, G. & Schwarz, T. L. The pathways of mitophagy for quality control and clearance of mitochondria. *Cell Death Differ.* **20**, 31-42 (2013).

86. Kanki, T. *et al.* Atg32 is a mitochondrial protein that confers selectivity during mitophagy. *Dev. Cell* **17**, 98-109 (2009).

87. Mao, K. *et al.* The scaffold protein Atg11 recruits fission machinery to drive selective mitochondria degradation by autophagy. *Dev. Cell* **26**, 9-18 (2013).

88. Otsu, K. *et al.* BCL2L13 is a mammalian homolog of the yeast mitophagy receptor Atg32. *Autophagy* **11**, 1932-1933 (2015).

89. Murakawa, T. *et al.* Bcl-2-like protein 13 is a mammalian Atg32 homologue that mediates mitophagy and mitochondrial fragmentation. *Nat. Commun.* **6**, 7527 (2015).

90. Kanki, T. & Klionsky, D. J. Mitophagy in yeast occurs through a selective mechanism. *J. Biol. Chem.* **283**, 32386-32393 (2008).

91. Clark, I. E. *et al.* Drosophila PINK1 is required for mitochondrial function and interacts genetically with Parkin. *Nature* **441**, 1162-1166 (2006).

92. Park, J. *et al.* Mitochondrial dysfunction in Drosophila PINK1 mutants is complemented by Parkin. *Nature* **441**, 1157-1161 (2006).

93. Narendra, D. *et al.* Parkin is recruited selectively to impaired mitochondria and promotes their autophagy. *J. Cell Biol.* **183**, 795-803 (2008).

94. Greene, A. W. *et al.* Mitochondrial processing peptidase regulates PINK1 processing, import and Parkin recruitment. *EMBO Rep.* **13**, 378-385 (2012).

95. Youle, R. J. & Narendra, D. P. Mechanisms of mitophagy. *Nat. Rev. Mol. Cell Biol.* **12**, 9-14 (2011).

96. Sarraf, S. A. *et al.* Landscape of the Parkin-dependent ubiquitylome in response to mitochondrial depolarization. *Nature* **496**, 372-376 (2013).

97. Chan, N. C. *et al.* Broad activation of the ubiquitin–proteasome system by Parkin is critical for mitophagy. *Hum. Mol. Gen.* (2011).

98. Okatsu, K. *et al.* PINK1 autophosphorylation upon membrane potential dissipation is essential for Parkin recruitment to damaged mitochondria. *Nat. Commun.* **3**, 1016 (2012).

99. Shiba-Fukushima, K. *et al.* PINK1-mediated phosphorylation of the Parkin ubiquitin-like domain primes mitochondrial translocation of Parkin and regulates mitophagy. *Sci. Rep.* **2**, 1002 (2012).

100. Koyano, F. *et al.* Ubiquitin is phosphorylated by PINK1 to activate parkin. *Nature* **510, 162–166** (2014).

101. Wong, Y. C. & Holzbaur, E. L. F. Optineurin is an autophagy receptor for damaged mitochondria in Parkin-mediated mitophagy that is disrupted by an ALS-linked mutation. *Proc. Natl. Acad. Sci. U.S.A.* **111**, E4439-E4448 (2014).

102. Lazarou, M. *et al.* The ubiquitin kinase PINK1 recruits autophagy receptors to induce mitophagy. *Nature* **524**, 309-314 (2015).

103. Geisler, S. *et al.* PINK1/Parkin-mediated mitophagy is dependent on VDAC1 and p62/SQSTM1. *Nat. Cell. Biol*.**12**, 119-131 (2010).

104. Zhang, J. & Ney, P. A. Role of BNIP3 and NIX in cell death, autophagy, and mitophagy. *Cell Death Differ.* **16**, 939-946 (2009).

105. Hanna, R. A. *et al.* Microtubule-associated protein 1 light chain 3 (LC3) interacts with Bnip3 protein to selectively remove endoplasmic reticulum and mitochondria via autophagy. *J. Biol. Chem.* **287**, 19094-19104 (2012).

106. Shi, R. Y. *et al.* BNIP3 Interacting with LC3 triggers excessive mitophagy in delayed neuronal death in stroke. *CNS Neurosci. Ther.* **20**, 1045-1055 (2014).

107. Schweers, R. L. *et al.* NIX is required for programmed mitochondrial clearance during reticulocyte maturation. *Proc. Natl. Acad. Sci. U.S.A.* **104**, 19500-19505 (2007).

108. Novak, I. *et al.* Nix is a selective autophagy receptor for mitochondrial clearance. *EMBO Rep.* **11**, 45-51 (2010).

109. Band, M. *et al.* Hypoxia-induced BNIP3 expression and mitophagy: *in vivo* comparison of the rat and the hypoxia-tolerant mole rat, Spalax ehrenbergi. *FASEB J.* **23**, 2327-2335 (2009).

110. Bellot, G. *et al.* Hypoxia-Induced autophagy is mediated through Hypoxia-inducible factor induction of BNIP3 and BNIP3L via their BH3 domains. *Mol. Cell. Biol.* **29**, 2570-2581 (2009).

111. Glick, D. *et al.* Bnip3 regulates mitochondrial function and lipid metabolism in the liver. *Mol. Cell. Biol.* **32**, 2570-2584 (2012).

112. Zhu, Y. *et al.* Modulation of serines 17 and 24 in the LC3-interacting region of Bnip3 determines pro-survival mitophagy versus apoptosis. *J. Biol. Chem.* **288**, 1099-1113 (2013).

113. Liu, L. *et al.* Mitochondrial outer-membrane protein FUNDC1 mediates hypoxia-induced mitophagy in mammalian cells. *Nat. Cell Biol.* **14**, 177-185 (2012).

114. Chen, G. *et al.* A regulatory signaling loop comprising the PGAM5 phosphatase and CK2 controls receptor-mediated mitophagy. *Mol. Cell* **54**, 362-377 (2014).

115. Wu, W. *et al.* ULK1 translocates to mitochondria and phosphorylates FUNDC1 to regulate mitophagy. *EMBO Rep.* **15**, 566-575 (2014).

116. Li, W. *et al.* MicroRNA-137 is a novel hypoxia-responsive microRNA that inhibits mitophagy via regulation of two mitophagy receptors FUNDC1 and NIX. *J. Biol. Chem.* **289**, 10691-10701 (2014).

117. Chu, C. T. *et al.* Cardiolipin externalization to the outer mitochondrial membrane acts as an elimination signal for mitophagy in neuronal cells. *Nat. Cell Biol.* **15**, 1197-1205 (2013).

118. Kagan, V. E. *et al.* NDPK-D (NM23-H4)-mediated externalization of cardiolipin enables elimination of depolarized mitochondria by mitophagy. *Cell. Death. Differ.* **23**, 1140-1151 (2016).

119. Melser, S. *et al.* Rheb regulates mitophagy induced by mitochondrial energetic status. *Cell Metab.* **17**, 719-730 (2013).

120. Miwa, S. *et al.* Mitochondrial turnover in liver is fast *in vivo* and is accelerated by dietary restriction: application of a simple dynamic model. *Aging Cell* **7**, 920-923 (2008).

121. Chan, X. a. C. Y. *et al.* Mitochondrial protein turnover: methods to measure turnover rates on a large scale. *J. Mol. Cell. Cardiol.* **78**, 54-61 (2015).

122. Lipsky, N. G. & Pedersen, P. L. Mitochondrial turnover in animal cells. Half-lives of mitochondria and mitochondrial subfractions of rat liver based on [14C]bicarbonate incorporation. *J. Biol. Chem.* **256**, 8652-8657 (1981).

123. Rakovic, A. *et al.* Phosphatase and Tensin Homolog (PTEN)-induced Putative Kinase 1 (PINK1)-dependent ubiquitination of endogenous Parkin attenuates mitophagy: study in human primary fibroblasts and induced pluripotent stem cell-derived neurons. *J. Biol. Chem.* **288**, 2223-2237

(2013).

124. Van Laar, V. S. *et al.* Bioenergetics of neurons inhibit the translocation response of Parkin following rapid mitochondrial depolarization. *Hum. Mol. Gen.* **20**, 927-940 (2011).

CHAPTER 2

RAPID PARALLEL MEASUREMENTS OF MACROAUTOPHAGY AND MITOPHAGY IN MAMMALIAN CELLS USING A SINGLE FLUORESCENT BIOSENSOR

From A. Sargsyan, J. Cai, L. B. Fandino, M. E. Labasky, T. Forostyan, L. K. Colosimo, S. J. Thompson, T. E. Graham. Rapid parallel measurements of macroautophagy and mitophagy in mammalian cells using a single fluorescent biosensor. Scientific Reports 5, 12397.
Copyright 2015 the authors, used with permission

www.nature.com/scientificreports

SCIENTIFIC REPORTS

OPEN

Rapid parallel measurements of macroautophagy and mitophagy in mammalian cells using a single fluorescent biosensor

Received: 31 March 2015
Accepted: 22 June 2015
Published: 28 July 2015

A. Sargsyan[1,2], J. Cai[1], L. B. Fandino[1], M. E. Labasky[1], T. Forostyan[1,3], L. K. Colosimo[1], S. J. Thompson[1] & T. E. Graham[1,2]

Mitochondrial dysfunction is implicated in many human diseases and occurs in normal aging. Mitochondrial health is maintained through organelle biogenesis and repair or turnover of existing mitochondria. Mitochondrial turnover is principally mediated by mitophagy, the trafficking of damaged mitochondria to lysosomes via macroautophagy (autophagy). Mitophagy requires autophagy, but is itself a selective process that relies on specific autophagy-targeting mechanisms, and thus can be dissociated from autophagy under certain circumstances. Therefore, it is important to assess autophagy and mitophagy together and separately. We sought to develop a robust, high-throughput, quantitative method for monitoring both processes in parallel. Here we report a flow cytometry-based assay capable of rapid parallel measurements of mitophagy and autophagy in mammalian cells using a single fluorescent protein biosensor. We demonstrate the ability of the assay to quantify Parkin-dependent selective mitophagy in CCCP-treated HeLa cells. In addition, we show the utility of the assay for measuring mitophagy in other cell lines, as well as for Parkin-independent mitophagy stimulated by deferiprone. The assay makes rapid measurements (10,000 cells per 6 seconds) and can be combined with other fluorescent indicators to monitor distinct cell populations, enabling design of high-throughput screening experiments to identify novel regulators of mitophagy in mammalian cells.

Mitochondria perform diverse cellular functions, including energy production, intermediary metabolism, and calcium and apoptosis regulation. Mitochondrial dysfunction, characterized by impaired oxidative phosphorylation and excessive production of reactive oxygen species (ROS), contributes to many human diseases[1–5]. Mitochondrial ROS regulate normal cellular functions and stress responses[6]; however, excessive ROS production can damage proteins, lipids, and other cellular components, including mitochondria themselves[7], leading to further worsening of mitochondrial dysfunction. Mitochondria possess several quality control mechanisms to counteract damage and maintain functionality[8–10]. Important among these is mitophagy, the trafficking of intact mitochondria or mitochondrial fission products via autophagy to lysosomes where they are degraded. Mitophagy is also required for developmental processes that require mitochondrial clearance, such as destruction of paternal mitochondria in oocytes after fertilization[11] and maturation of erythrocytes[12], eye lens epithelium[13], and adipocytes[14]. Perturbations in mitophagy have been implicated in heart disease[15–17], neurodegeneration[18–20], metabolic syndrome, diabetes[21,22] and

[1]Molecular Medicine Program and Division of Endocrinology, Metabolism & Diabetes, Department of Medicine, University of Utah, Salt Lake City, UT, USA 84112. [2]Department of Biochemistry, University of Utah,Salt Lake City, UT, USA 84112. [3]Department of Oncological Sciences, University of Utah, Salt Lake City, UT, USA 84112. Correspondence and requests for materials should be addressed to T.E.G. (email: tgraham@u2m2.utah.edu)

cancer[23,24]. Impairment of autophagy or mitophagy drastically alters mitochondrial function and cell fate in many cell types, indicating the importance of these pathways.

Mitophagy requires intact autophagy; however, induction of autophagy alone is not sufficient for mitophagy to occur. Increasing evidence indicates that mitophagy is a highly selective process. Whether or not individual mitochondria are trafficked into the autophagy pathway depends on factors such as mitochondrial membrane potential and display of certain proteins or lipids in the mitochondrial outer membrane that act as molecular adaptors to engage mitochondria with nascent autophagasome membranes[25–29]. These molecular cues are capable of relaying the integrity and functional state of individual mitochondria, such that damaged or impaired mitochondria are targeted for destruction and functional mitochondria are preserved. Similar mechanisms also appear to coordinate induction of mitophagy during development in certain cell types. Therefore, when assessing potential mechanisms involved in regulating mitophagy, there is value in assessing the states of both autophagy and mitophagy, together and separately.

HeLa cervical carcinoma cells treated with carbonyl cyanide m-chlorophenylhydrazone (CCCP) are a widely studied model of selective mitophagy. CCCP uncouples the electron transport chain and causes varying degrees of mitochondrial inner membrane depolarization. In most cells, CCCP induces generalized autophagy[30,31], along with mitophagy that selectively targets depolarized mitochondria for destruction[32]. Activation of the Parkin E3 ubiquitin ligase, initiated by Pink1 stabilization on depolarized mitochondria, is a proposed mechanism for selectivity in this process[33]. HeLa are particularly noteworthy as a model for Parkin-dependent selective mitophagy because they do not express endogenous Parkin, making it possible to assess the requirement for Parkin by expressing it ectopically[34].

We sought to employ the CCCP-treated HeLa cell as a model for developing an assay capable of rapid, highly quantitative parallel measurements of autophagy and mitophagy, with the long term goal of enabling high throughput screens for regulators of mitophagy in mammalian cells. The Rosella biosensor has been used to measure mitophagy in yeast[35,36]. Rosella is a chimera of two tandem fluorescent proteins: pHluorin a pH-sensitive green fluorescent protein[37], and dsRed.T3[38], a non-pH-sensitive red fluorescent protein (Fig. 1A). Attaching Rosella to specific cellular 'cargos' makes it possible to monitor their separate delivery to the acidic compartments of lysosomes via autophagy. We hypothesized that Rosella-LC3 and Mito-Rosella could be used together for simultaneous measurement of autophagy and mitophagy in a single parallel assay capable of demonstrating the requirement for Parkin in selective mitophagy in CCCP-treated HeLa cells. Here we report the performance characteristics of Rosella-LC3 and Mito-Rosella biosensors in single-cell and flow cytometry (FCM)-based parallel autophagy/mitophagy assays, and describe the potential of this method for conducting rapid, high-throughput assays in human cells.

Results

Mito-Rosella localization and pH-dependence. Transiently transfected Mito-Rosella specifically and completely labeled mitochondria (Fig. 1B), whereas Rosella lacking a targeting sequence showed diffuse localization (Suppl. Fig. 1). Rosella green fluorescence was reduced 70% without affecting red fluorescence when culture media pH was reduced to 5.0, and recovered rapidly with return to pH 7.4. (Fig. 1C,D). Expression of Rosela-LC3 or Mito-Rosella did not alter the dynamics or extent of mitophagy and autophagy compared to control transfection, as measured by Western blot analysis of mitochondrial markers (Suppl. Fig. 2A) and endogenous LC3 lipidation (Suppl. Fig. 2B).

CCCP-induced redistribution of Rosella-LC3 and Mito-Rosella to lysosomal compartments. Vehicle (DMSO)-treated HeLa cells expressing Rosella-LC3 exhibited dual-labeled green/red puncta throughout the cytoplasm, consistent with the characteristic appearance of autolysosomes (Fig. 1E, i–iv). In cells treated with CCCP (10 μM), red-only vesicles were present at 6 hr after treatment (Fig. 1E, v–viii) and increased in number at 24 hr after treatment (Fig. 1E, ix–xii). Vehicle-treated HeLa cells co-expressing Mito-Rosella and Parkin exhibited dual-labeled green/red mitochondria throughout the cytoplasm (Fig. 1E, xiii–xvi). Treatment with CCCP resulted in appearance of Mito-Rosella in red-only vesicles, indicative of redistribution to acidic lysosomal compartments, located in the cytoplasm at 6 hr after treatment (Fig. 1E, xvii–xx), and accumulating near the perinuclear lysosomal compartments at 24 hr after treatment (Fig. 1E, xxi–xxiv).

Parkin-dependent selective mitophagy demonstrated by differential responses of Rosella-LC3 and mito-Rosella. To demonstrate the dependence of mitophagy on Parkin expression in CCCP-treated HeLa cells, we analyzed autophagy (*i.e.,* LC3-Rosella) and mitophagy (*i.e.,* Mito-Rosella) responses in the presence or absence of co-expressed Parkin. HeLa cells transiently transfected with Rosella-LC3 were treated with vehicle (DMSO) or CCCP for 24 hr. In vehicle-treated cells, Rosella-LC3 produced primarily dual-labeled green/red autophagic puncta (Fig. 2A, i–iii), while CCCP treatment induced large perinuclear accumulations of red-only LC3, indicating redistribution of autophagasomes to low pH lysosomal compartments (Fig. 2A, iv–vi). Treatment with Bafilomycin-A1 (BafA1), an inhibitor of the lysosomal V-ATPase that maintains lysosome pH, caused accumulation of dually labeled green/red LC3 puncta (Fig. 2A, vii–ix), indicative of autophagasomes or autolysosomes collecting under conditions

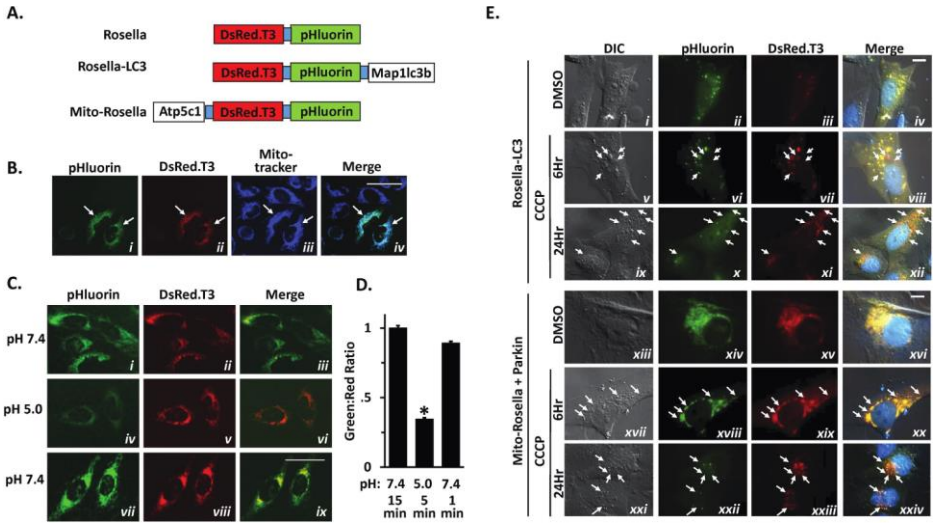

Figure 1. Rosella pH-responsive fluorescent biosensors. (**A**) Schematic representation of Rosella, Rosella-LC3, and Mito-Rosella fluorescent protein biosensor constructs. Rosella (top) is a chimeric protein containing the pH-stable DsRed.T3 red fluorescent protein and the pH-sensitive pHluorin green fluorescent protein. Rosella-LC3 (middle) consists of the complete open reading frame (ORF) of human LC3B (Map1lc3b) joined in-frame with the 3′ end of the Rosella ORF (coding the C-terminus) without a stop codon. Mito-Rosella (bottom) consists of the complete human ATP synthase subunit gamma (Atp5c1) ORF without a stop codon fused in-frame with the 5′ end of the Rosella ORF (coding the N-terminus). (**B**) Representative micrographs of HeLa cells transiently transfected with expression plasmids for Mito-Rosella and treated with Mitotracker Deep Red FM to image mitochondria independently of Rosella. The merged panel shows overlap of fluorescence from the green, red, and far-red channels in two cells expressing Mito-Rosella (white arrows). (**C**) Representative micrographs of green and red channel fluorescence of Mito-Rosella in cells subjected to sequential incubations in culture media adjusted to pH 7.4 (for 15 min; starting point), pH 5.0 (for 5 min), and then pH 7.4 again (for 1 min). (**D**) Quantification of green to red fluorescence ratios measured in single cells subjected to pH changes described above for (**C**). Bars represent mean ± SEM of ratios for n = 50–60 cells per condition. $^*p < 0.05$, based on unpaired T-test. For panels B and C: scale bars indicate a length of 50 μm. (**E**) Representative widefield micrographs of HeLa cells transiently transfected with expression plasmids for Rosella-LC3 (panels i to xii) and Mito-Rosella (panels xiii to xxiv) with Parkin, treated with CCCP (10 μM) or vehicle for 6 and 24 hr. In merged images arrows represent acidified Rosella-LC3 (panels viii and xii) and acidified Mito-Rosella (panels xx and xxiv). DIC, differential interference contrast microscopy. Scale bars indicate a length of 10 μm.

of impaired lysosome acidification. Co-expressing Parkin did not alter the number, size or localization pattern of LC3-containing structures, relative to control cells under the same conditions (Fig 2A, x–xviii).

In vehicle-treated cells transfected with Mito-Rosella, mitochondria were primarily dual-labeled green/red and exhibited normal cytosolic localization (Fig. 2B, i–iii). CCCP treatment (10 μM, 24 hr) did not alter mitochondrial fluorescence or localization in control cells (Fig. 2B, iv–vi). In cells expressing Parkin, CCCP induced redistribution and accumulation of red-only mitochondria near the central lysosomal compartments (Fig. 2B, xiii–xv) in a BafA1-dependent manner (Fig. 2B, xvi–xviii). Therefore, LC3-Rosella and Mito-Rosella responses replicate prior observations that autophagy occurs in a Parkin-independent manner whereas mitophagy occurs in a selective, Parkin-dependent manner in CCCP-treated HeLa cells.

Autophagy and mitophagy were quantified in single cells by blinded scoring of Rosella-LC3 and Mito-Rosella responses, respectively. CCCP induced autophagy in 11.2 ± 2.6% of cells at 6 hr (vs. 2.4 ± 1.0% in CCCP + BafA1-treated cells, $p < 0.05$, Fig. 2C) and 67.5 ± 2.2% of cells at 24 hr (vs. 4.0 ± 1.4% in CCCP + BafA1-treated cells, $p < 10^{-8}$, Fig. 2C). Interestingly, cells in vehicle-treated media exhibited increased autophagy after 24 hr (17 ± 1.4% vs. 1.4 ± 0.9% baseline, $p < 0.001$, Fig. 2C), though to a much

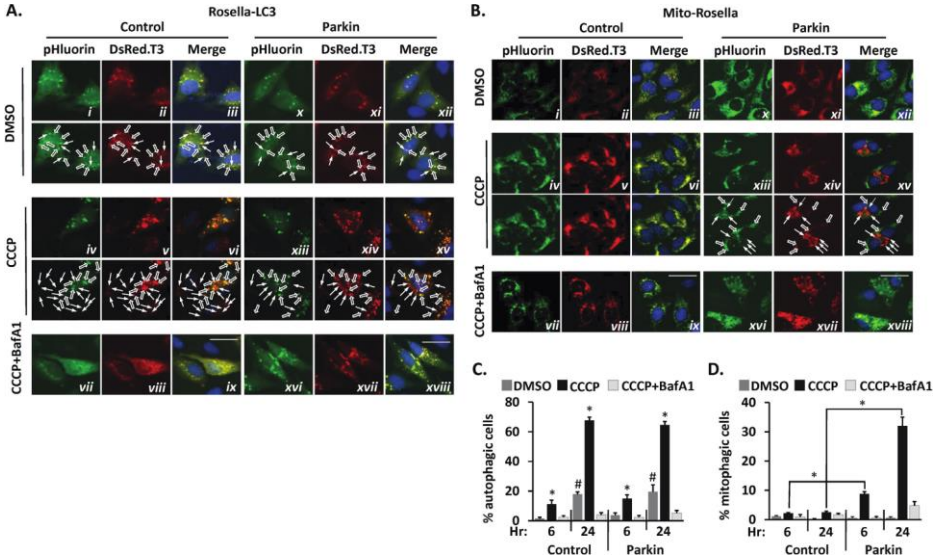

Figure 2. Single-cell measurements of autophagy and mitophagy based on biosensor responses to CCCP treatment. (**A**) Representative micrographs of HeLa cells transiently co-transfected with Rosella-LC3 expression plasmid plus Parkin expression plasmid or 'empty' plasmid (Control). Cells were treated for 24 hr with: Vehicle alone (DMSO), CCCP (10 μM), or CCCP (10 μM) + lysosomal inhibitor Bafilomycin-A1 (BafA1, 100 nM). CCCP-treated cells displayed accumulation of primarily red Rosella-LC3 fluorescence near the central lysosomal compartments (solid arrows in identical, labeled panels below panels vi and xv), while vehicle treated cells primarily display co-localization between red and green signals (hollow arrows in identical, labeled panels below panels iii and xii). Co-treatment with BafA1 (panels ix and xviii) prevented CCCP-induced relocation of Rosella-LC3 to the central lysosomal compartment, causing it to accumulate in autophagasomes within the cytoplasm (panels ix and xviii). (**B**) Representative micrographs of HeLa cells co-transfected with Mito-Rosella plus either Parkin or Control plasmids, and treated exactly as described above for (A). CCCP treatment caused an accumulation of red-only Mito-Rosella-labeled mitochondria in the central lysosomal compartments in Parkin co-transfected cells but not in control cells (solid arrows in identical, labeled panel below panel xv), and this was inhibited by BafA1 treatment (panel xviii). In contrast, DMSO-treated Parkin-expressing cells (panel xii) and control cells treated with vehicle (DMSO) or CCCP (panels iii and vi), there is a complete co-localization of green/red fluorescence. Quantification of percentage of cells exhibiting induction of (**C**) autophagy or (**D**) mitophagy, as determined by categorizing individual cells on the basis of presence/absence of visible accumulations of red biosensor fluorescence in the lysosomal compartments as in (A) and (B) above. For panels C and D: bars represent mean ± SEM of percentages of cells from n = 4 biological replicates, with >120 cells categorized per replicate. For panels A and B: scale bars indicate a length of 25 μm. For panel C: $^{*}p < 0.05$ vs. DMSO treated cells at the same time-point; and $^{\#}p < 0.05$ vs. 6 hr time-point by unpaired T-test. For panel D: $^{*}p < 0.05$ by unpaired T-test for the indicated comparisons between cells co-transfected with Parkin vs. Control plasmid.

lesser extent than CCCP treatment. Co-expression of Parkin did not alter the autophagic response in vehicle or CCCP-treated cells (p = NS for LC3-Rosella alone vs. LC3-Rosella co-expressed with Parkin at 6 or 24 hr time-points after treatment, Fig. 2C). In cells expressing Mito-Rosella, CCCP-induced mitophagy solely in cells co-expressing Parkin (8.8 ± 0.8% with Parkin vs. 2.2 ± 0.2% without Parkin at 6 hr, $p < 0.001$; and 32 ± 3.0% with Parkin vs. 2.5 ± 0.4% without Parkin at 24 hr, $p < 10^{-4}$, Fig. 2D).

Flow-cytometry based parallel analyses of autophagy and mitophagy using Rosella biosensors. The robust Rosella biosensor responses observed in single cell measurements suggested they could be adapted for flow cytometry (FCM)-based assays, which are capable of making rapid, highly-quantitative measurements. We measured effects of CCCP treatment in cells transfected with

Rosella-LC3 or Mito-Rosella and Parkin, using standard FCM methods. In cells expressing Rosella-LC3, CCCP induced a BafA1-sensitive reduction in green fluorescence (green-shift) indicating induction of autophagy (detected in $34.3 \pm 1.2\%$, $44.3 \pm 0.6\%$, and $60.0 \pm 1.9\%$ of cells measured at 6, 12 or 24 hr, respectively; Fig 3A,C). In cells expressing Mito-Rosella with Parkin, CCCP also induced a BafA1-sensitive green-shift indicating mitophagy (detected in $25 \pm 0.2\%$, 49.8 ± 1.8 and $59.4 \pm 1.3\%$ of cells measured at 6, 12, or 24 hr after treatment, respectively; $p < 10^{-4}$ vs. cells treated with CCCP + BafA1 for each of the three time-points; Fig. 3B,D). These responses correlated with Western blot analysis of LC3 processing (Fig. 3D) and disappearance of mitochondrial markers (Fig. 3F).

A spectrally distinct fluorescent population marker (iRFP) can be used in screens to assess regulators of autophagy/mitophagy. High-throughput screens utilizing DNA or RNA expression libraries frequently employ fluorescent proteins to monitor transfection/transduction efficiencies as a means of improving signal-to-noise ratio. Since standard FCM instruments measure several fluorescent channels simultaneously, we tested whether a third fluorescent marker could be used in conjunction with green/red Rosella biosensors to monitor responses selectively in transfected cells only. To test this, we transiently transfected Parkin coupled via a T2A sequence[39] to near-infrared fluorescent protein[40] (iRFP) in cells stably expressing Mito-Rosella (Fig. 3G). Transient transfection efficiencies in HeLa are ~60–70%, so that a significant number of cells go untransfected under these conditions. The FCM analysis was gated for iRFP fluorescence as the indicator of Parkin expression (Suppl. Fig. 5). Cells expressing Parkin (60% the total population) exhibited robust CCCP-induced mitophagy, whereas untransfected cells showed no mitophagy (Fig. 3H). Therefore, use of a spectrally distinct fluorescent marker in conjunction with Rosella enables robust analysis even under imperfect transfection/transduction conditions.

Characteristics of Rosella-based flow cytometry parallel autophagy/mitophagy assay in HeLa cells. We performed additional studies to characterize the performance of the FCM assay for mitophagy. We determined the sensitivity of the assay for detecting CCCP-induced mitophagy at earlier time-points. As shown in Suppl. Fig. 3A, a statistically significant increase in mitophagy was detected at 2 hr after treatment with CCCP ($7.4 \pm 0.4\%$ vs. $5.4 \pm 0.3\%$ for CCCP + BafA1 treatment, $p < 0.01$). We also compared the efficiency of Parkin translocation to mitochondria at 6 and 24 hr after treatment with 10 μM CCCP. As expected, there was extensive translocation of Parkin to mitochondria at 6 and 24 hr ($70.1 \pm 2.3\%$ and $95.4 \pm 1.7\%$, respectively). The percentage of cells displaying mitophagy at these time-points (Fig. 3D) is less than the percentage displaying Parkin translocation (Suppl. Fig. 3B), which agrees with prior observations that Parkin translocation to mitochondria occurs more rapidly and efficiently than mitochondrial clearance by mitophagy in CCCP-treated HeLa cells[32]. However, rates of mitophagy in the HeLa model can be increased by treatment with higher concentrations of CCCP, as a dose-response study showed 20 μM CCCP induced greater mitophagy than the 10 μM concentration used in our studies (Suppl. Fig. 3C). To determine whether the relative amount of Mito-Rosella expression alters measurements of rates of mitophagy, we studied cells co-transfected with a fixed amount of Parkin and varying amounts of Mito-Rosella. As shown in Suppl. Fig. 3D, there is no significant difference in the quantities of CCCP-induced mitophagy measured over a 3-fold range of transfected Mito-Rosella.

It has been reported that under certain conditions, CCCP may directly alter lysosomal function[41]. Since the FCM-based Rosella method relies on acidification of lysosomes to detect delivery of autophagic cargo, we tested whether CCCP treatment alters lysosome acidity in our model. As shown in Suppl. Fig. 4A,B, there were no changes in lysosome acidification induced by CCCP under the conditions of our experiments, as measured by Lysotracker red uptake. Since CCCP-induced, Parkin-dependent mitophagy relies on depolarization of mitochondria, we also tested the efficiency of CCCP in depolarizing mitochondria in our model. As shown in Suppl. Fig. 4C–D, CCCP induced substantial depolarization of mitochondria at 6, 12, and 24 hr after treatment, as measured by uptake of the membrane potentiometric dye TMRE. Interestingly, at 24 hr after treatment with CCCP, a partial recovery of mitochondrial membrane potential was evident (74.4% depolarization at 24 hr vs. 94.4% and 91.6% at 6 and 12 hr, respectively), which could potentially affect the maximal rates of mitophagy measured at 24 hr in this model.

To determine the utility of the Mito-Rosella-based assay for measuring mitophagy induced by other stimuli, we tested its ability to quantify mitophagy in HeLa cells treated with the iron chelator, 3-Hydroxy-1,2-dimethyl-4(1H)-pyridone (deferiprone, or DFP), which is reported to induce mitophagy independently of Parkin[42]. As shown in Fig. 4A–C, treatment of HeLa cells expressing Mito-Rosella (without Parkin) with DFP (1 mM) induced mitophagy at 12 and 24 hr after treatment (Fig. 4A,B). The induction of mitophagy by DFP correlated with Western blot analysis showing a decrease in mitochondrial markers (Fig. 4C). We also tested the ability of the Rosella-based mitophagy assay to quantify mitophagy in other cell types beside HeLa. As shown in Fig. 4D,E, the assay readily detects mitophagy in CCCP-treated HEK-293 kidney epithelial cells, which are known to express endogenous Parkin[31,32,43,44], as well as in CCCP treated HCT-116 colorectal carcinoma cells co-transfected with Parkin. In addition, the Mito-Rosella-based assay exhibits similar capacity to measure mitophagy in HepG2 hepatocarcinoma cells, H9C2 cardiomyocytes, and bovine aortic endothelial cells (*data not shown*).

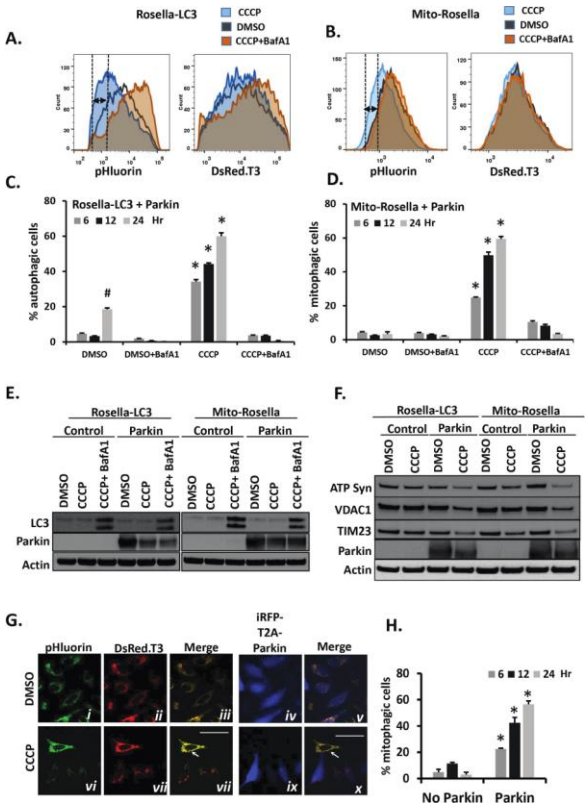

Figure 3. Parallel quantification of autophagy and mitophagy under the same conditions by flow cytometry (FCM) measurement of biosensor responses. Representative histograms of pHluorin/green and DsRed.T3/red fluorescence intensities of HeLa cells transiently transfected with plasmids expressing (**A**) Rosella-LC3 and Parkin, or (**B**) Mito-Rosella and Parkin, and treated for 24 hr with: DMSO (vehicle), CCCP (10 μM), or CCCP (10 μM) + Baf1A (100 nM); histograms depict intensities of n = 10,000 cells per condition. CCCP induced a significant reduction (dashed lines and arrow) in pHluorin/green fluorescence but not in DsRed.T3/red fluorescence of both Rosella-LC3 and Mito-Rosella. Quantitation of cells with (**C**) increased autophagy or (**D**) increased mitophagy based on detection of changes in green vs. red fluorescence intensities in gated FCM scattergram analysis (see also Suppl. Fig. 5A–B); bars represent means of 3 biological replicates ± SEM, N = 10,000 cells analyzed per replicate; $^{*}p < 0.001$ vs. CCCP + BafA1; $^{\#}p < 0.001$ vs. DMSO at 6 time-point (see also Suppl. Fig. 5A–B). (**E**) Western blots of LC3 processing in cells co-transfected with Rosella biosensors plus Parkin or Control plasmids and treated 24 hr as indicated. (**F**) Western blots of mitochondrial markers in cells co-transfected with plasmids for each of the Rosella biosensors plus Parkin or Control plasmid. (**G**) Representative micrographs of HeLa cells stably expressing Mito-Rosella and transiently transfected with a bicistronic iRFP-T2A-Parkin expression plasmid; iRFP fluorescence was readily visualized and exhibited a diffuse localization in successfully transfected cells (panels iv and ix). As expected, DMSO did not induce mitophagy in cells expressing Parkin (iRFP positive cells; panels iii–v). Consistent with our other findings, CCCP treatment did not induce mitophagy in iRFP-negative cells lacking Parkin (panels vi–x, solid white arrow), but induced mitophagy in iRFP-positive cells expressing Parkin (panels viii–x). (**H**) FCM analysis was used to demonstrate the requirement of Parkin expression for CCCP-induced mitophagy. Cells stably expressing Mito-Rosella and transiently transfected with iRFP-T2A-Pakin were first gated according to negative vs. positive iRFP-fluorescence (*i.e.,* No Parkin vs. Parkin expression, respectively), and then analyzed separately to detect mitophagic cells (see Suppl. Fig. 5D), using the same method described for Fig. 3C,D.

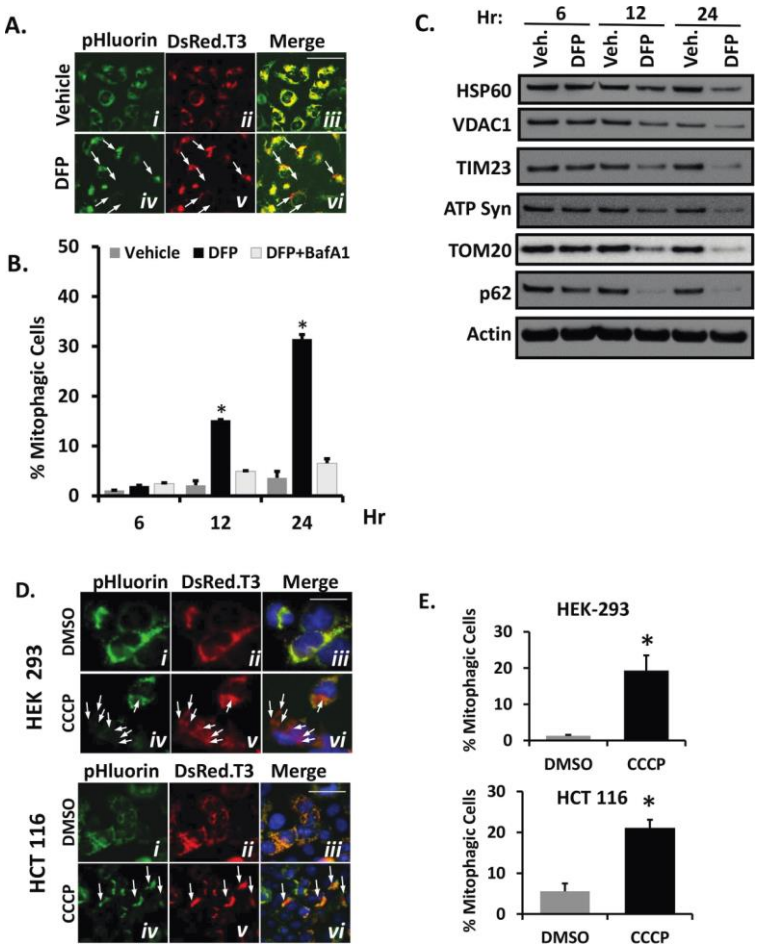

Figure 4. Quantification of CCCP induced mitophagy in HEK-293 and HCT-116 cells and deferiprone (DFP)-induced mitophagy in HeLa cells. (**A**) Representative micrographs of HeLa cells transfected with Mito-Rosella and then treated with 1mM of 3-Hydroxy-1,2-dimethyl-4(1H)-pyridone (deferiprone, DFP) or Vehicle (phosphate-buffered saline, PBS) for 24 hr. DFP treatment caused an accumulation of red-only Mito-Rosella labeled mitochondria (panel vi, solid arrows) while in vehicle treated cells there was complete co-localization between red/green signals (panel iii). Scale bar indicate a length of 50 μm. (**B**) Percentage of Mito-Rosella expressing cells showing increased mitophagy after 1 mM DFP treatment at indicated time-points as quantified by mito-Rosella FCM assay. Bars represent mean of 3 biological replicates ± SEM, N = 10,000 cells analyzed per replicate; $^{*}p < 0.001$ vs DFP + BafA1 (**C**) Western blots of markers of mitochondrial content–HSP60, ATP synthase, VDAC1, TIM23 and TOM20 (top four panels) and p62 (autophagy marker) and actin (gel loading control) in cell treated with DFP or Vehicle (PBS) control for the indicated time-points. (**D**) Representative micrographs of HEK-293 cells transfected with Mito-Rosella alone (top panels) and HCT-116 cells (bottom panels) transfected with Mito-Rosella plus HA-Parkin; cells were treated with CCCP (10 μM) or vehicle as indicated; treatment durations were 24 hr for HEK-293 cells or 6 hr for HCT-116 cells. CCCP treatment induced accumulation of red-only Mito-Rosella indicating mitophagy (white arrows). Scale bars indicate a length of 25 μm. (**E**) Percentage of Mito-Rosella expressing HEK-293 and HCT-116 cells showing increased mitophagy after CCCP treatment as quantified by mito-Rosella assay.

Discussion

Degradation of mitochondria by macroautophagy, also known as 'mitophagy', is important for mitochondrial function and has been implicated in human disease processes. Mitophagy requires autophagy, and so autophagy and mitophagy must be assessed in parallel when considering regulation of mitophagy. Here we report a novel, flow cytometry (FCM)-based assay for measuring autophagy and mitophagy in parallel using a single fluorescent biosensor, Rosella, targeted to different cellular compartments. We demonstrate the performance of this assay in measuring Parkin-mediated mitophagy in CCCP-treated HeLa, a well-characterized model of selective mitophagy, in HEK-293 and HCT-116 cells treated with CCCP, and in Parkin-independent mitophagy in cells treated with DFP. Measuring 10,000 cells requires 6 seconds of analysis time (<10 min for 96 separate conditions). Therefore, this parallel assay for autophagy/mitophagy has the capacity to make hundreds to thousands of measurements in minutes to hours. Moreover, by combining these methods with iRFP as a marker of genetic manipulation (as shown in Fig. 3G,H), the assay should be capable of screening large libraries of cDNA, RNAi, TALEN, or Crispr-Cas9 sgRNA to identify regulators of selective mitophagy.

Our findings indicate that LC3-Rosella and Mito-Rosella can be employed in parallel to measure both generalized macroautophagy and selective mitophagy; and importantly, the two biosensors used together can readily detect dissociation between autophagy and mitophagy when it occurs (*e.g.,* in HeLa cells treated with CCCP but not expressing Parkin). Other fluorescent markers have been used for monitoring delivery of autophagic cargo lysosomes, including tandem mCherry-eGFP[45,46], mRFP-GFP[47], and RFP-eGFP[48] constructs, and the pH-sensitive Keima[49] fluorescent protein; however, this is the first demonstration of an FCM-based high-throughput method for measuring autophagy and mitophagy in parallel in mammalian cells.

Monitoring of mitochondrial content by means of Western blotting of mitochondrial protein markers, uptake of mitochondria-specific dyes, or measurement of mitochondrial DNA provides information about the cellular content of mitochondria at any given point in time. However, because the net content of mitochondria reflects simultaneous mitochondrial biogenesis and mitochondrial turnover, mediated in part by mitophagy, these methods may underestimate mitophagy when there is substantial mitochondrial biogenesis. Because measurement of mitochondrial flux to the lysosome by the Mito-Rosella method is a more direct measurement of mitophagy (*i.e.,* trafficking via autophagy and terminal delivery of mitochondria to the functional lysosome), there is less potential for it to be affected by mitochondrial biogenesis than surrogate measurements of mitophagy based on mitochondrial content.

Moreover, several of the mitochondrial dyes used to quantify mitochondria–including those described as 'non-potentiometric'[50] can be affected by conditions that alter membrane potential[51,52] and should be used with caution. For example, staining of mitochondria with 10-N-nonyl acridine orange (NaO), a dye that interacts specifically with cardiolipin on the mitochondrial membrane, is highly dependent on mitochondrial energy state[53]. Moreover, recent reports that externalization of cardiolipin to the outer mitochondrial membrane plays a role in initiation of mitophagy[24] raises questions about how this process might influence measurements of mitochondrial mass using NaO. In addition, a recent report by Padman *et al.*[41] showed redistribution of mitochondrial dyes (DiOC6, TMRM, MTR, and MTG) from mitochondria to lysosomes after CCCP treatment. Another aspect of non-potentiometric mitochondrial dyes is that they typically have affinity for some specific chemical group on/in mitochondria, and these dyes can therefore potentially stain mitochondria even after delivery to lysosomes via mitophagy, which could result in overestimation of intact mitochondrial mass.

Because Rosella monitors terminal delivery of cargo to lysosomes, the assay cannot provide information about lysosome-independent mechanisms for mitochondrial degradation[54], or budding of mitochondrial-derived vesicles (MDVs) that may traffic to other compartments[55]. A potential limitation of this method is that Rosella biosensors could potentially detect lysosome-independent acidification of cargos; conversely, they could underestimate delivery of cargos when lysosomal pH is elevated by other factors[41]. Therefore, pilot studies to assess intracellular localization of different biosensor-tagged cargos by fluorescence microscopy and sensitivity to BafA1 treatment are advisable when applying these methods to new conditions or when attaching Rosella to different cargos.

Taken together, these findings indicate Rosella biosensor measurements are amenable to use in high-throughput screening assays designed to identify chemical or genetic factors that regulate autophagy or mitophagy in mammalian cells, and can readily detect selective regulation of mitophagy as a dissociation between the two processes when it occurs. We are currently applying the Rosella-based autophagy/mitophagy assays to screen shRNAi and cDNA libraries in an effort to identify new regulators in mammalian cells, and we are producing transgenic mice expressing Rosella-LC3 and Mito-Rosella biosensors for measuring autophagic and mitophagic fluxes to lysosomes in different tissues *in vivo*.

Materials and Methods

Cell culture. HeLa, HEK-293 and HCT-116 cells were from ATCC (American Type Culture Collection), and cultured in DMEM for HeLa and HEK-293 (Life Technologies) and McCoy's 5a Medium Modified (Life Technologies) for HTC-116 and supplemented with 10% heat-inactivated fetal bovine serum (Atlanta Biologicals), penicillin, and streptomycin (Life Technologies), and maintained in a 5% CO_2, 37 °C humidified incubator. Media was changed every third day, and culture passage number was maintained under fifteen.

Expression plasmids. The Rosella biosensor was described in previous publications[35,36]. The full-length open reading frame (ORF) of human microtubule-associated protein 1A/1B-light chain 3 (Map1lc3b) was joined in-frame to the 3′ end of the Rosella ORF (coding the C-terminus) in the pDest expression vector, generating the Rosella-LC3 biosensor (Fig. 1A), for use in detecting delivery of autophagosomes to lysosomes (*i.e.,* generalized macroautophagy). The ATP synthase subunit gamma (Atp5c) full-length ORF minus the terminal stop codon was joined in-frame to 5′ of the Rosella ORF (end (coding the N-terminus) in the pCIneo expression plasmid (Clontech), generating the Mito-Rosella biosensor (Fig. 1A) for detecting delivery of mitochondria to lysosomes (*i.e.*, mitophagy). pRK5-HA-Parkin (Addgene plasmid 17613) was a gift from Dr. Ted Dawson (Johns Hopkins University), pIRFP (Addgene plasmid 31857; based on vector backbone pEGFP-C1) was a gift from Dr. Vladislav Verkhusha (Yeshiva University). iRFP-T2A-Parkin vector was generated from IRFP-T2A-TREX2 in pExodus CMV vector (Addgene plasmid #50419), a gift from Dr. Andrew Scharenberg (Seattle's Children Hospital), by substituting TREX2 with Parkin. pmTurquoise2-Mito (Addgene plasmid 36208) was a gift from Dr. Dorus Gadella (University of Amsterdam) and mCherry-Parkin (Addgene plasmid 23956) was a gift from Dr. Richard Youle (NINDS). HeLa cells with stable expression of Rosella-LC3 or Mito-Rosella were generated by cloning the biosensor ORFs into a PiggyBac transposon transfer vector (System Biosciences, product #B510B-1), which was then co-transfected with the Super PiggyBac Transposase expression vector (System Biosciences, product #PB210PA-1); stable cell lines were developed by repeated passaging in the presence of puromycin (2 μg/mL, InvivoGen) for 3 weeks, followed by sterile flow cytometry-automated cell sorting to isolate cells with increased green and red channel fluorescence. After sorting, stable lines were cultured continuously in media containing Puromycin (2 μg/mL).

Microscopy and flow cytometry (FCM). Figure 1E cells were plated on 60 mm glass bottom poly-D-lysine coated plates, transfected with Rosella-LC3 or Mito-Rosella with Parkin. 24 hr post transfection cells were treated as indicated and live images were obtained with Nikon Eclipse Ti-E widefield inverted microscope equipped with 405 nm diode laser, 488 nm Argon gas and 543 nm Helium-neon gas lasers and DAPI (450–465 nm) FITC (505–535 nm) and TRITC (580–620) filter sets using 100X oil immersion objective. For all other images: Cells were grown on 6 or 12 well plates and images of unfixed, live cells were obtained using an EVOS-fl inverted LED fluorescence microscope. pHluorin emission (510 ± 42 nm), DsRed.T3 emission (593 ± 40 nm) and iRFP emission (692 ± 40 nm) were measured after excitation with (470 ± 22 nm), (531 ± 40 nm) and (628 ± 40 nm) LED illuminations respectively. ImageJ software were used for quantitative analysis. Individual cells in micrographs were scored as being positive or negative for autophagy or mitophagy, based on the presence/absence of visible accumulations of red biosensor fluorescence in the central lysosomal compartments with distinct "red only" fluorescence. For FCM, cells were grown on 12 well plates until reaching 90% confluency and treated with CCCP (10 μM) and/or bafilomycin A (100 nM,) for indicated durations. Cells were harvested for analysis by washing twice with PBS, trypsinizing with TrypLE (Life Technologies), and transferring to 96 well plate wells containing 0.3 mL PBS. Cells were analyzed using a BD FACSCanto analyzer on high throughput mode. pHluorin emission (530 ± 30 nm), DsRed.T3 emission (585 ± 15 nm) and iRFP emission (780 ± 60 nm) were measured after excitation with 488, 561 and 640 nm lasers, respectively. 5,000 to 10,000 live cells were analyzed per condition, with fluorescent detection in green and red channels, and when required for detecting iRFP, the near-infrared (Cy7) channel. Increased autophagy or mitophagy were determined for individual cells by detecting decreased green vs. red fluorescence, based on gating determined by the green and red fluorescence of vehicle (DMSO)-treated control cells. To eliminate potential confounding effects of lysosome-independent changes in mitochondrial pH, Bafilomycin A1-treated cells were used as a control condition under situations where potential acidification of media or cytoplasm might occur (*e.g.,* prolonged CCCP treatment in Fig. 3H).

Antibodies and chemicals. Primary antibodies used in this study: rabbit anti-LC3A/B, rabbit anti-Parkin rabbit anti-HSP60 (1:1000, Cell Signaling, products #4108S, #4211S and #12165S , respectively); mouse anti-TIM23 (1:1000, BD Biosciences, product #611222); mouse anti-VDAC1, mouse anti-TOM20, and mouse anti-p62 (Santa Cruz, 1: 500, sc-58649, sc-17764, and sc-28359, respectively); rabbit anti-ATP synthase gamma (1:1000, GeneTex, product #GTX-114275), mouse anti-Actin (1:3000, Genescript, product #A00702) and rabbit anti-GFP (Genescript, product #A01388-40). Secondary antibodies were: HPR conjugated goat anti-rabbit and goat anti-mouse (1:2500, products #170-6515 and #172-1011, respectively). CCCP and DMSO were obtained from Sigma. Bafilomycin A1 was obtained from LC Laboratories. Mitotracker Deep Red FM, Lysotracker Red DND 99, and TMRE, and Hoechst 33342 were obtained from Life Technologies. 3-Hydroxy-1,2-dimethyl-4(1H)-pyridone was from Sigma.

Western blot analysis. Cells were washed twice in PBS and lysed with ice-cold RIPA buffer (Santa-Cruz) containing HALT protease/phosphatase cocktail (Pierce/Thermo Scientific). Lysates were incubated on ice for 30 min with gentle, constant agitation. Lysates were centrifuged at 12,000 × g for 20 min at 4 °C to pellet nuclei and other insoluble material. Lysates were treated with Novex sample buffer and heated 10 min at 90 °C. SDS-PAGE was performed on 4–12% Tris-Bis gels (Life Technologies) with MES-based running buffer containing anti-oxidant additive, according to the manufacturer's instructions. Gels were transferred to nitrocellulose (iBlot system, Life technologies). Western blot membranes

were blocked with 5% BSA in TBS-T buffer for 1 hour at room temperature, followed by incubation with 5% BSA in TBS-T containing primary antibodies at the indicated concentrations (see Methods, above) overnight at 4 °C with gentle rocking; in the morning, blots were washed in TBS-T and incubated 1 hr at room temperature in 5% BSA in TBS-T containing HRP-conjugated secondary antibodies (1:2500), washed again in TBS-T, and incubated in luminescent peroxidase substrate (ThermoFisher). Imaging of Western blot band luminescence was performed with a GeneGnome imager (Syngene); and band intensities were quantified using Gene Snap software (Syngene).

References

1. Boland, M. L., Chourasia, A. H. & Macleod, K. F. Mitochondrial dysfunction in cancer. *Front. Oncol.* **3,** 292 (2013).
2. Kobayashi, S. & Liang, Q. Autophagy and mitophagy in diabetic cardiomyopathy. *Biochim. Biophys. Acta (BBA) - Molecular Basis of Disease* **1852,** 252–261 (2015).
3. Lin, M. T. & Beal, M. F. Mitochondrial dysfunction and oxidative stress in neurodegenerative diseases. *Nature* **443,** 787–795 (2006).
4. Lowell, B. B. & Shulman, G. I. Mitochondrial Dysfunction and Type 2 Diabetes. *Science* **307,** 384–387 (2005).
5. Bratic, A., Larsson, N.-G., xF & ran The role of mitochondria in aging. *J. Clin. Invest.* **123,** 951–957 (2013).
6. Hamanaka, R. B. & Chandel, N. S. Mitochondrial reactive oxygen species regulate cellular signaling and dictate biological outcomes. *Trends Biochem. Sci.* **35,** 505–513.
7. Choksi, K. B., Boylston, W. H., Rabek, J. P., Widger, W. R. & Papaconstantinou, J. Oxidatively damaged proteins of heart mitochondrial electron transport complexes. *Biochim. Biophys. Acta* **1688,** 95–101 (2004).
8. Taylor, E. B. & Rutter, J. Mitochondrial quality control by the ubiquitin-proteasome system. *Biochem. Soc. Trans.* **39,** 1509–1513 (2011).
9. Ashrafi, G. & Schwarz, T. L. The pathways of mitophagy for quality control and clearance of mitochondria. *Cell Death Differ.* **20,** 31–42 (2013).
10. Sugiura, A., McLelland, G. L., Fon, E. A. & McBride, H. M. A new pathway for mitochondrial quality control: mitochondrial-derived vesicles. *EMBO J.* **33,** 2142–2156 (2014).
11. Al Rawi, S. *et al.* Postfertilization Autophagy of Sperm Organelles Prevents Paternal Mitochondrial DNA Transmission. *Science* **334,** 1144–1147 (2011).
12. Schweers, R. L. *et al.* NIX is required for programmed mitochondrial clearance during reticulocyte maturation. *Proc. Natl. Acad. Sci. USA.* **104,** 19500–19505 (2007).
13. Costello, M. J. *et al.* Autophagy and mitophagy participate in ocular lens organelle degradation. *Exp. Eye Res.* **116,** 141–150 (2013).
14. Goldman, S. J., Zhang, Y. & Jin, S. Autophagic Degradation of Mitochondria in White Adipose Tissue Differentiation. *Antioxid. Redox Signal.* **14,** 1971–1978 (2011).
15. Ikeda, Y. *et al.* Endogenous Drp1 mediates mitochondrial autophagy and protects the heart against energy stress. *Circ. Res.* **116,** 264–278 (2015).
16. Andres, A. M. *et al.* Mitophagy is required for acute cardioprotection by simvastatin. *Antioxid Redox Signal* **21,** 1960–1973 (2014).
17. Huang, C. *et al.* Preconditioning involves selective mitophagy mediated by Parkin and p62/SQSTM1. *PLoS One* **6,** e20975 (2011).
18. Pickrell, A. M. & Youle, R. J. The roles of PINK1, parkin, and mitochondrial fidelity in Parkinson's disease. *Neuron* **85,** 257–273 (2015).
19. Ye, X., Sun, X., Starovoytov, V. & Cai, Q. Parkin-mediated mitophagy in mutant hAPP neurons and Alzheimer's disease patient brains. *Hum. Mol. Genet.* **24,** 2938–2951 (2015).
20. Wong, Y. C. & Holzbaur, E. L. Optineurin is an autophagy receptor for damaged mitochondria in parkin-mediated mitophagy that is disrupted by an ALS-linked mutation. *Proc. Natl. Acad. Sci. USA.* **111,** E4439–4448 (2014).
21. Soleimanpour, S. A. *et al.* The diabetes susceptibility gene Clec16a regulates mitophagy. *Cell* **157,** 1577–1590 (2014).
22. Seillier, M. *et al.* Defects in mitophagy promote redox-driven metabolic syndrome in the absence of TP53INP1. *EMBO Mol. Med.* (2015). doi: 10.15252/emmm.201404318
23. Lu, H. *et al.* Regulation and function of mitophagy in development and cancer. *Autophagy* **9,** 1720–1736 (2013).
24. Fujiwara, M. *et al.* Parkin as a tumor suppressor gene for hepatocellular carcinoma. *Oncogene* **27,** 6002–6011 (2008).
25. Liu, L. *et al.* Mitochondrial outer-membrane protein FUNDC1 mediates hypoxia-induced mitophagy in mammalian cells. *Nat. Cell Biol.* **14,** 177–185 (2012).
26. Chu, C. T. *et al.* Cardiolipin externalization to the outer mitochondrial membrane acts as an elimination signal for mitophagy in neuronal cells. *Nat. Cell Biol.* **15,** 1197–1205 (2013).
27. Novak, I. *et al.* Nix is a selective autophagy receptor for mitochondrial clearance. *EMBO Rep* **11,** 45–51 (2010).
28. Shi, R. Y. *et al.* BNIP3 interacting with LC3 triggers excessive mitophagy in delayed neuronal death in stroke. *CNS Neurosci. Ther.* **20,** 1045–1055 (2014).
29. Strappazzon, F. *et al.* AMBRA1 is able to induce mitophagy via LC3 binding, regardless of PARKIN and p62/SQSTM1. *Cell Death Differ.* **22,** 419–432 (2015).
30. Chen, D. *et al.* CCCP-Induced LC3 Lipidation Depends on Atg9 Whereas FIP200/Atg13 and Beclin 1/Atg14 are Dispensable. *Biochem. Biophys. Res. Commun.* **432,** 226–230 (2013).
31. Ding, W. X. *et al.* Nix is critical to two distinct phases of mitophagy, reactive oxygen species-mediated autophagy induction and Parkin-ubiquitin-p62-mediated mitochondrial priming. *J. Biol. Chem.* **285,** 27879–27890 (2010).
32. Narendra, D., Tanaka, A., Suen, D.-F. & Youle, R. J. Parkin is recruited selectively to impaired mitochondria and promotes their autophagy. *J. Cell Biol.* **183,** 795–803 (2008).
33. Narendra, D. P. *et al.* PINK1 is selectively stabilized on impaired mitochondria to activate Parkin. *PLoS Biol.* **8,** e1000298 (2010).
34. Matsuda, N. *et al.* PINK1 stabilized by mitochondrial depolarization recruits Parkin to damaged mitochondria and activates latent Parkin for mitophagy. *J. Cell Biol.* **189,** 211–221 (2010).
35. Rosado, C. J., Mijaljica, D., Hatzinisiriou, I., Prescott, M. & Devenish, R. J. Rosella: a fluorescent pH-biosensor for reporting vacuolar turnover of cytosol and organelles in yeast. *Autophagy* **4,** 205–213 (2008).
36. Mijaljica, D., Prescott, M. & Devenish, R. J. A Fluorescence Microscopy Assay for Monitoring Mitophagy in the Yeast Saccharomyces cerevisiae. *J. Vis. Exp.: JoVE*, 2779 (2011).
37. Miesenbock, G., De Angelis, D. A. & Rothman, J. E. Visualizing secretion and synaptic transmission with pH-sensitive green fluorescent proteins. *Nature* **394,** 192–195 (1998).
38. Bevis, B. J. & Glick, B. S. Rapidly maturing variants of the Discosoma red fluorescent protein (DsRed). *Nat Biotech* **20,** 83–87 (2002).

39. Kim, J. H. *et al.* High cleavage efficiency of a 2A peptide derived from porcine teschovirus-1 in human cell lines, zebrafish and mice. *PLoS One* **6,** e18556 (2011).
40. Filonov, G. S. *et al.* Bright and stable near-infrared fluorescent protein for *in vivo* imaging. *Nat. Biotechnol.* **29,** 757–761 (2011).
41. Padman, B. S., Bach, M., Lucarelli, G., Prescott, M. & Ramm, G. The protonophore CCCP interferes with lysosomal degradation of autophagic cargo in yeast and mammalian cells. *Autophagy* **9,** 1862–1875 (2013).
42. Allen, G. F., Toth, R., James, J. & Ganley, I. G. Loss of iron triggers PINK1/Parkin-independent mitophagy. *EMBO Rep* **14,** 1127–1135 (2013).
43. Fu, M. *et al.* Regulation of mitophagy by the Gp78 E3 ubiquitin ligase. *Mol. Biol. Cell* **24,** 1153–1162 (2013).
44. Zou, J. *et al.* Autophagy inhibitor LRPPRC suppresses mitophagy through interaction with mitophagy initiator Parkin. *PLoS One* **9,** e94903 (2014).
45. Gump, J. M. *et al.* Autophagy variation within a cell population determines cell fate through selective degradation of Fap-1. *Nat. Cell Biol.* **16,** 47–54 (2014).
46. Pankiv, S. *et al.* p62/SQSTM1 binds directly to Atg8/LC3 to facilitate degradation of ubiquitinated protein aggregates by autophagy. *J. Biol. Chem.* **282,** 24131–24145 (2007).
47. Kimura, S., Noda, T. & Yoshimori, T. Dissection of the autophagosome maturation process by a novel reporter protein, tandem fluorescent-tagged LC3. *Autophagy* **3,** 452–460 (2007).
48. Li, L., Wang, Z. V., Hill, J. A. & Lin, F. New autophagy reporter mice reveal dynamics of proximal tubular autophagy. *J. Am. Soc. Nephrol.* **25,** 305–315 (2014).
49. Katayama, H., Kogure, T., Mizushima, N., Yoshimori, T. & Miyawaki, A. A sensitive and quantitative technique for detecting autophagic events based on lysosomal delivery. *Chem. Biol.* **18,** 1042–1052 (2011).
50. Cottet-Rousselle, C., Ronot, X., Leverve, X. & Mayol, J. F. Cytometric assessment of mitochondria using fluorescent probes. *Cytometry A* **79,** 405–425 (2011).
51. Keij, J. F., Bell-Prince, C. & Steinkamp, J. A. Staining of mitochondrial membranes with 10-nonyl acridine orange, MitoFluor Green, and MitoTracker Green is affected by mitochondrial membrane potential altering drugs. *Cytometry* **39,** 203–210 (2000).
52. Jacobson, J., Duchen, M. R. & Heales, S. J. Intracellular distribution of the fluorescent dye nonyl acridine orange responds to the mitochondrial membrane potential: implications for assays of cardiolipin and mitochondrial mass. *J. Neurochem.* **82,** 224–233 (2002).
53. Garcia Fernandez, M. I., Ceccarelli, D. & Muscatello, U. Use of the fluorescent dye 10-N-nonyl acridine orange in quantitative and location assays of cardiolipin: a study on different experimental models. *Anal. Biochem.* **328,** 174–180 (2004).
54. Lyamzaev, K. G. *et al.* Novel mechanism of elimination of malfunctioning mitochondria (mitoptosis): formation of mitoptotic bodies and extrusion of mitochondrial material from the cell. *Biochim. Biophys. Acta* **1777,** 817–825 (2008).
55. Braschi, E. *et al.* Vps35 mediates vesicle transport between the mitochondria and peroxisomes. *Curr. Biol.* **20,** 1310–1315 (2010).

Acknowledgements

The authors thank Dr. Rodney Devenish, Dr. Mark Prescott, and Dr. Carlos J. Rosado of Monash University, Melbourne, Australia, and Dr. Jared Rutter, Dr. Dennis Winge, Dr. Dana Carroll, and Dr. Don McClain of University of Utah, Salt Lake City, UT, for providing helpful advice on design and interpretation of these studies. The authors thank Dr. Elizabeth Leibold, for providing important reagents. The authors also thank the Flow Cytometry Core Facility and Fluorescent Microscopy Core Facility, parts of the Health Sciences Cores at the University of Utah, for training and assistance in flow cytometry and imaging. Microscopy equipment was obtained using NCRR Shared Equipment Grant #1S10RR024761. The work was supported by NIH R01 DK100826, American Diabetes Association Core Basic Science Award 7-13-BS-056, and Department of Veterans Affairs Biomedical Laboratory Research and Development Merit Review Award I01 BX000937 to TEG, and a Howard Hughes Medical Institute Med-Into-Grad Award 56006777 to AS.

Author Contributions

A.S. and T.E.G. designed the studies, oversaw conduct of individual experiments, and wrote the main manuscript text. J.C., L.B.F., M.E.L., T.F., L.K.C. and S.J.T. assisted A.S. with conduct of individual experiments and provided essential technical support in Figs 1–4 and Suppl. Figs 1–5.

Additional Information

Supplementary information accompanies this paper at http://www.nature.com/srep

Competing financial interests: The authors have no competing interests to declare related to this area of research. TEG serves on the Medical Advisory Board of Health Diagnostic Laboratory, Inc., Richmond, VA, and on the Scientific Advisory Board of Progenitor Life Sciences, Inc., Salt Lake City, UT.

How to cite this article: Sargsyan, A. *et al.* Rapid parallel measurements of macroautophagy and mitophagy in mammalian cells using a single fluorescent biosensor. *Sci. Rep.* **5**, 12397; doi: 10.1038/srep12397 (2015).

This work is licensed under a Creative Commons Attribution 4.0 International License. The images or other third party material in this article are included in the article's Creative Commons license, unless indicated otherwise in the credit line; if the material is not included under the Creative Commons license, users will need to obtain permission from the license holder to reproduce the material. To view a copy of this license, visit http://creativecommons.org/licenses/by/4.0/

CHAPTER 3

MITOCHONDRIAL PYRUVATE METABOLISM INDUCES PSEUDOHYPOXIA AND MITOPHAGY

Ashot Sargsyan

Abstract

Abnormal accumulation of TCA cycle metabolites stabilizes hypoxia inducible factor 1α (HIF-1α) that results in profound transcriptional and metabolic changes. In many cases, accumulation of succinate and fumarate, and subsequent stabilization of HIF-1α, is thought to be causative for cancers such as paragangliomas, phaeochromocytomas, leiomyosarcoma, and renal cell carcinomas. Moreover, lactate and pyruvate, the end products of glycolysis, also stabilize HIF-1α by direct inhibition of prolyl hydroxylases, which are required for HIF-1α degradation. In this report, we show that in many cancer cell lines mitochondrial pyruvate metabolism induces the stabilization of HIF-1α and requires mitochondrial entry of pyruvate. Pyruvate metabolism induces mitophagy mediated by HIF-1α and its downstream target BNIP3. We also show that inhibition of mitochondrial pyruvate carrier abrogates stabilization of HIF-1α and BNIP3. Notably, this pseudohypoxic stabilization of HIF-1α by pyruvate could be induced by glycolysis derived pyruvate, suggesting this process could have physiological relevance. Moreover, we show that antioxidant N-acetylcysteine (NAC) is sufficient to block HIF-1α stabilization. Based on our findings, we propose that stabilization of HIF-1α and mitophagy are protective against excessive reactive oxygen species (ROS) damage to mitochondria, possibly by removing damaged mitochondria, thereby maintaining mitochondrial health. Pioglitazone, a drug that has widespread usage in diabetes treatment, abrogates stabilization of HIF-1α caused by mitochondrial pyruvate metabolism, likely by inhibition of the mitochondrial pyruvate carrier complex. Whether the ability of pioglitazone to block the

stabilization of HIF-1α has any clinical significance in type two diabetes treatment awaits further investigation.

Introduction

The decision to utilize pyruvate through mitochondria or to convert it to lactate is one of the crucial steps of cellular carbohydrate metabolism. In differentiated cells most of the pyruvate is taken up by mitochondria where it is utilized in the TCA cycle[1]. In contrast, most cancer cells rely on glycolysis[2] and divert pyruvate to lactate that is excreted from cells[3]. Furthermore, stem cells appear to rely on glycolysis and tend to lose their stemness with increased mitochondrial metabolism[4,5]. In cancer cells, glycolysis supports the increased anabolic requirements of cells, while pyruvate to lactate conversion regenerates ample NAD+ that, in turn, supports glycolysis. The increased glycolytic dependence of cancer cells was first described by Otto Warburg and subsequently is called the Warburg effect[6]. For several decades, cancer cells' "unwillingness'' to utilize pyruvate in mitochondria was attributed to defective mitochondria, although in recent years, several lines of evidence suggest that most cancer cells have fully functional mitochondria. Furthermore, studies have shown that the Warburg effect is mostly driven by oncogenic mutations and hypoxia. This is evident in solid tumors[7] where lack of blood flow and subsequent scarcity of oxygen activates hypoxia inducible transcription factor 1 (HIF-1) a key regulator of the oxygen sensing pathway. HIF-1 facilitates adaptation to hypoxia at cellular and organismal levels. The HIF-1 transcription factor is a heterodimer consisting of alpha and beta

subunits, where HIF-1β is constitutively expressed while expression of HIF-1α is highly regulated by cellular oxygen tension. With ample cellular oxygen concentrations, HIF-1α is hydroxylated[8, 9] at two prolyl residues (402 and 564) in its oxygen-dependent degradation domain (ODD) by prolyl hydroxylase domain (PHD) proteins[10]. Proline hydroxylation serves as a recognition signal for the Von Hippel–Lindau (VHL) tumor-suppressor protein of the ubiquitin ligase complex, that ubiquitinates and targets HIF-1α for proteasomal degradation. Another oxygen dependent regulation of HIF-1α activity is asparagine 803 hydroxylation by Factor Inhibiting HIF (FIH) asparaginyl hydroxylase[11, 12] , which disrupts the interaction of HIF-1α with the p300/CBP coactivator inhibiting its transcriptional activity. Under low cellular oxygen tension, the rate of hydroxylation of prolyl residues significantly decreases and HIF-1α is not recognized by VHL for ubiquitination. This leads to stabilization of HIF-1α and subsequent translocation to nucleus, where the HIF 1 heterodimer binds to the hypoxia responsive elements in promoter regions of a vast number of genes responsible for adaptation to low oxygen levels. HIF-1α initiated transcriptional changes lead to organismal level adaptations such as increased angiogenesis and red blood cell production, and to cellular responses such as increased glycolytic enzyme expression and repression of oxidative metabolism. Transcriptional changes induced by HIF-1α could also induce carcinogenesis and mediate drug resistance in cancers. It is important to note that mitochondria and the TCA cycle are directly involved in regulation of HIF-1α stabilization. During the hydroxylation reaction PHDs utilize alpha ketoglutarate (αKG), a metabolite of TCA cycle. Any metabolic perturbation that results in a

change of αKG levels can potentially influence HIF-1α stabilization. In addition, activation of HIF-1α decreases the flow of pyruvate into mitochondria by virtue of pyruvate dehydrogenase kinase overexpression and activation that inhibits the pyruvate dehydrogenase complex[13, 14]. Certain aberrant TCA metabolites are known to inhibit prolyl hydroxylases[15, 16] and stabilize hypoxia HIF-1α in a variety of cancer types[17-20]. In most cases, inhibition of PHDs are directly linked to mutations in the succinate dehydrogenase[21, 22], fumarate hydratase[23], and isocitrate dehydrogenase[24] genes. Mutations in both SDH and FH result in accumulation of succinate and fumarate respectively, while isocitrate dehydrogenase 1 mutations result in a formation of 2-hydroxyglutarate[25], a competitive inhibitor of PHD [26], and in depletion of αKG, a cofactor in HIF-1α degradation. It has also been shown that fumarate reacts with the antioxidant glutathione and forms succinated glutathione which eventually leads to excessive ROS production and stabilization of HIF-1α[27]. Furthermore, glucose and glycolysis end products lactate and pyruvate can inhibit prolyl hydroxylases and induce the hypoxic response[28, 29]. While there is substantial evidence of pyruvate stabilization of HIF-1α, the role of mitochondrial pyruvate metabolism in this process has not been elucidated. We wanted to investigate whether inhibitory effects of pyruvate on prolyl hydroxylases require mitochondrial metabolism, or whether cytoplasmic pyruvate can stabilize HIF-1α directly. Furthermore, glycolytic and TCA cycle mediated HIF-1α stabilization have been mostly studied in the context of cancer, while the physiological importance of normal glucose metabolism in HIF-1α stabilization is not well understood. This is particularly important since in most

laboratory settings the majority of model cell lines are grown in 10 to 25 mM glucose solution often substituted with 1 mM pyruvate, concentrations that are multiples of their physiological values. This could lead to overwhelming the mitochondria with pyruvate and lead to metabolic reprograming of the cells. In this work, we studied the effects of pyruvate metabolism in context of HIF-1α induction and subsequent metabolic changes.

Results

Mitochondrial pyruvate metabolism stabilizes HIF-1α and induces mitophagy.

To test whether glycolysis or pyruvate metabolism in mitochondria induce stabilization of HIF-1α, we fed different cell lines with either 10 mM glucose or 10 mM pyruvate. Since pyruvate can only be utilized in mitochondria to produce energy via TCA cycle and oxidative phosphorylation, while glucose could be consumed by glycolysis to produce pyruvate, we hypothesized that any changes seen in HIF-1α stabilization could be attributed to presence or absence of glycolysis. In four cell lines, we tested, (HepG2, HEK 293, Hela, and SH-SY5Y) pyruvate stabilized HIF-1α after 24 h incubation with 10 mM pyruvate (Figure 3.1, A). Interestingly, we noticed that HIF-1α stabilization was the highest in HepG2 cells. Furthermore, Hela cells had elevated level of HIF-1α with glucose compared to other cell lines we tested, but less in intensity than pyruvate treated cells. Since the highest level of stabilization was achieved in HepG2 cells, we decided to use HepG2 cells as our preferred cell line in further analysis. In HepG2 cells incubation

with 10 mM pyruvate noticeably stabilized HIF-1α after 4 h, with gradual increase up to 10 h (the last time point in this series of experiments). A slight increase in HIF-1α levels was also recorded in glucose treated cells, suggesting that glycolysis derived pyruvate could stabilize HIF-1α (Figure 3.1, B). Moreover, we noticed that increasing pyruvate concentration results in increased HIF-1α accumulation, but at 25 mM concentration this effect was diminished (Figure 3.1, C). Interestingly, addition of 10 mM glucose with 10 mM pyruvate completely abrogated stabilization of HIF-1α, suggesting that glycolysis can restore degradation of HIF-1α. HIF-1α is known to mediate mitophagy [30], partially through upregulation of BCL2/Adenovirus E1B 19kDa Interacting Protein 3 (BNIP3)[31, 32]. In our experiments, we noticed increased expression of BNIP3 and a decrease in mitochondrial proteins VDAC1, FUNDC1, and TIM23 (Figure 3.1, B and C). Importantly, addition of 10 mM glucose to pyruvate blocked stabilization of HIF-1α and reduced the expression of BNIP3, suggesting that HEPG2 cells prefer glycolysis over oxidative phosphorylation, and further implying that HIF-1α stabilization is dependent on mitochondrial respiration rather than pyruvate presence in the cytoplasm. Moreover, glucose addition restored the levels of mitochondrial proteins. Treatment with Echinomycin, a HIF-1α inhibitor, significantly decreased the expression of BNIP3, suggesting BNIP3 expression is under direct control of HIF-1α. Furthermore, in Hela cells, knockdown of HIF-1α abrogates expression of BNIP3 after pyruvate treatment and increases mitochondrial protein levels as measured by western blotting (Figure 3.2). To further test whether HIF-1α stabilization is due to the mitochondrial pyruvate

metabolism, we incubated HepG2 and Hela cells with glucose and pyruvate as before, but with addition of mitochondrial pyruvate carrier inhibitor UK5099 [33, 34]. Addition of UK5099 abrogated stabilization of HIF-1α and expression of BNIP3 protein, confirming that HIF-1α stabilization is dependent on mitochondrial entry of pyruvate (Figure 3.3, A and B). Interestingly, inhibition of lysosomal V-ATPases with 100nM Bafilomycin A1 markedly increased stabilization of HIF-1α, suggesting that HIF-1α is at least partially degraded via lysosomes[35]. UK5099 significantly increased glucose clearance from the media with HepG2 cells, suggesting that even with glycolysis HepG2 cells use some of the pyruvate derived through glycolysis in mitochondria (Figure 3.3, C). In contrast, UK5099 significantly decreased the clearance of pyruvate from media, although it did not reach the level of initial pyruvate concentration. Moreover, addition of UK5099 to glucose incubated cells increased the acidification of the media, indicating that blocking mitochondrial pyruvate metabolism increases cellular needs for glycolysis, presumably to meet energetic needs of the cell. In contrast, there was no acidification of media while grown on pyruvate with or without UK5099. This was also evident from metabolomics analysis, where we found negligible amounts of lactate in pyruvate fed cells when compared to glucose fed cells (Figure 3.4). This finding is particularly surprising since HIF-1α upregulates the expression of lactate dehydrogenase A (LDHA) [36] and should have increased conversion of pyruvate to lactate. It has been reported that increased levels of pyruvate can inhibit the lactate dehydrogenase enzyme[37-39]. Although we did not test this hypothesis, it is possible that pyruvate inhibits LDH in our system as well. To test whether the ability of

UK5099 to destabilize HIF-1α is indeed due to its effects on mitochondria and not HIF-1α itself, we incubated cells with an iron chelator deferiprone with or without UK5099. Under iron chelation UK5099 failed to block the stabilization of HIF-1α, indicating that UK5099 cannot rescue iron deficiency.

Mitochondrial pyruvate metabolism increases

TCA cycle metabolites

Since many TCA cycle metabolites are known to stabilize HIF-1α, we questioned whether that would be a mechanism of HIF-1α stabilization in our model system. To identify possible metabolite(s) responsible for HIF-1α stabilization, we incubated HepG2 cells with pyruvate and glucose for 24 h and subjected the cells to metabolomics analysis using gas chromatography-mass spectrometry (GC-MS). All TCA metabolites that have been shown to inhibit PHDs were increased with pyruvate treatment. Succinate was increased by 3.8-fold, while fumarate and malate were increased by 6.8 and 12-fold respectively (Figure 3.5, A). In addition, we measured a 10-fold increase in 2-hyroxyglutarte levels. 2-hydroxyglutarete is a competitive inhibitor of prolyl hydroxylases, but in the presence of a high level of alpha ketoglutarate is unable to inhibit αKG-dependent dioxygenases[26, 40]. There was also a 59-fold increase in alpha ketoglutarate levels, which is a cofactor the in HIF-1α hydroxylation reaction. These findings are particularly surprising since αKG is known to alleviate pseudohypoxia induced by high levels of succinate and fumarate [41]. Since αKG was the most upregulated TCA metabolite in our screen, we suspected there could be an inhibition of alpha

ketoglutarate dehydrogenase (OGDH) enzyme. This was confirmed by assessment of enzymatic activity of OGDH in isolated mitochondria from cells incubated with either 10 mM glucose or pyruvate for 24 h. We found that OGDH activity is decreased by 80% after pyruvate treatment, while citrate synthase activity was decreased slightly (11%) (Figure 3.5, B). We wanted to know whether inhibition of OGDH and PDH, and therefore inhibition of the TCA cycle, will rescue the HIF-1α stabilization phenotype. Treatment with CPI 630, a lipoic acid derivative that inhibits OGDH and pyruvate dehydrogenase complex [42], was sufficient to block the induction of HIF-1α (Figure 3.5, C), confirming that functional TCA cycle is needed for stabilization of HIF-1α. High levels of αKG in our system suggested that succinate and fumarate are unlikely to mediate stabilization of HIF-1α due to their presumed competitive binding to PHDs against αKG. Nevertheless, we tested whether succinate, fumarate (methyl and ethyl esters), αKG, or citrate could stabilize HIF-1α in HepG2 cells. None of the tested metabolites could stabilize HIF-1α to the levels comparable with pyruvate (Figure 3.5, D). Interestingly, dimethyl ketoglutarate (2MKG), an ester of αKG that is widely used as cell permeable analog of αKG, stabilized HIF-1α, and this stabilization could not be blocked with UK5099 (Figure 3.6, A). This compound also induced mitophagy in Hela cells after 24 h incubation as measured by mito-Rosella[43] (Figure 3.6, B). It has been reported that 2MKG directly inhibits prolyl hydroxylases, independently of its property to increase intracellular αKG concentrations[44, 45].

Cellular production of pyruvate is sufficient to stabilize HIF-1α

In our initial experiments with HepG2 cells, significant stabilization of HIF-1α was achieved only with supraphysiological concentrations of pyruvate (2 to 10 mM), while cellular pyruvate levels are reported to be around 200 μM[46] and circulating pyruvate levels in blood are about 50 μM[47]. Although this is an interesting observation, it hardly could be applied to any physiological condition. In contrast to HepG2 cells, 10 mM glucose was sufficient to stabilize HIF-1α in Hela cells. Importantly, this observation is also dependent on pyruvate and its mitochondrial metabolism, since treatment with UK5099 completely abrogated stabilization of HIF-1α (Figure 3.3, A). This observation is particularly significant since it implies that stabilization of HIF-1α could be achieved with pyruvate derived from glycolysis. Since both glucose and pyruvate induced HIF-1α, as a control treatment for Hela cells we used all deficient (no carbon source) media or 10 mM glutamine containing media. Both media did not stabilize HIF-1α, nor induce expression of BNIP3 (Figure 3.3, D). Although glutamine should feed into the TCA cycle by glutaminolysis, it did not change HIF-1α protein levels, suggesting that mitochondrial metabolism per se is not sufficient to induce HIF-1α.

As another pharmacological inhibitor of the MPC complex, we used pioglitazone[48, 49], a member of thiazolidinedione family of insulin sensitizers. As expected, pioglitazone abrogated stabilization of both glucose and pyruvate induced HIF-1α stabilization and BNIP3 expression. To test whether pioglitazone inhibits HIF-1α stabilization by inhibition of MPC1 and not due to its PPAR-Y agonist properties, we incubated cells with 10 mM methyl and ethyl pyruvate with

and without pioglitazone. These esters can freely cross mitochondrial membranes and are cleaved in the matrix of mitochondria to generate pyruvate. In these settings pioglitazone was unable to block the stabilization of HIF-1α and BNIP3, confirming that HIF-1α stabilization is dependent on mitochondrial pyruvate metabolism (Figure 3.7). Furthermore, we noticed that pyruvate treatment in Hela cells induces selective degradation of OGDH, while HSP60 protein levels were not changed to the same extent. Moreover, addition of pioglitazone or NAC can restore the levels of OGDH, suggesting that this process is mediated by mitochondrial pyruvate metabolism and production of ROS (Figure 3.8).

Pyruvate metabolism induces ROS

Another widely reported mechanism of HIF-1α stabilization is mediated by Reactive Oxygen Species (ROS). Reactive oxygen species could inhibit prolyl hydroxylases and stabilize HIF-1α[50] or at least they are required for HIF-1α stabilization[51-54]. OGDH is a significant ROS producer and has been reported to be a source and a target of ROS[55-57]. Another closely related 2-oxoacid dehydrogenase complex, pyruvate dehydrogenase, has been reported to produce ROS as well[58]. To test whether this mechanism could be responsible for induction of HIF-1α stabilization in our model, we first tested whether pyruvate increases the mitochondrial membrane potential when compared to glucose in HepG2 cells (Figure 3.9, A). Pyruvate induced an increase in the mitochondrial membrane potential that can be reversed with addition of UK5099, indicating increase oxidative phosphorylation activity. As expected, superoxide production was

increased with pyruvate incubation as measured with dihydroethidium (DHE) staining, but UK5099 failed to decrease the amount of superoxide detected (Figure 3.9, B and C). Although this is counterintuitive, similar results were obtained by other groups as well and were attributed to antioxidant properties of pyruvate itself[59, 60]. Nevertheless, addition of the antioxidant N-acetyl cysteine (NAC) was sufficient to disrupt the stabilization of HIF-1α in HepG2 cells (Figure 3.9, D) and in Hela cells (not shown). Since UK5099 failed to decrease the production of ROS but was sufficient to stop the stabilization of HIF-1α, we speculate that ROS alone is not a sufficient to induce HIF-1α. Moreover, we treated the cells with antimycin and rotenone to induce ROS, and both drugs were unable to induce HIF-1α in HepG2 cells. Of interest, Rotenone and Antimycin treatment in combination with 10 mM pyruvate disrupted stabilization of HIF-1α.

Conclusion

In this body of work, we identified that mitochondrial pyruvate metabolism is sufficient to stabilize HIF-1α, and it can be regulated by manipulation of the mitochondrial pyruvate carrier. We also showed that antioxidants can abrogate this stabilization, although induction of ROS was not a sufficient condition to replicate HIF-1α stabilization. Surprisingly, feeding mitochondrial metabolism with succinate, fumarate, or αKG did not replicate HIF-1α stabilization, suggesting that TCA cycle entry point is critical for this phenomenon. Another possible mechanism that we did not test was the elevated levels of TCA cycle metabolites along with ROS and 2-hydroxyglutarate; perhaps they could all act in concert to stabilize HIF-

1α. This type of conditions could be virtually impossible to recreate. The observation that pioglitazone inhibits stabilization of HIF-1α is particularly interesting, since pioglitazone and other TZD family medications are still prescribed to treat diabetes.

Discussion

Stabilization of HIF-1α by low oxygen tension upregulates glycolytic genes[61] and reduces pyruvate utilization by mitochondria. This is partially mediated by inhibitory phosphorylation of pyruvate dehydrogenase by pyruvate dehydrogenase kinase and by increased shunting of pyruvate to lactate. In hypoxia, this phenomenon is critical for cellular homeostasis and serves to match the available oxygen to substrate oxidation. However, during pseudohypoxia, stabilization of HIF-1α under ample oxygen availability could not serve this purpose. Increased pyruvate uptake by mitochondria is thought to increase the activity of OXPHOS and as a byproduct, increase the production of reactive oxygen species[62, 63]. Here, we suggest that activation of hypoxic response by pyruvate metabolism could be a defense mechanism against excessive ROS production and cellular damage. We suggest that the hypoxic response is activated to limit the flow of pyruvate to mitochondria and limit the ROS production. Mitophagy mediated by HIF-1α could be another way to keep the mitochondrial pool healthier by degrading damaged mitochondria. A similar hypothesis has been tested by Melser and colleagues where they showed that cells grown on glutamine exhibit increased mitophagy mediated by RHEB and NIX, and abrogation of mitophagy results in more ROS

damage [64]. HIF mediated protective mechanisms against oxidative injury have been reported in kidney and intestine during ischemia and reperfusion[65, 66] . Moreover, it has been shown that metabolic reprogramming by HIF-1α reduces ROS levels in murine cancer models as well[67].

Traditionally, stabilization of HIF-1α by means other than hypoxia has been considered a pathological state. Our observation that mitochondrial pyruvate metabolism can stabilize HIF-1α even when cells are treated with 10 millimolar glucose is interesting. It is possible that low steady state levels of HIF-1α can contribute to mitochondrial homeostasis by activating basal mitophagy and by regulating pyruvate flow to mitochondria. Moreover, we show that pioglitazone, a diabetes medication that is still in use, could reverse mitochondrial pyruvate induced HIF-1α stabilization. Pioglitazone and other medications of the same family have an extensive list of side effects ranging from bone density lose to fluid retention and cardiovascular risks. It remains to be studied whether beneficial or side effects of TZDs are somehow connected to their ability to inhibit stabilization of HIF-1α.

Materials and methods

Cell culture

Hela, HEK-293, HepG2, and SH-SY5Y cells were from ATCC (American Type Culture Collection), and cultured in DMEM (Life Technologies) with 10% heat-inactivated fetal bovine serum (Atlanta Biologicals), penicillin, and streptomycin (Life Technologies), and maintained in a 5% CO_2, 37^{O}C humidified incubator.

Custom formulated media was made by addition of different carbon sources to DMEM without glucose, pyruvate, and amino acids (US Biological) and pH was corrected to 7.4. Methyl and ethyl pyruvate, pyruvate, glucose, galactose, dimethyl alpha-ketoglutarate, dimethyl and diethyl esters of succinate and fumarate, were obtained from Sigma.

Expression plasmids and siRNA transfection

Mito-Rosella was previously described[43]. Briefly, cells were seeded in 12 well plates and transfected with mito-Rosella upon 80% confluency. Cells were transfected with Polyjet transfection reagent (Signagen). After 48 h cells were washed with PBS twice and incubated with experimental media, with addition of E64/Leupepeptin cocktail, to prevent lysosomal degradation. Cells were assessed for mitophagy after 24 h incubation and imaged with EVOS-fi inverted LED fluorescence microscope. ImageJ software were used for quantitative analysis. SiRNA transfections were carried out with Rnaimax transfection reagent (Invitrogen), per manufacturer's instruction. Gene knockout was tested after 48 h of incubation. SiRNAs HIF-1α and scrambled control were purchased from Invitrogen. SiRNA against BNIP3 were synthesized in University of Utah DNA synthesis core and had the following sequence: 5'-GGACGAAGUAGCUCCAAGATT-3 and (reverse) 5'-UCUUGGAGCUACUUCGUCCTT-3'.

Mitochondrial membrane potential and ROS production assessment

Mitochondrial membrane potential and ROS production were measured by TMRE and DHE (Life Technologies), per the manufacturer's instructions, using a BD FACSCanto analyzer on high throughput mode. For ROS production analysis, cells were grown on 12 well plates until reaching 90% confluency and loaded with DHE for 15 min, washed 3 times with PBS and incubated with experimental media for indicated durations. For TMRE fluorescence intensity analysis, cells first were incubated with experimental conditions for 6 h, then incubated with TMRE for 15 min. Cells were harvested for analysis by washing twice with PBS, trypsinizing and transferring to 96 well plate wells containing 0.3 mL PBS and fluorescent intensities were measured by FCM. For all conditions, 3 biological replicates with at least 10000 cells were used. Oligomycin and CCCP were used as positive and negative controls for TMRE. Antimycin A and antimycin A plus NAC were used as controls for DHE experiments.

Antibodies and chemicals

Primary antibodies used in this study: mouse anti-HIF1α(# 610958), rabbit anti-BNIP3, rabbit anti-LC3A/B, rabbit anti-HSP60, rabbit anti-MPC1, rabbit anti-OGDH (Cell Signaling, #44060S, #4108S, #12165S, #14462S, and #13407S); mouse anti-TIM23 (1:1000, BD Biosciences, product #611222); mouse anti-VDAC1, mouse anti-TOM20, rabbit anti-SDHB (Santa Cruz, 1: 500, sc-58649, sc-17764, sc-25851); rabbit anti-ATP synthase gamma (GeneTex, product #GTX-

114275), rabbit anti-FUNDC1(Aviva Systems Biology, # ARP53280_P050) mouse anti-βTubulin (Genescript, product # A01410). Secondary antibodies were: HPR conjugated goat anti-rabbit and goat anti-mouse (1:2500, products #170-6515 and #172-1011, respectively). Bafilomycin A1 was obtained from LC Laboratories. Mitotracker Deep Red FM, DHE, TMRE, and Hoechst 33342 were obtained from Life Technologies. 3-Hydroxy-1,2-dimethyl-4(1H)-pyridone (Diferiprone) was from Sigma. Echniomycin, UK5099 and pioglitazone were purchased from Cayman Chemicals. Rosiglitazone and ciglitazone were purchased from Sigma.

Western blot analysis

Cells were washed with phosphate buffered saline twice and scraped off the plate with RIPA buffer (Santa-Cruz) containing protease/phosphatase cocktail (Santa-Cruz). Lysates were incubated on ice for 30 min with gentle, constant agitation, then centrifuged at 12,000 ×g for 20 min at 4 ºC to pellet nuclei and other insoluble material. Equal amount of proteins were reconstituted in Novex sample buffer and heated 10 min at 90ºC. SDS-PAGE was performed on 4-12% Tris-Bis gels (Life Technologies) with MES-based running buffer containing antioxidant additive, per the manufacturer's instructions. Gels were transferred to nitrocellulose (iBlot system, Life technologies). Nitrocellulose membranes were blocked with 5% BSA in TBS containing 0.2% Tween 20, and incubated with primary antibodies overnight. The following day membranes were washed and incubated with HPR conjugated secondary antibodies for an hr. GeneGnome imager (Syngene) was used for imaging of western blot membranes and band

intensities were quantified using Gene Snap software (Syngene).

Metabolomics

Cells were trypsinized and washed twice with ice-cold PBS and snap frozen in liquid nitrogen. Metabolites were extracted with 90% methanol and dried in a speed-vac. Analysis was performed with a Waters GCT Premier mass spectrometer coupled with an Agilent 6890 gas chromatograph and a Gerstel MPS2 auto sampler. Data were collected and analyzed using QuanLynx, and MassLynx 4.1 software. For all conditions, at least five biological replicates were analyzed.

Enzyme activity assays

Semipure mitochondria obtained by differential centrifugation were used for citrate synthase and OGDH activity assays. The citrate synthase activity assay was obtained from Sigma. The OGDH activity assay was performed as described in Lei and Cooper[68].

References

1. Vander Heiden, M. G. *et al.* Understanding the Warburg effect: the metabolic requirements of cell proliferation. *Science* **324**, 1029-1033 (2009).

2. Altenberg, B. & Greulich, K. O. Genes of glycolysis are ubiquitously overexpressed in 24 cancer classes. *Genomics* **84**, 1014-1020 (2004).

3. Lunt, S. Y. & Vander Heiden, M. G. Aerobic Glycolysis: meeting the metabolic requirements of cell proliferation. *Annu. Rev. Cell Dev. Biol.* **27**, 441-464 (2011).

4. Folmes, C. D. *et al.* Energy metabolism plasticity enables stemness programs. *Ann. N. Y. Acad. Sci.* **1254**, 82-89 (2012).

5. Ito, K. & Suda, T. Metabolic requirements for the maintenance of self-renewing stem cells. *Nat. Rev. Mol. Cell Biol.* **15**, 243-256 (2014).

6. Warburg, O. *et al.* The metabolism of tumors in the body. *J. Gen. Physiol.* **8**, 519-530 (1927).

7. Denko, N.C. Hypoxia, HIF1 and glucose metabolism in the solid tumour. *Nat. Rev. Cancer* **8**, 705-713 (2008).

8. Ivan, M. *et al.* HIFalpha targeted for VHL-mediated destruction by proline hydroxylation: implications for O2 sensing. *Science* **292**, 464-468 (2001).

9. Jaakkola, P. *et al.* Targeting of HIF-alpha to the von Hippel-Lindau ubiquitylation complex by O2-regulated prolyl hydroxylation. *Science* **292**, 468-472 (2001).

10. Bruick, R. K. & McKnight, S. L. A conserved family of prolyl-4-hydroxylases that modify HIF. *Science* **294**, 1337-1340 (2001).

11. Mahon, P. C. *et al.* FIH-1: a novel protein that interacts with HIF-1alpha and VHL to mediate repression of HIF-1 transcriptional activity. *Genes Dev.* **15**, 2675-2686 (2001).

12. Lando, D. *et al.* FIH-1 is an asparaginyl hydroxylase enzyme that regulates the transcriptional activity of hypoxia-inducible factor. *Genes Dev.* **16**, 1466-1471 (2002).

13. Kim, J. W. *et al.* HIF-1-mediated expression of pyruvate dehydrogenase kinase: a metabolic switch required for cellular adaptation to hypoxia. *Cell Metab.* **3**, 177-185 (2006).

14. Papandreou, I. *et al.* HIF-1 mediates adaptation to hypoxia by actively

downregulating mitochondrial oxygen consumption. *Cell Metab.* **3**, 187-197.

15. Koivunen, P. *et al.* Inhibition of hypoxia-inducible factor (HIF) hydroxylases by citric acid cycle intermediates: possible links between cell metab. and stabilization of HIF. *J. Biol. Chem.* **282**, 4524-4532 (2007).

16. Hewitson, K. S. *et al.* Structural and mechanistic studies on the inhibition of the hypoxia-inducible transcription factor hydroxylases by tricarboxylic acid cycle intermediates. *J. Biol. Chem.* **282**, 3293-3301 (2007).

17. Baysal, B. E. *et al.* Mutations in SDHD, a mitochondrial complex II gene, in hereditary paraganglioma. *Science* **287**, 848-851 (2000).

18. Niemann, S. & Muller, U. Mutations in SDHC cause autosomal dominant paraganglioma, type 3. *Nat. Genet.* **26**, 268-270 (2000).

19. Tomlinson, I. P. *et al.* Germline mutations in FH predispose to dominantly inherited uterine fibroids, skin leiomyomata and papillary renal cell cancer. *Nat. Genet.* **30**, 406-410 (2002).

20. Yan, H. *et al.* IDH1 and IDH2 mutations in gliomas. *N. Engl. J. Med.* **360**, 765-773 (2009).

21. Selak, M. A. *et al.* Succinate links TCA cycle dysfunction to oncogenesis by inhibiting HIF-alpha prolyl hydroxylase. *Cancer Cell* **7**, 77-85 (2005).

22. King, A. *et al.* Succinate dehydrogenase and fumarate hydratase: linking mitochondrial dysfunction and cancer. *Oncogene* **25**, 4675-4682 (0000).

23. Sudarshan, S. *et al.* Fumarate hydratase deficiency in renal cancer induces glycolytic addiction and hypoxia-inducible transcription factor 1alpha stabilization by glucose-dependent generation of reactive oxygen species. *Mol. Cell. Biol.* **29**, 4080-4090 (2009).

24. Izquierdo-Garcia, J. L. *et al.* IDH1 mutation induces reprogramming of pyruvate metabolism. *Cancer Res.* **75**, 2999-3009 (2015).

25. Dang, L. *et al.* Cancer-associated IDH1 mutations produce 2-hydroxyglutarate. *Nature* **462**, 739-744 (2009).

26. Xu, W. *et al.* Oncometabolite 2-hydroxyglutarate is a competitive inhibitor of alpha-ketoglutarate-dependent dioxygenases. *Cancer Cell* **19**, 17-30 (2011).

27. Sullivan, L. B. *et al.* The proto-oncometabolite fumarate binds glutathione to amplify ROS-dependent signaling. *Mol. Cell* **51**, 236-248 (2013).

28. Lu, H. *et al.* Hypoxia-inducible factor 1 activation by aerobic glycolysis

implicates the Warburg effect in carcinogenesis. *J. Biol. Chem.* **277**, 23111-23115 (2002).

29. Lu, H. *et al.* Reversible inactivation of HIF-1 prolyl hydroxylases allows cell metab. to control basal HIF-1. *J. Biol. Chem.* **280**, 41928-41939 (2005).

30. Zhang, H. *et al.* Mitochondrial autophagy is an HIF-1-dependent adaptive metabolic response to hypoxia. *J. Biol. Chem.* **283**, 10892-10903 (2008).

31. Zhang, J. & Ney, P. A. Role of BNIP3 and NIX in cell death, autophagy, and mitophagy. *Cell Death Differ.* **16**, 939-946 (2009).

32. Band, M. *et al.* Hypoxia-induced BNIP3 expression and mitophagy: in vivo comparison of the rat and the hypoxia-tolerant mole rat, Spalax ehrenbergi. *FASEB J.* **23**, 2327-2335 (2009).

33. Halestrap, A. P. The mitochondrial pyruvate carrier. kinetics and specificity for substrates and inhibitors. *Biochem. J.* **148**, 85-96 (1975).

34. Bricker, D. K. *et al.* A mitochondrial pyruvate carrier required for pyruvate uptake in yeast, Drosophila, and humans. *Science* **337**, 96-100 (2012).

35. Hubbi, M. E. *et al.* Chaperone-mediated autophagy targets hypoxia-inducible factor-1α (HIF-1α) for lysosomal degradation. *J. Biol. Chem.* **288**, 10703-10714 (2013).

36. Firth, J. D., Ebert, B. L., Pugh, C. W. & Ratcliffe, P. J. Oxygen-regulated control elements in the phosphoglycerate kinase 1 and lactate dehydrogenase A genes: similarities with the erythropoietin 3' enhancer. *Proc. Natl. Acad. Sci. U.S.A.* **91**, 6496-6500 (1994).

37. Coulson, C. J. & Rabin, B. R. Inhibition of lactate dehydrogenase by high concentrations of pyruvate: The nature and removal of the inhibitor. *FEBS Lett.* **3**, 333-337 (1969).

38. Gutfreund, H. *et al.* The kinetics of the reversible inhibition of heart lactate dehydrogenase through the formation of the enzyme–oxidized nicotinamide–adenine dinucleotide–pyruvate compound. *Biochem. J.* **106**, 683-687 (1968).

39. Wang, C. S. Inhibition of human erythrocyte lactate dehydrogenase by high concentrations of pyruvate. Evidence for the competitive substrate inhibition. *Eur. J. Biochem.* **78**, 569-574 (1977).

40. Evans, B., Griner, E. & Reproducibility Project: Cancer, B. Registered report: Oncometabolite 2-hydroxyglutarate is a competitive inhibitor of alpha-ketoglutarate-dependent dioxygenases. *Elife* **4**, e07420 (2015).

41. MacKenzie, E. D. *et al.* Cell-permeating alpha-ketoglutarate derivatives alleviate pseudohypoxia in succinate dehydrogenase-deficient cells. *Mol. Cell. Biol.* **27**, 3282-3289 (2007).

42. Stuart, S. D. *et al.* A strategically designed small molecule attacks alpha-ketoglutarate dehydrogenase in tumor cells through a redox process. *Cancer Metab* **2**, 4 (2014).

43. Sargsyan, A. *et al.* Rapid parallel measurements of macroautophagy and mitophagy in mammalian cells using a single fluorescent biosensor. *Sci. Rep.* **5**, 12397 (2015).

44. Hou, P. *et al.* Intermediary metabolite precursor dimethyl-2-ketoglutarate stabilizes hypoxia-inducible factor-1alpha by inhibiting prolyl-4-hydroxylase PHD2. *PLoS One* **9**, e113865 (2014).

45. Kuo, C. Y. *et al.* HIF-1-alpha links mitochondrial perturbation to the dynamic acquisition of breast cancer tumorigenicity. *Oncotarget* **7**, 34052-34069 (2016).

46. Zhu, A. *et al.* A sensitive fluorimetric assay for pyruvate. *Anal. Biochem.* **396**, 146-151 (2010).

47. Landon, J., Fawcett, J. K. & Wynn, V. Blood pyruvate concentration measured by a specific method in control subjects. *J. Clin. Pathol.* **15**, 579-584 (1962).

48. Divakaruni, A. S. *et al.* Thiazolidinediones are acute, specific inhibitors of the mitochondrial pyruvate carrier. *Proc. Natl. Acad. Sci. U. S. A.* **110**, 5422-5427 (2013).

49. Colca, J. R. *et al.* Identification of a mitochondrial target of thiazolidinedione insulin sensitizers (mTOT)—relationship to newly identified mitochondrial pyruvate carrier proteins. *PLoS One* **8**, e61551 (2013).

50. Jung, S. N. *et al.* Reactive oxygen species stabilize hypoxia-inducible factor-1 alpha protein and stimulate transcriptional activity via AMP-activated protein kinase in DU145 human prostate cancer cells. *Carcinogenesis* **29**, 713-721 (2008).

51. Brunelle, J. K. *et al.* Oxygen sensing requires mitochondrial ROS but not oxidative phosphorylation. *Cell Metab.* **1**, 409-414 (2005).

52. Guzy, R. D. *et al.* Mitochondrial complex III is required for hypoxia-induced ROS production and cellular oxygen sensing. *Cell Metab*. **1**, 401-408 (2005).

53. Mansfield, K. D. *et al.* Mitochondrial dysfunction resulting from loss of

cytochrome c impairs cellular oxygen sensing and hypoxic HIF-alpha activation. *Cell Metab.* **1**, 393-399 (2005).

54. Chandel, N. S. *et al.* Reactive oxygen species generated at mitochondrial complex III stabilize hypoxia-inducible factor-1alpha during hypoxia: a mechanism of O2 sensing. *J. Biol. Chem.* **275**, 25130-25138 (2000).

55. Tretter, L. & Adam-Vizi, V. Alpha-ketoglutarate dehydrogenase: a target and generator of oxidative stress. *Philos. Trans. R. Soc. Lond. B. Biol. Sci.* **360**, 2335-2345 (2005).

56. Starkov, A. A. *et al.* Mitochondrial alpha-ketoglutarate dehydrogenase complex generates reactive oxygen species. *J. Neurosci.* **24**, 7779-7788 (2004).

57. Tretter, L. & Adam-Vizi, V. Generation of reactive oxygen species in the reaction catalyzed by alpha-ketoglutarate dehydrogenase. *J. Neurosci.* **24**, 7771-7778 (2004).

58. Quinlan, C. L. *et al.* The 2-oxoacid dehydrogenase complexes in mitochondria can produce superoxide/hydrogen peroxide at much higher rates than complex I. *J. Biol. Chem.* **289**, 8312-8325 (2014).

59. Schell, J. C. *et al.* A role for the mitochondrial pyruvate carrier as a repressor of the Warburg effect and colon cancer cell growth. *Mol. Cell* **56**, 400-413 (2014).

60. Zhong, Y. *et al.* Application of mitochondrial pyruvate carrier blocker UK5099 creates metabolic reprogram and greater stem-like properties in LnCap prostate cancer cells *in vitro*. *Oncotarget* **6**, 37758-37769 (2015).

61. Semenza, G. L. *et al.* Transcriptional regulation of genes encoding glycolytic enzymes by hypoxia-inducible factor 1. *J. Biol. Chem.* **269**, 23757-23763 (1994).

62. Yu, T. *et al.* Increased production of reactive oxygen species in hyperglycemic conditions requires dynamic change of mitochondrial morphology. *Proc. Natl. Acad. Sci. U. S. A.* **103**, 2653-2658 (2006).

63. Kowaltowski, A. J. *et al.* Mitochondria and reactive oxygen species. *Free Radic. Biol. Med.* **47**, 333-343 (2009).

64. Melser, S. *et al.* Rheb regulates mitophagy induced by mitochondrial energetic status. *Cell Metab.* **17**, 719-730 (2013).

65. Kojima, I. *et al.* Protective Role of Hypoxia-Inducible Factor-2α against Ischemic Damage and Oxidative Stress in the Kidney. *J. Am. Soc. Nephrol.* **18**, 1218-1226 (2007).

66. Hart, M. L. *et al.* Hypoxia-inducible factor-1α–dependent protection from intestinal ischemia/reperfusion injury involves ecto-5′-nucleotidase (CD73) and the A2B adenosine receptor. *J. Immunol. (Baltimore, Md. : 1950)* **186**, 10.4049/jimmunol.0903617 (2011).

67. Zhao, T. *et al.* HIF-1-mediated metabolic reprogramming reduces ROS levels and facilitates the metastatic colonization of cancers in lungs. *Sci. Rep.* **4**, 3793 (2014).

68. Lai, J. C. K. & Cooper, A. J. L. Brain α-Ketoglutarate dehydrogenase complex: kinetic properties, regional distribution, and effects of inhibitors. *J. Neurochem.* **47**, 1376-1386 (1986).

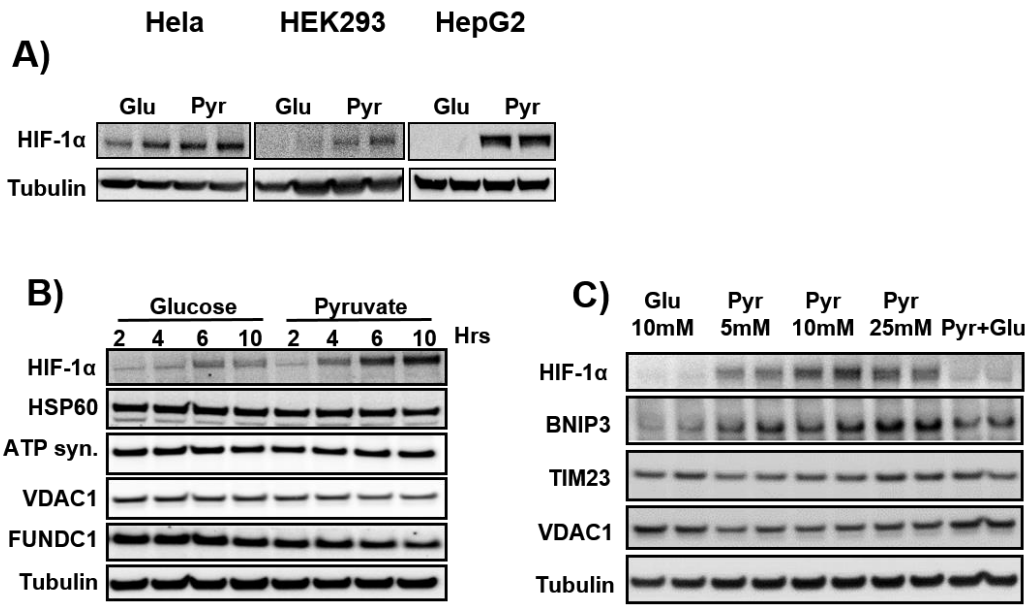

Figure 3.1. Pyruvate stabilizes HIF-1α and induces expression of BNIP3
A) Hela, HEK 293 and HepG2 cells were treated for 24 h with either 10mM of glucose or 10 mM pyruvate and HIF-1α stabilization was assessed by western blots. Pyruvate stabilized HIF-1α in all cell lines, while glucose stabilized HIF-1α in Hela cells**. B)** HepG2 cells were treated with 10 mM glucose and 10 mM pyruvate for indicated times. Pyruvate induced stabilization of HIF-1α while reducing mitochondrial proteins HSP60, VDAC1, and FUNDC1. C**)** Dose dependent stabilization of HIF-1α and BNIP3 expression by pyruvate in HepG2 cells after 24 h of treatment. Addition of 10 mM glucose to 10 mM pyruvate completely abrogates stabilization of HIF-1α and decreases the expression of BNIP3. Increased pyruvate concentration correlates with decreased mitochondrial proteins TIM23 and VDAC1.

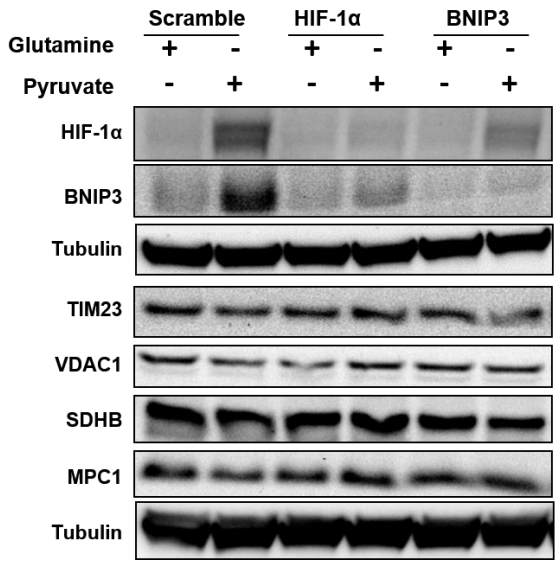

Figure 3.2. Expression of BNIP3 and mitophagy are mediated by HIF-1α: Hela cells were transfected with siRNAs against HIF-1α and BNIP3 and after 48 h were incubated with 10 mM glutamine or 10 mM pyruvate. After 24 h cells were harvested and western blot was performed. In the absence of HIF-1α pyruvate was unable to increase the expression of BNIP3. There is also marked increase in MPC1, TIM23 and SDHB proteins in the absence of HIF-1α.

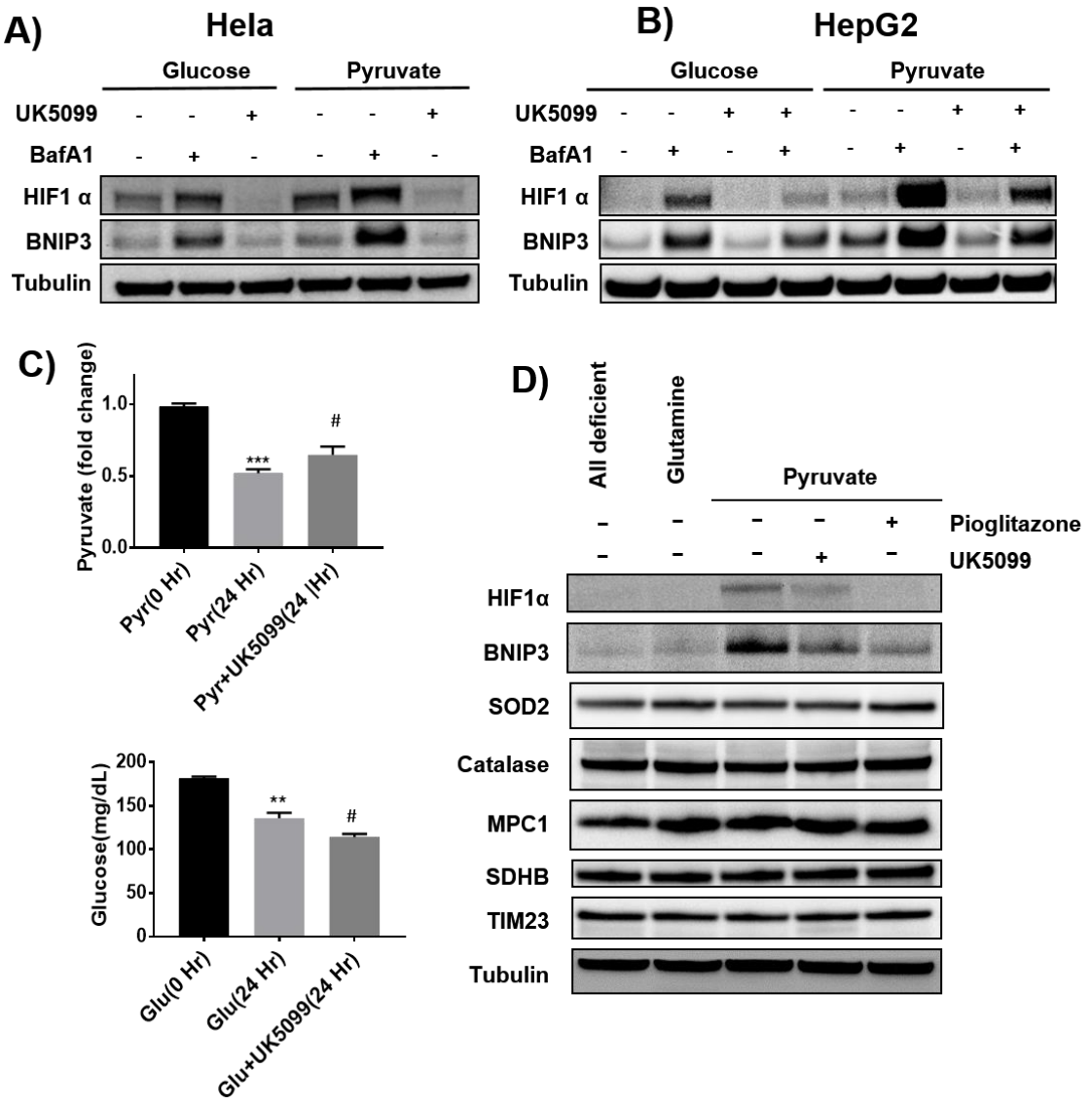

Figure 3.3. HIF-1α stabilization is dependent on mitochondrial pyruvate metabolism: A). Hela cells were incubated for 24 h with either 10mM of glucose or 10 mM pyruvate and HIF-1α stabilization and BNIP3 expression was assessed by WB. With both treatments 200 nM UK5099 blocked the stabilization of HIF-1α and decreased the expression of BNIP3**. B)** HepG2 cells were incubated for 24 h with either 10mM of glucose or pyruvate and HIF-1α stabilization and BNIP3 expression was assessed by WB. 200 nM UK5099 could block the stabilization of HIF-1α. **C)** Clearance of pyruvate and glucose from media after 24 h incubation with UK5099 **D)** Starvation or 10mM Glutamine do not stabilize HIF-1α and BNIP3, indicating that mitochondrial metabolism (TCA cycle) is not sufficient for induction of HIF-1α. In contrast, UK5099 and pioglitazone can downregulate the stabilization of HIF-1α and BNIP3.

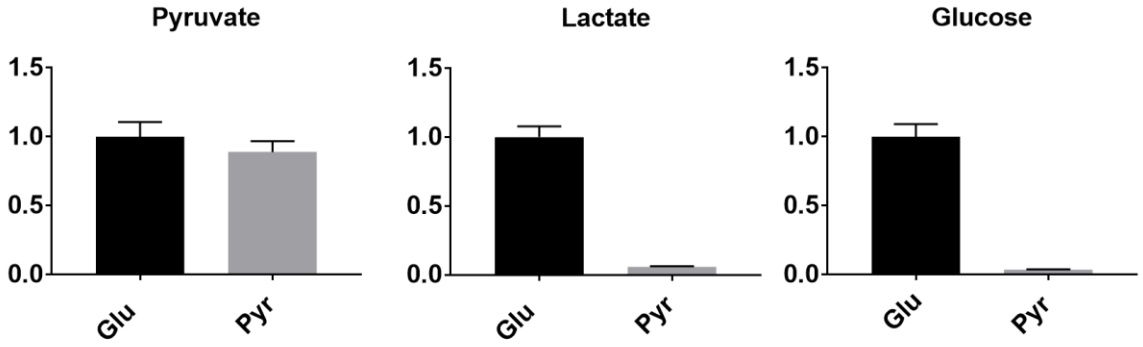

Figure 3.4. Glucose and glycolysis product levels: Pyruvate, lactate, and glucose levels in glucose and pyruvate treated HepG2 cells after 24 h. Pyruvate levels are not different, indicating that majority of cellular pyruvate is converted to TCA cycle intermediates. Lactate is almost undetectable in pyruvate treated cells. As expected there was no glucose present in pyruvate treated cells.

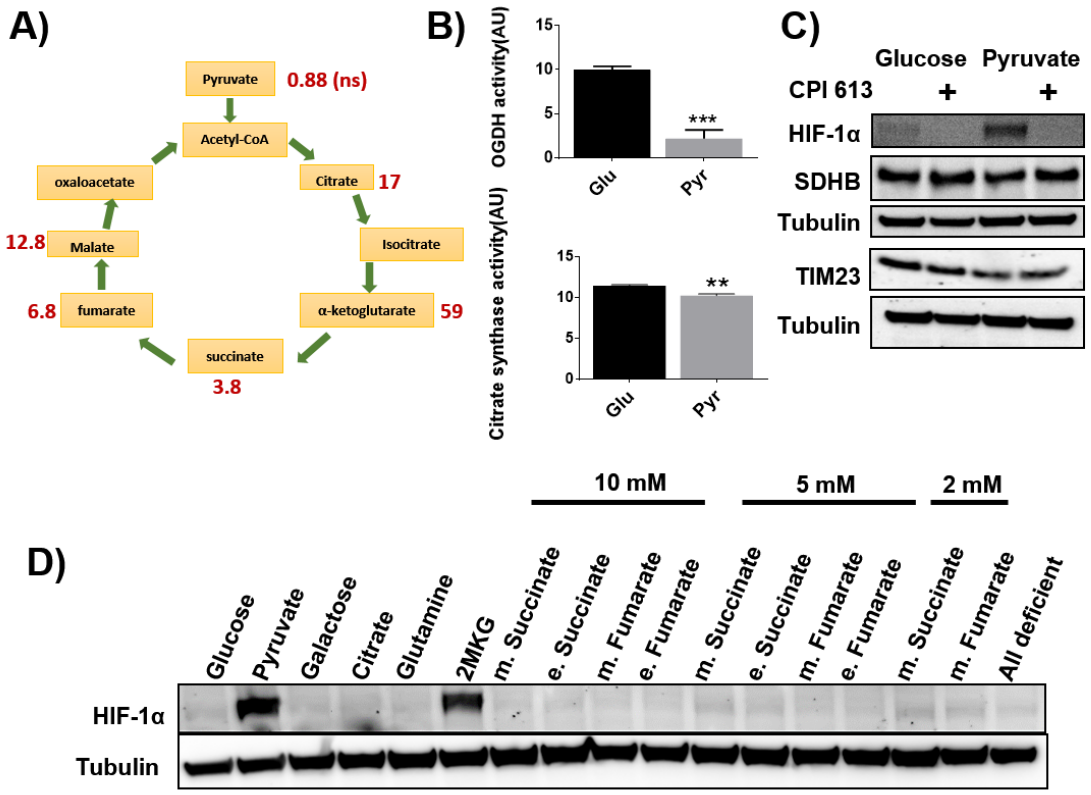

Figure 3.5. Pyruvate metabolism inhibits OGDH in HepG2 cells: A) Fold changes of metabolites (Pyr treated/ Glu treated) after 24 h of incubation with Glucose or Pyruvate. **B)** Enzymatic activity of OGDH and citrate synthase after 24 h of incubation with 10 mM Glucose or Pyruvate. **C)** Pyruvate dehydrogenase (PDH) and α-ketoglutarate dehydrogenase (OGDH) inhibitor CPI 613 abrogates stabilization of HIF-1α and restores mitochondrial protein levels **D)** Stabilization of HIF-1α is not replicated with either succinate and fumarate, citrate (10 mM), glutamine (10 mM). ***p<0.0005, **p<0.005, calculated by student's t-test.

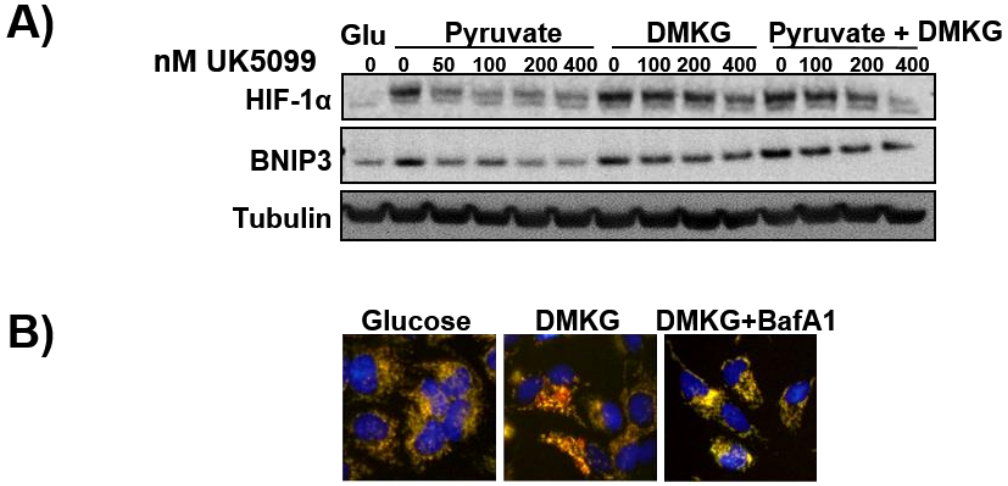

Figure. 3.6. Dimethyl 2-ketoglutarate induces stabilization of HIF-1α and mitophagy. **A)** HepG2 cells were treated with either 10 mM pyruvate or 2 mM of dimethyl 2-ketoglutarate (DMKG) separately or together, with varying concentrations of UK5099 and HIF-1α stabilization and BNIP3 expression were assessed after 24 h with western blotting. UK5099 can inhibit stabilization of HIF-1α induced by pyruvate, but not HIF-1α induced by DMKG or DMKG or pyruvate. **B)** Representative images of mito-Rosella transfected Hela cells, treated either with 10 mM glucose or 2mM DMKG with and without 100 nM of Bafilomycin A1. Red fluorescence corresponds to mitochondria delivered to lysosomes for degradation.

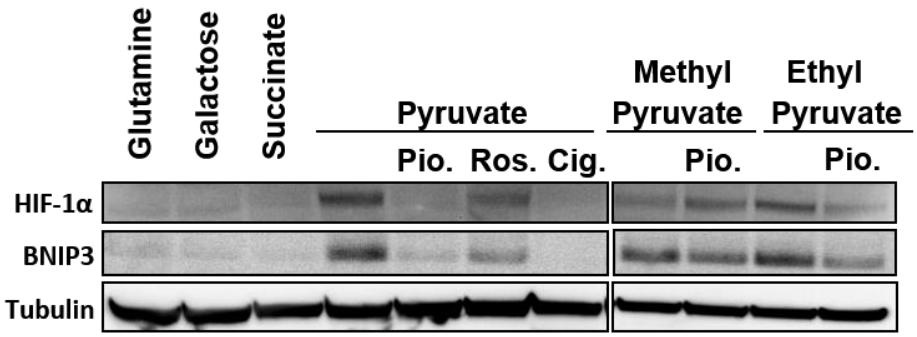

Figure 3.7. TZDs are effective inhibitors of pyruvate mediated pseudohypoxia. Hela cells were treated with indicated carbon source and pyruvate with and without pioglitazone, rosiglitazone and ciglitazone. All three could inhibit stabilization of HIF-1α and BNIP3, with Rosiglitazone being the least effective. Pioglitazone was not sufficient to inhibit stabilization of HIF-1α induced by esters of pyruvate, indicating that mitochondrial pyruvate metabolism is essential for the stabilization of HIF-1α.

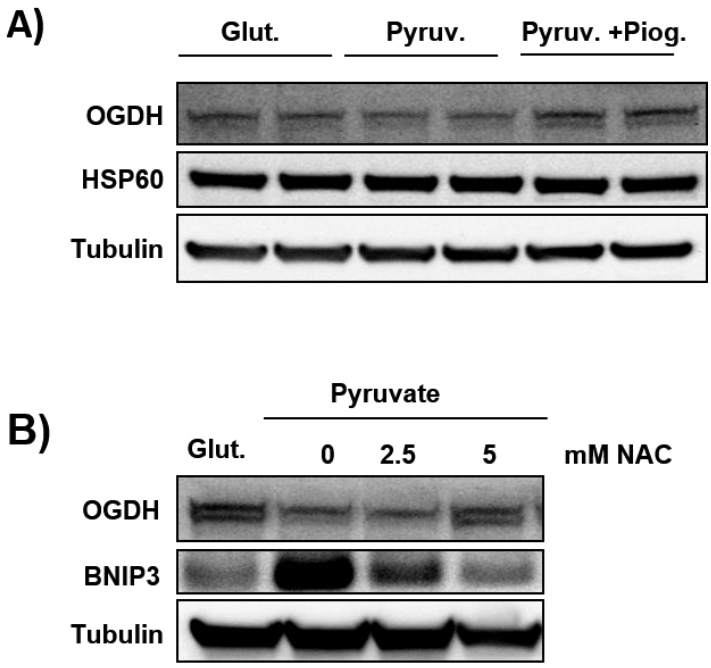

Figure 3.8. Pyruvate induces degradation of OGDH that is reversed by pioglitazone and NAC. A) Hela cells were incubated with 10 mM of glutamine or pyruvate and pyruvate plus 10 µM pioglitazone for 24 h and western blot was performed. Pyruvate induces decrease in OGDH that can be reversed with pioglitazone. **B)** Hela cells were incubated with 10 mM of glutamine or pyruvate with increasing concentration of NAC. 5 mM NAC is sufficient to block the degradation of OGDH.

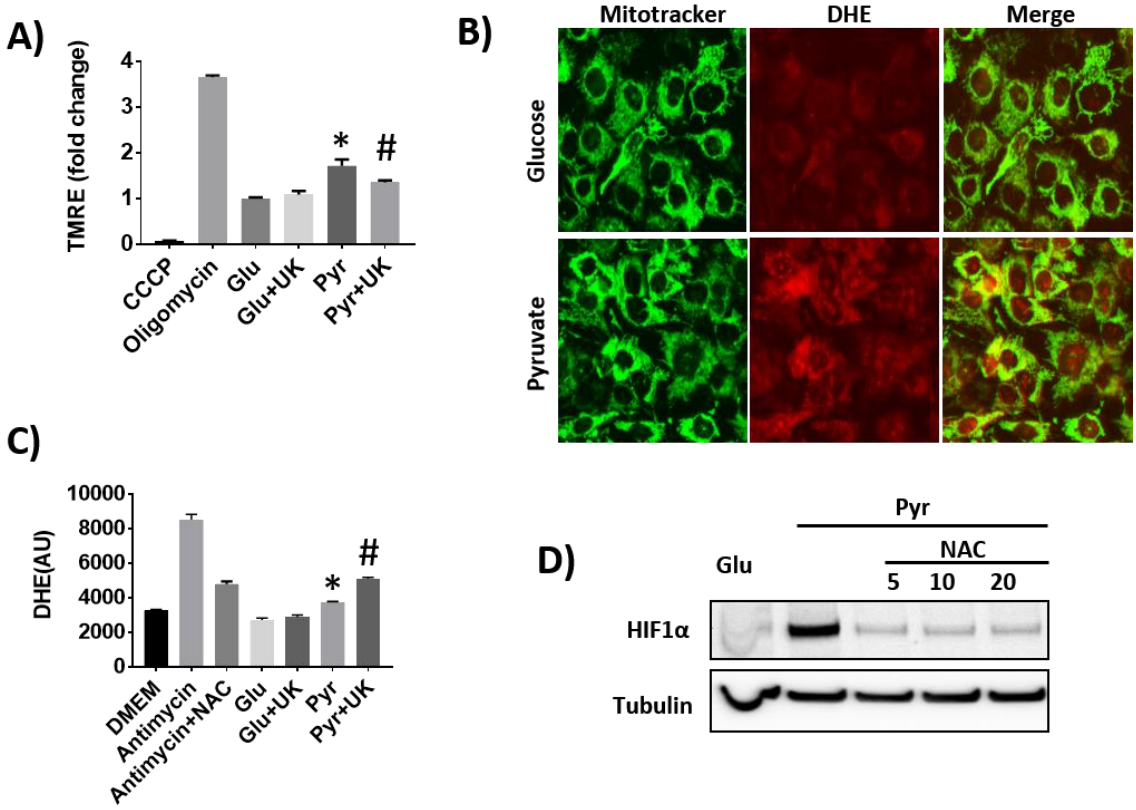

Figure 3.9. Pyruvate metabolism increases ROS production: A) TMRE fluorescence intensities as measured with flow cytometry after 6 h incubation with indicated conditions, pyruvate induces increase in mitochondrial membrane potential in HepG2 cells. **B)** Representative images of Mitotracker Deep Red FM and DHE loaded HepG2 cells after 6 h of incubation with 10 mM glucose or pyruvate. **C)** DHE fluorescence intensities as measured with flow cytometry after 6 h incubation with indicated conditions. **D**) Antioxidant NAC blocks the stabilization of HIF-1α. *p< 0.05 between pyruvate and glucose treated cells, #p< 0.05 between pyruvate and pyruvate plus UK5099 treated cells.

CHAPTER 4

CONCLUSION

Mito-Rosella

Mitochondrial quality control and particularly mitochondrial degradation recently has gained more attention as a significant component of cellular and organismal homeostasis. In the last decade, there were many substantial discoveries connecting mitophagy to human disease. Identification of Parkinson's disease related proteins PINK1 and Parkin involvement in mitochondrial degradation is one example. Moreover, PINK1 and Parkin are now shown to be involved in many other physiological and pathophysiological processes such as cancers[1-4] and heart function [5-8]. BNIP3, another mitophagic protein, is implicated in liver health and BNIP3 deficient mice exhibit increased inflammation and steatohepatitis[9] . Together these findings underline the importance of mitophagy in human health and disease. Despite to these important findings, our understanding of mitophagy is not complete. This partly could be explained by the limited scope of the methods used to identify mitophagy. In this body of work, we have developed pH sensor, Rosella-based rapid and sensitive method of mitophagy detection that detects delivery of mitochondria to functional lysosomes. Moreover, this method could be applied to single cell analysis as well as to high throughput screenings and allows direct comparison of mitophagy to autophagy. Single cell analysis is particularly useful in applications that induce minimal mitophagy, while high throughput analysis is suitable for more robust mitophagy inducers like iron chelation and CCCP. Additionally, this method allows for continuous monitoring of mitophagy in cells, since it does not require cell fixation. Currently, the method we developed is used in number of laboratories across the

world to identify new regulators of mitophagy. Additionally, there are efforts to develop transgenic mouse expressing mito-Rosella. This will allow researchers to examine mitophagy at an organismal levels in various murine disease models. Furthermore, mito-Rosella was instrumental in identification of pyruvate as an inducer of HIF-1α and mitophagy that was described in Chapter 3.

Mitochondrial pyruvate metabolism induces pseudohypoxia and mitophagy

Stabilization of hypoxia inducible factor 1α is indispensable for adaptations to hypoxia. However, HIF-1α is also implicated in tumorigenesis and proliferation of cancer cells. In different tumors and experimental cancer models, HIF-1α can be stabilized by several mechanisms, including hypoxia, mutations in HIF-1α degradation pathway genes, and aberrant accumulation of TCA cycle metabolites and byproducts. It has been shown that glycolysis end products can also stabilize HIF-1α by direct inhibition of prolyl hydroxylases. In this report, we uncovered yet another mechanism of HIF-1α stabilization that requires mitochondrial pyruvate metabolism. Moreover, we showed that inhibition of the mitochondrial pyruvate carrier by UK5099 or by pioglitazone can restore the degradation of HIF-1α. This stabilization is also dependent on the presence of reactive oxygen species since antioxidant NAC and ascorbic acid can restore the degradation of HIF-1α. Interestingly, feeding mitochondria with substrates such as succinate, fumarate, and glutamine is not sufficient to induce stabilization. We conclude that mitochondrial metabolism itself is not sufficient to induce stabilization of HIF-1α,

and specifically requires pyruvate as a substrate. Moreover, we showed that pyruvate that is derived from glycolysis is sufficient to induce this process. The last observation is particularly interesting since it implies that stabilization of HIF-1α could potentially take place in normal cellular conditions without external sources of pyruvate.

Future directions

Why does pyruvate induce stabilization of HIF-1α? Mitochondrial pyruvate metabolism increases OXPHOS activity by supplying NADH and $FADH_2$. This, in turn, should increase the production of ROS by OXPHOS, which is damaging to mitochondria themselves as well as to other cellular compartments. Stabilization of HIF-1α could limit the damaging effects of ROS by two distinct mechanisms. First, since HIF-1α induces mitophagy, it is possible that stabilization of HIF-1α and subsequent mitophagy are designed to digest defective mitochondria that arise from ROS damage. Second, HIF-1α is also known to inhibit oxidative metabolism by upregulation of glycolysis and by inhibition of pyruvate dehydrogenase complex that results in decreased pyruvate uptake by mitochondria. Future studies will determine whether HIF-1α plays protective role from ROS damage. Additionally, the observation that pioglitazone and other TZD members can inhibit stabilization of HIF-1α by pyruvate opens several questions that remains to be studied. Are TZDs' abilities to inhibit mitochondrial pyruvate metabolism and promote degradation of HIF-1α involved in their pharmacological effects? Could they be used to promote HIF-1α degradation and decrease tumor burden in SDHB and FH

mutated cancer models? We believe that these questions warrant future studies and will broaden our understanding of HIF-1α involvement in cellular homeostasis under non-hypoxic conditions.

References

1. Sun, X. *et al.* Parkin deficiency contributes to pancreatic tumorigenesis by inducing spindle multipolarity and misorientation. *Cell Cycle* **12**, 1133-1141 (2013).

2. Poulogiannis, G. *et al.* PARK2 deletions occur frequently in sporadic colorectal cancer and accelerate adenoma development in Apc mutant mice. *Proc. Natl. Acad. Sci. U.S.A.* **107**, 15145-15150 (2010).

3. Veeriah, S. *et al.* Somatic mutations of the Parkinson's disease-associated gene PARK2 in glioblastoma and other human malignancies. *Nat. Genet.* **42**, 77-82 (2010).

4. Fujiwara, M. *et al.* Parkin as a tumor suppressor gene for hepatocellular carcinoma. *Oncogene* **27**, 6002-6011 (2008).

5. Andres, A.M. *et al.* Mitophagy is required for acute cardioprotection by simvastatin. *Antioxid. Redox Signal.* **21**, 1960-1973 (2014).

6. Huang, C. *et al.* Preconditioning involves selective mitophagy mediated by Parkin and p62/SQSTM1. *PLoS One* **6**, e20975 (2011).

7. Hoshino, A. *et al.* Cytosolic p53 inhibits Parkin-mediated mitophagy and promotes mitochondrial dysfunction in the mouse heart. *Nat. Commun.* **4**, 2308 (2013).

8. Billia, F. *et al.* PTEN-inducible kinase 1 (PINK1)/Park6 is indispensable for normal heart function. *Proc. Natl. Acad. Sci. U.S.A.* **108**, 9572-9577 (2011).

9. Glick, D. *et al.* BNip3 regulates mitochondrial function and lipid metabolism in the liver. *Mol. Cell. Biol.* **32**, 2570-2584 (2012).

APPENDIX

HEPATOCYTES ARE THE PRINCIPAL SOURCE OF CIRCULATING RBP4 IN MICE

Spencer J. Thompson*, Ashot Sargsyan*, Seung-Ah Lee,
Jason J. Yuen, Jinjin Cai, Rana Smalling,
Norbert Ghyselinck, Manuel Mark,
William S. Blaner, Timothy E. Graham

*Both authors contributed equally to this work.

From Thompson et al. Hepatocytes are the principal source of circulating RBP4 in mice. Diabetes 2016 Oct; db160286.
Copyright 2016 American Diabetes Association. Used with permission

Diabetes Volume 66, January 2017 1

Spencer J. Thompson,[1] Ashot Sargsyan,[1,2] Seung-Ah Lee,[3] Jason J. Yuen,[3] Jinjin Cai,[1,2] Rana Smalling,[2] Norbert Ghyselinck,[3] Manuel Mark,[3,4] William S. Blaner,[5] and Timothy E. Graham[1,2]

Hepatocytes Are the Principal Source of Circulating RBP4 in Mice

Diabetes 2017;66:1–6 | DOI: 10.2337/db16-0286

RBP4 is produced mainly by hepatocytes. In type 2 diabetes and obesity, circulating RBP4 is increased and may act systemically to cause insulin resistance and glucose intolerance. Observations that adipocyte RBP4 mRNA increases in parallel with circulating RBP4 in these conditions, whereas liver RBP4 mRNA does not, led to a widely held hypothesis that elevated circulating RBP4 is a direct result of increased production by adipocytes. To test this, we generated mice with hepatocyte-specific deletion of *RBP4* (liver RBP4 knockout or LRKO mice). Adipose tissue RBP4 expression and secretion remained intact in LRKO mice and increased as expected in the setting of diet-induced insulin resistance. However, circulating RBP4 was undetectable in LRKO mice. We conclude that adipocyte RBP4 is not a significant source of circulating RBP4, even in the setting of insulin resistance. Adipocyte RBP4, therefore, may have a more important autocrine or paracrine function that is confined within the adipose tissue compartment.

Liver is the main organ for vitamin A (retinol) storage in vertebrates (1). Hepatocytes distribute retinol to other tissues through a circulating carrier protein, serum retinol-binding protein (RBP4) (2). RBP4 is expressed primarily in hepatocytes and to a lesser extent in adipocytes and other cell types and functions as the sole specific blood transport protein for retinol (2). RBP4 expressed in hepatocytes binds intracellular retinol and is secreted into the circulation as retinol-bound holo-RBP4, which delivers retinol to multiple tissues (2).

Circulating RBP4 concentrations are increased in humans and rodents with obesity and type 2 diabetes (3,4). Several lines of evidence suggest RBP4 acts systemically in a classic endocrine fashion to dysregulate insulin-glucose homeostasis in these conditions (3,4). In mice, increasing serum RBP4 by genetic or pharmacological approaches causes insulin resistance and glucose intolerance, whereas lowering serum RBP4 improves insulin sensitivity and enhances glucose tolerance (3). Elevated serum RBP4 induces the gluconeogenic enzyme phosphoenolpyruvate carboxykinase in liver and impairs insulin signaling in skeletal muscle (3). RBP4 has been suggested to play a key role in coordinating cellular immunity to induce adipose tissue inflammation in obesity (5).

Extensive work in human subjects (children and adults) from diverse clinical contexts, resulting in hundreds of publications over the past decade, has confirmed strong correlations of serum RBP4 with diabetes and diabetic complications, insulin resistance, metabolic syndrome, polycystic ovarian syndrome, metabolic complications of pregnancy, atherosclerosis, heart disease, stroke, and certain cancers (6–13). Moreover, humans harboring a genetic polymorphism (−803G>A) of *Rbp4*, which regulates transcription factor binding to the *Rbp4* promoter (14), exhibit elevated serum RBP4 (15) and up to a 2.7-fold greater risk of incident diabetes (16). Nevertheless, how serum RBP4 regulates insulin-glucose homeostasis

[1]Molecular Medicine Program, Department of Medicine, Division of Endocrinology, Metabolism, and Diabetes, Department of Nutrition, and Department of Biological Chemistry, University of Utah School of Medicine, Salt Lake City, UT

[2]George E. Wahlen Department of Veterans Affairs Medical Center, Salt Lake City, UT

[3]Département de Génétique Fonctionnelle et Cancer, Institut de Génétique et de Biologie Moléculaire et Cellulaire; Centre National de la Recherche Scientifique; INSERM; and Université de Strasbourg, Illkirch, France

[4]Hôpitaux Universitaires de Strasbourg, Strasbourg, France

[5]Department of Medicine and Institute of Human Nutrition, Columbia University College of Physicians and Surgeons, New York, NY

Corresponding author: Timothy E. Graham, tim.graham@progenitorlifesciences.com.

Received 29 February 2016 and accepted 14 October 2016.

This article contains Supplementary Data online at http://diabetes.diabetesjournals.org/lookup/suppl/doi:10.2337/db16-0286/-/DC1.

S.J.T. and A.S. contributed equally to this work.

© 2016 by the American Diabetes Association. Readers may use this article as long as the work is properly cited, the use is educational and not for profit, and the work is not altered. More information is available at http://www.diabetesjournals.org/content/license.

remains poorly understood, including which tissues contribute to elevated serum RBP4 during insulin resistance.

To our knowledge, the contribution of RBP4 produced within adipose tissue to the circulating RBP4 pool has never been formally tested. We determined the relative contributions of adipose and other extrahepatic tissues to circulating RBP4 concentrations in vivo by generating and characterizing mice with hepatocyte-specific genetic deletion of *Rbp4* (liver-specific RBP4 knockout [LRKO] mice). We report the unexpected finding that LRKO mice lack detectable RBP4 in circulation.

RESEARCH DESIGN AND METHODS

Animal Husbandry, Diets, and Genotyping

$Rbp4^{(loxP/loxP)}$ mice on mixed C57BL/6J × 129Sv background (17) (a gift from P. Chambon, University of Strasbourg), were crossed with albumin promoter (*Alb*)-Cre transgenic mice (18) (a gift from M. Magnuson, The Jackson Laboratories, Bar Harbor, ME; strain #003574) to produce $Rbp4^{(loxP/+)}$/*Alb*-$Cre^{(Tg/0)}$ mice, which were interbred to produce F2 mice with hepatocyte-specific genetic knockout (KO) of *Rbp4* (i.e., $Rbp4^{(loxP/loxP)}$/*Alb*-$Cre^{(Tg/0)}$ mice, called LRKO mice). Littermates with genotypes $Rbp4^{(+/+)}$/*Alb*-$Cre^{(0/0)}$, $Rbp4^{(+/+)}$/*Alb*-$Cre^{(Tg/0)}$, and $Rbp4^{(loxP/loxP)}$/*Alb*-$Cre^{(0/0)}$ served as controls. The various genotypes used for controls showed no statistically significant differences in metabolic parameters or serum RBP4 levels. Mice were maintained in an American Association of Laboratory Animal Care–accredited temperature and humidity–controlled vivarium with 12-h light/dark cycles. Studies were approved by the Institutional Animal Care and Use Committee at the University of Utah. Standard chow diet (Teklad 2920 × 0; Harlan-Teklad) or high-fat (HF) diet (55% fat calories) (Teklad 93075) were administered from weaning until sacrifice at 20–22 weeks. The nonirradiated chow diet contained 15 International Units/g vitamin A as retinyl acetate. The γ-irradiated HF/high-sucrose (HS) diets contained 26 International Units/g retinyl acetate (before γ-irradiation for sterilization); according to the manufacturer, the dose of γ-irradiation used causes a 35–45% reduction in bioavailable vitamin A in rodent diets. Genotyping for *Rbp4* alleles and *Alb*-Cre transgene was performed as previously described (17,18).

Quantitative RT-PCR

Commercial reagents (miRNeasy; QIAGEN) were used to isolate purified mRNA, and cDNA was immediately generated by Transcriptor First-Strand cDNA Synthesis Kit (Roche). For quantitative RT-PCR, RBP4 transcripts were amplified using primers 5′-GACAAGGCTCGTTTCTCTGG-3′ and 5′-AAAGGAGGCTACACCCCAGT-3′ (University of Utah Genomics Core) and detected with the FastStart Universal SYBR Green Master (Rox) kit (Roche) on a 7900HT Fast Real-Time PCR System (Applied Biosystems).

Hepatic Portal Vein Blood Sampling

Mice were anesthetized with 3–5% isofluorane before exposing the hepatic portal vein with a ventral incision. Hepatic portal blood was then collected with a 27-gauge insulin syringe. Blood was allowed to clot for 15 min and centrifuged at 1,500*g* for 10 min. Serum was then collected and analyzed by Western blotting. The protocol was adapted for mice (19).

Western Blotting

Serum was analyzed by SDS-PAGE and Western blotting for RBP4 as previously described (3,20). Commercially available purified RBP4 isolated from pooled human donor plasma (Hytest) was used as a positive control. For explant analysis, one-half perigonadal fat pad per animal was isolated, weighed, minced with fine scissors, washed by buoyancy centrifugation, and incubated overnight in media (DMEM; Gibco). The media volumes were adjusted so that total explant tissue weight per volume of media was equal for every sample. RBP4 was isolated by immunoprecipitation (by using polyclonal rabbit anti-human RBP4 [A0040; Dako]) from the conditioned media and then detected as above; the upper part of the SDS-PAGE gel was cut to prevent interference in Western blotting from the heavy chain of the immunoprecipitating antibody. This technique produced total precipitation of RBP4 in the serum of control mice (Supplementary Fig. 4). Transferrin antibody was from Bethyl Laboratories (Cat. A80-128) and transthyretin (TTR) (prealbumin) antibody was purchased Santa Cruz Biotechnology (Cat. sc-377517).

Metabolic Measurements

Serum insulin was measured by commercial ELISA (Crystal Chem). Serum glucose was measured in whole blood by glucometer (Bayer). Intraperitoneal glucose tolerance testing (1 g/kg body weight) and insulin tolerance testing (1 unit/kg body weight insulin aspart; Novo Nordisk) were performed as previously described (3). Urine RBP4 levels were determined by ELISA by using a monoclonal IgA-based assay (21) according to the manufacturer's instructions (Adipogen). Body composition was measured by whole-body nuclear magnetic resonance (minispec; Bruker). Retinol and retinyl esters (REs) were measured as previously described for serum, tissue, and cells. The RE fraction contains the summed levels of retinyl palmitate, retinyl oleate, retinyl stearate, and retinyl linoleate. These four REs account for >95% of the RE present in liver.

Statistical Analysis

Two-way ANOVA was used to test for significant differences in groupings based on the independent factors of genotype and diet. Insulin tolerance test (ITT) area over the curve and glucose tolerance test (GTT) area under the curve were calculated as the change in glucose (mg/dL) from the baseline (time 0) value integrated over time (min).

RESULTS

LRKO mice were born at expected Mendelian frequencies and did not differ from littermate controls in growth, body weight, or adiposity on normal chow diet (Table 1).

Table 1—Metabolic characterization of LRKO mice

	Control chow	LRKO chow	Control HF/HS	LRKO HF/HS
Body composition				
Body weight (g)	31.6 ± 0.9	29.2 ± 0.6	31.6 ± 0.7	35.4 ± 1.1*†
Change in weight after weaning (g)	22.0 ± 0.8	19.8 ± 0.6	22.5 ± 0.7	25.1 ± 1.3*†
Percent fat mass (%)	19.1 ± 3.0	14.3 ± 2.5	23.8 ± 2.6	29.2 ± 3.4*†
Metabolic phenotype				
Food intake (g/body weight/day)	0.102 ± 0.002	0.099 ± 0.002	0.127 ± 0.025*	0.131 ± 0.031*
Fasted glucose (mg/dL)	62.5 ± 4.1	62.75 ± 1.9	61.8 ± 3.5	61.3 ± 0.4
Fed glucose (mg/dL)	111.8 ± 7.5	119.3 ± 12.6	120.3 ± 9.3	106.5 ± 4.8
Fasted insulin (ng/mL)	0.30 ± 0.04	0.30 ± 0.02	0.31 ± 0.05	0.35 ± 0.06
Fed insulin (ng/mL)	0.53 ± 0.07	0.78 ± 0.21	1.00 ± 0.24*	1.23 ± 0.15*
ITT (area over the curve)	11,944 ± 625	11,833 ± 730	8,678 ± 1,335*	7,980 ± 1,191*
GTT (area under the curve)	27,030 ± 1,445	26,009 ± 1,558	37,542 ± 1,863*	37,490 ± 2,026*
Retinoid phenotype				
Serum RBP4 by ELISA (μg/mL)	100.7 ± 9.6	ND	115.58 ± 8.2	ND
Serum ROH (μg/dL)	25.9 ± 2.3	1.7 ± 0.2†		
Liver ROH (nmol/g)	126 ± 12	125 ± 19		
Liver RE (nmol/g)	4,818 ± 166	4,392 ± 285		
Hepatocyte ROH (nmol/10^6 cells)	0.0600 ± 0.004	0.0478 ± 0.004		
Hepatocyte RE (nmol/10^6 cells)	9.5 ± 1.6	6.9 ± 0.8		
HSC RE (nmol/10^6 cells)	138.8 ± 18.6	98.6 ± 34.0		

Data are mean ± SEM. Male mice; ages 20–22 weeks; chow or HF/HS diets started at weaning. n = 9–10 per group for RBP4 ELISA; n = 5–6 per group for other studies. Units for ITT and GTT area over/under the curve are mg · dL^{-1} · min^{-1}. Maximum sensitivity of assay is 0.06 ng/mL. HSC, hepatic stellate cell; ND, not detected; ROH, retinol. *$P < 0.05$ vs. chow; †$P < 0.05$ vs. control on same diet, by two-way ANOVA.

Cre-mediated *LoxP* site recombination of *Rbp4* was detected in the liver of LRKO mice but not in brain, skeletal muscle, brown adipose tissue, or any of three different white adipose tissue depots surveyed (Fig. 1*A*). Hepatocyte-specific *Rbp4* recombination diminished RBP4 expression in liver without affecting RBP4 expression in fat (Fig. 1*B*).

Because adipose RBP4 is upregulated in insulin-resistant states (3,4), we fed LRKO and control mice an HF/HS diet to induce insulin resistance. Food intake did not differ between genotypes. Control mice fed HF/HS exhibited resistance to diet-induced obesity, consistent with their 129Sv mixed genetic background (22), but still developed insulin resistance and glucose intolerance (ITT response decreased 28%, and GTT response increased 39%; $P < 0.05$ for each result) (Table 1 and Supplementary Fig. 2*A* and *B*). Conversely, LRKO mice fed HF/HS exhibited small, but significant gains in body weight (12% increase over chow-fed LRKO mice; $P < 0.05$) and greater adiposity (29.2 ± 3.4% fat mass in LRKO mice vs. 23.8 ± 2.6% fat mass in control mice; $P < 0.05$) (Table 1) yet developed similar degrees of insulin resistance and glucose intolerance (ITT response decreased 33%, and GTT increased 41%; $P < 0.05$ vs. chow-fed LRKO mice and nonsignificant vs. control mice for each result) (Table 1 and Supplementary Fig. 2*A* and *B*). HF/HS feeding increased adipose tissue RBP4 mRNA independently of genotype (48% greater in HF/HS-fed vs. chow-fed mice; $P < 0.05$) (Fig. 1*B*), which is consistent with other mouse models of insulin resistance (3). Similar to the phenotype of germline *Rbp4* KO mice (total-body *Rbp4* KO mice) reported previously (23), LRKO mice exhibited greatly reduced serum retinol (<7% of control mouse levels; $P < 0.05$) (Table 1). However, liver retinol and RE content did not differ between LRKO and control mice when analyzed in whole tissue or in isolated parenchymal hepatocytes and hepatic stellate cells (Table 1), and liver weight did not differ between genotypes (data not shown).

Of note, RBP4 was not detected in serum from the general or portal circulation of LRKO mice, even in response to HF/HS feeding–induced insulin resistance (Fig. 2*A* and *B*). Perigonadal white adipose tissue explants taken from LRKO and control mice secreted equal amounts of RBP4 into culture media (Fig. 2*C* and Supplementary Fig. 3*A*). Explant secretion was increased by HF/HS feeding in-dependently of genotype (Fig. 2*D*). In the absence of its hepatocyte-secreted binding partner TTR, serum RBP4 is filtered through the glomerulus and excreted into urine (2). Serum TTR did not differ between genotypes (Supple-mentary Fig. 4). However, adipocytes do not express TTR, so we reasoned that RBP4 produced in its absence would un-dergo more rapid renal clearance. To test this, we measured urine RBP4 levels. However, RBP4 was detected in urine of control mice but not in urine of LRKO mice (Fig. 2*E*).

DISCUSSION

Together these findings indicate that mice lacking hepatocyte-derived RBP4 exhibit no detectable circulating RBP4, which is not due to increased renal excretion of RBP4 or the absence of adipocyte RBP4 expression/secretion. Therefore, hepatocytes appear to be the principal, and perhaps sole, source of circulating RBP4 in mice. The clear dissociation between adipose RBP4 production and

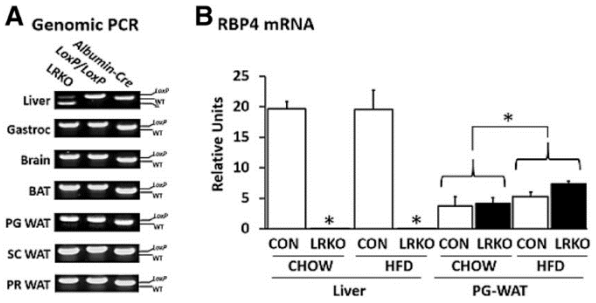

Figure 1—LRKO mice. *A*: Representative PCR analysis of genomic DNA prepared from tissues of LRKO, *Rbp4*$^{(fl/fl)}$, and albumin promoter-Cre$^{(Tg/0)}$ transgenic mice. The lower-molecular-weight Cre-*LoxP* recombinant allele (Δ) is observed solely in the liver of LRKO mice and not in other tissues surveyed. *B*: Measurement of adipose tissue RBP4 mRNA by quantitative RT-PCR demonstrates a reduction of liver RBP4 mRNA to levels near the limit of detection in LRKO mice and induction of adipose tissue RBP4 mRNA by HF/HS feeding independently of genotype. Data are mean ± SEM (n = 5 per group). Statistical testing for liver and adipose tissue, respectively: *P < 0.05 vs. control and *P < 0.05 for chow-fed vs. HF/HS-fed groups (as indicated by brackets), by two-way ANOVA. BAT, brown adipose tissue; CON, control; Gastroc, gastrocnemius; HFD, high-fat diet; PG, perigonadal; PR, perirenal; SC, subcutaneous; WAT, white adipose tissue; WT, wild type.

circulating RBP4 in LRKO mice indicates that adipocyte-secreted RBP4 is most likely confined to autocrine or paracrine actions within adipose tissue, even in the setting of insulin resistance.

Of note, LRKO mice fed chow do not exhibit the enhanced insulin sensitivity and glucose tolerance previously observed in total-body RBP4 KO mice (3), suggesting that an additional loss of RBP4 expressed in extrahepatic tissues (possibly adipocyte RBP4) is necessary for the favorable metabolic phenotype of the total-body RBP4 KO mice. However, these observations are complicated by the obesity-resistant, 129Sv mixed background of the mice studied. In future studies, characterization of the metabolic phenotype of adipocyte-specific RBP4 KO mice compared with LRKO mice will be important, ideally on a homogenous genetic background. Furthermore, although total-body RBP4 KO mice acquire increased RE and retinol stores with aging (24), this was not apparent in our 5-month-old LRKO mice (Table 1). Otherwise, phenotypes of LRKO mice and total-body RBP4 KO mice are similar; neither line exhibited protection from diet-induced insulin resistance or hyperglycemia (Table 1). Of note, LRKO mice unexpectedly developed slightly greater diet-induced weight gain and adiposity than littermate controls (Table 1), despite the obesity-resistant 129Sv mixed genetic background. Further study will clarify whether the observed increase in adiposity is a consistent feature of the LRKO phenotype in other genetic backgrounds.

Why does RBP4 secretion by adipocytes not produce circulating RBP4 in LRKO mice? Adipocyte RBP4 might be degraded rapidly within adipose tissue in vivo by undetermined mechanisms. However, we did not detect RBP4 proteolytic products in serum, adipose tissue, or adipose explant-conditioned media of LRKO or control mice by Western blotting with various combinations of N- or C-terminus–directed antibodies (data not shown). Work by Moraes-Vieira et al. (5) in mice expressing human RBP4 ectopically in muscle (muscle creatine kinase promoter-hRBP4 transgenic mice) suggested an alternative explanation: hRBP4 produced in muscle, which can be differentiated from endogenous mouse RBP4, accumulates in adipose tissue in vivo, where it activates CD11c^{+} cells (macrophage antigen-presenting cells and dendritic cells) and produces adipose tissue inflammation and systemic insulin resistance. Moreover, recent work by Lee et al. (25) showed that overexpression of hRBP4 in adipocytes causes increased levels of adipose tissue RBP4 but does not increase total circulating RBP4. Taken together, these findings suggest that circulating RBP4 may bind and accumulate in fat through yet-to-be-determined binding sites, and adipocyte-secreted RBP4 primarily remains within the adipose compartment. A survey of gene expression in adipose tissue of LRKO mice revealed no statistically significant differences between genotypes in mRNA levels of the RBP4 receptors Stra6 and Stra6L, which could potentially mediate RBP4 binding in fat, or in mRNA of classic retinoic acid target genes Rarβ, Crbp1, and Cyp26a1 (Supplementary Fig. 5*A*); additionally, no differences in mRNA of proinflammatory cytokines tumor necrosis factor-α and Mcp1 or in markers of macrophage infiltration Cd68 and F4/80 were found (Supplementary Fig. 5*B*).

There are several considerations in interpreting these findings. First, studies should be designed to determine whether the relative contributions of adipose and other extrahepatic tissues to circulating RBP4 levels differ between mice and humans. Second, although LRKO mice with diet-induced obesity exhibit no circulating RBP4, adipocyte RBP4 could make a greater contribution to circulating levels in the setting of severe obesity, as observed in *ob/ob* or *db/db* mice (26) or in morbidly obese

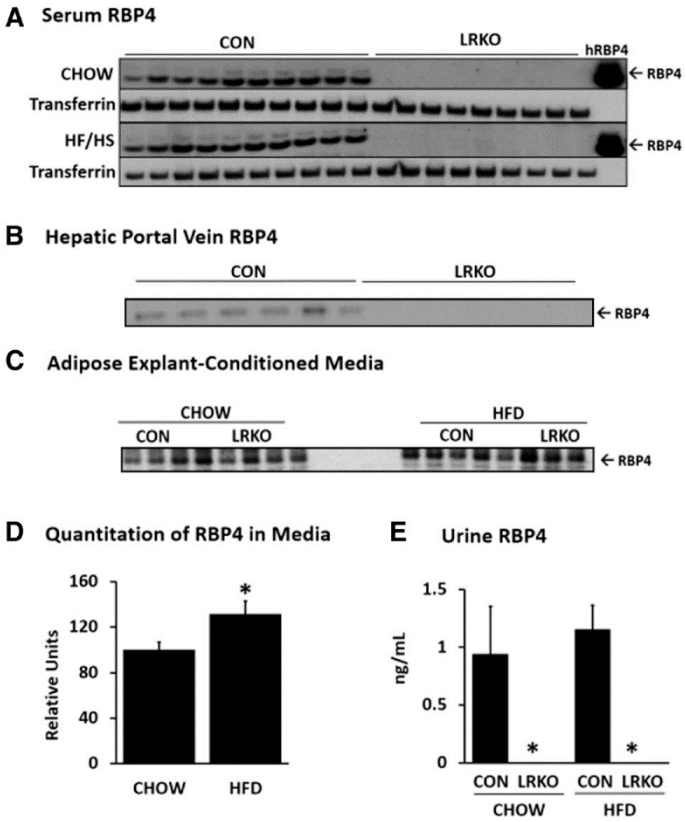

Figure 2—RBP4 is secreted by adipose tissue explants but is not detected in serum or urine of LRKO mice. *A*: RBP4 protein levels are undetectable in serum of LRKO mice fed either a normal chow or an HF/HS diet as determined by Western blotting. Transferrin was used as a loading control. The hRBP4 lane contains 10 ng purified human RBP4. No immunoreactivity is evident in LRKO serum. *B*: RBP4 protein levels are undetectable in serum collected from the hepatic portal vein as determined from Western blotting. *C*: RBP4 protein secretion by adipose explants of LRKO and control littermates fed a normal chow or an HF/HS diet. *D*: Quantitation of Western blot data in adipose explant–conditioned media shown in panel *C*. HF/HS feeding caused an ~25% increase in explant RBP4 secretion, independently of genotype. **P* < 0.05 vs. chow-feeding (n = 4 per group), by two-way ANOVA. *E*: RBP4 protein is not detected in urine of LRKO mice by ELISA. **P* < 0.05 vs. control (n = 5 per group), by two-way ANOVA. Data are mean ± SEM. CON, control; HFD, high-fat diet.

humans, although the current findings suggest that this contribution might be minor. Third, adipocyte RBP4 could regulate serum RBP4 indirectly by altering hepatocyte RBP4 secretion or renal RBP4 clearance through as yet undetermined mechanisms. Finally, the finding that RBP4 does not function as a circulating adipokine in the classic endocrine sense does not negate or otherwise contradict the hundreds of publications that link elevated serum RBP4 to clinical features of insulin resistance, type 2 diabetes, dyslipidemia, cardiovascular disease, and cancer in humans; however, it does suggest that other parameters such as RBP4 production by hepatocytes, affinity of RBP4-TTR interactions, and RBP4 renal clearance may be more important determinants of RBP4 concentrations in these conditions. Further studies will clarify the dynamics of RBP4 secretion and action within the adipose tissue compartment and determine the extent to which (and mechanisms by which) adipocyte RBP4 and other extrahepatic RBP4 sources contribute to systemic insulin-glucose homeostasis.

Acknowledgments. The authors thank Sihem Boudina, John David Symons, Corrine Welt, Thunder Jalili, Micah Drummond, and Anandh Babu Pon

Velayutham of the University of Utah for intellectual contributions to the discussion of the study design and data interpretation.

Funding. This work was supported by a Howard Hughes Medical Institute Med into Grad Award (to A.S.); by an American Heart Association Predoctoral Fellowship award (to R.S. and T.E.G.); and by U.S. Department of Veterans Affairs Biomedical Laboratory Research and Development Merit Review Award BX000937, American Diabetes Association Core Basic Science Award 7-13-BS-05, and National Institute of Diabetes and Digestive and Kidney Diseases grant R01-DK-100826 (to T.E.G.).

Duality of Interest. No potential conflicts of interest relevant to this article were reported.

Author Contributions. S.J.T., A.S., and T.E.G. designed and executed the experiments, interpreted the data, and wrote the manuscript. S-A.L., J.J.Y., and W.S.B. measured the retinol and REs in whole liver and isolated hepatocytes and hepatic stellate cells. J.C. and R.S. contributed to the data analysis of metabolic phenotype and RBP4 mRNA measurements. N.G. and M.M. developed and shared the flox-RBP4 mice for these studies. T.E.G. is the guarantor of this work and, as such, had full access to all the data in the study and takes responsibility for the integrity of the data and the accuracy of the data analysis.

References

1. Blaner WS, Olson JA. *Retinol and Retinoic Acid Metabolism*. New York, NY, Raven Press, 1994
2. Saprano DB, Blaner WS. *Plasma Retinol-Binding Protein*. New York, NY, Raven Press, 1994
3. Yang Q, Graham TE, Mody N, et al. Serum retinol binding protein 4 contributes to insulin resistance in obesity and type 2 diabetes. Nature 2005;436:356–362
4. Graham TE, Yang Q, Blüher M, et al. Retinol-binding protein 4 and insulin resistance in lean, obese, and diabetic subjects. N Engl J Med 2006;354:2552–2563
5. Moraes-Vieira PM, Yore MM, Dwyer PM, Syed I, Aryal P, Kahn BB. RBP4 activates antigen-presenting cells, leading to adipose tissue inflammation and systemic insulin resistance. Cell Metab 2014;19:512–526
6. Aigner E, Bachofner N, Klein K, et al. Retinol-binding protein 4 in polycystic ovary syndrome—association with steroid hormones and response to pioglitazone treatment. J Clin Endocrinol Metab 2009;94:1229–1235
7. Cho YM, Youn BS, Lee H, et al. Plasma retinol-binding protein-4 concentrations are elevated in human subjects with impaired glucose tolerance and type 2 diabetes. Diabetes Care 2006;29:2457–2461
8. El-Mesallamy HO, Hamdy NM, Zaghloul AS, Sallam AM. Serum retinol binding protein-4 and neutrophil gelatinase-associated lipocalin are interrelated in pancreatic cancer patients. Scand J Clin Lab Invest 2012;72:602–607
9. Su YX, Hong J, Yan Q, et al. Increased serum retinol-binding protein-4 levels in pregnant women with and without gestational diabetes mellitus. Diabetes Metab 2010;36:470–475
10. Kadoglou NP, Lambadiari V, Gastounioti A, et al. The relationship of novel adipokines, RBP4 and omentin-1, with carotid atherosclerosis severity and vulnerability. Atherosclerosis 2014;235:606–612
11. Reinehr T, Stoffel-Wagner B, Roth CL. Retinol-binding protein 4 and its relation to insulin resistance in obese children before and after weight loss. J Clin Endocrinol Metab 2008;93:2287–2293
12. Cheng Y, Liu C, Zhang N, Wang S, Zhang Z. Proteomics analysis for finding serum markers of ovarian cancer. Biomed Res Int 2014;2014:179040
13. Balagopal P, Graham TE, Kahn BB, Altomare A, Funanage V, George D. Reduction of elevated serum retinol binding protein in obese children by lifestyle intervention: association with subclinical inflammation. J Clin Endocrinol Metab 2007;92:1971–1974
14. Munkhtulga L, Nagashima S, Nakayama K, et al. Regulatory SNP in the RBP4 gene modified the expression in adipocytes and associated with BMI. Obesity (Silver Spring) 2010;18:1006–1014
15. Munkhtulga L, Nakayama K, Utsumi N, et al. Identification of a regulatory SNP in the retinol binding protein 4 gene associated with type 2 diabetes in Mongolia. Hum Genet 2007;120:879–888
16. van Hoek M, Dehghan A, Zillikens MC, Hofman A, Witteman JC, Sijbrands EJ. An RBP4 promoter polymorphism increases risk of type 2 diabetes. Diabetologia 2008;51:1423–1428
17. Ghyselinck NB, Vernet N, Dennefeld C, et al. Retinoids and spermatogenesis: lessons from mutant mice lacking the plasma retinol binding protein. Dev Dyn 2006;235:1608–1622
18. Postic C, Shiota M, Niswender KD, et al. Dual roles for glucokinase in glucose homeostasis as determined by liver and pancreatic beta cell-specific gene knock-outs using Cre recombinase. J Biol Chem 1999;274:305–315
19. Scholtens E, Mulder GJ. A simple method of obtaining multiple blood samples from the portal vein and the hepatic vein in the rat in vivo. Experientia 1983;39:1176–1177
20. Mody N, Graham TE, Tsuji Y, Yang Q, Kahn BB. Decreased clearance of serum retinol-binding protein and elevated levels of transthyretin in insulin-resistant ob/ob mice. Am J Physiol Endocrinol Metab 2008;294:E785–E793
21. Park SE, Lee NS, Park JW, et al. Association of urinary RBP4 with insulin resistance, inflammation, and microalbuminuria. Eur J Endocrinol 2014;171:443–449
22. Bachmanov AA, Reed DR, Tordoff MG, Price RA, Beauchamp GK. Nutrient preference and diet-induced adiposity in C57BL/6ByJ and 129P3/J mice. Physiol Behav 2001;72:603–613
23. Quadro L, Blaner WS, Salchow DJ, et al. Impaired retinal function and vitamin A availability in mice lacking retinol-binding protein. EMBO J 1999;18:4633–4644
24. Paik J, Vogel S, Quadro L, et al. Vitamin A: overlapping delivery pathways to tissues from the circulation. J Nutr 2004;134:276S–280S
25. Lee SA, Yuen JJ, Jiang H, Kahn BB, Blaner WS. Adipocyte-specific overexpression of retinol-binding protein 4 causes hepatic steatosis in mice. Hepatology 2016;64:1534–1546
26. Wang B, Chandrasekera PC, Pippin JJ. Leptin- and leptin receptor-deficient rodent models: relevance for human type 2 diabetes. Curr Diabetes Rev 2014;10:131–145